

CREEP BEHAVIOR OF NATURAL FIBER REINFORCED POLYMER COMPOSITES

A Dissertation

Submitted to the Graduate Faculty of the
Louisiana State University and
Agricultural and Mechanical College
in partial fulfillment of the
requirements for the degree of
Doctor of Philosophy

In

The School of Renewable Natural Resources

by

Yanjun Xu

B.E., Sichuan University, June 2002

M.E., Sichuan University, June 2005

December 2009

ACKNOWLEDGEMENTS

It is my pleasure to acknowledge some people who contributed to this dissertation.

I am heartily thankful to my advisor, Dr. Qinglin Wu, for his guidance and support during my PhD study. His diligence and intelligence have motivated me to excel not only in this program, but also in my future career.

I would also like to thank my committee members, Dr. Quang V. Cao, Dr. Ioan I. Negulescu, Dr. Su-Seng Pang, and Dr. Paul Russo. Their suggestions and advices were very valuable and constructive in my research and dissertation writing.

My special thanks go to my friend and lab mate, Dr. Yong Lei, for his help during this program. My other lab mates, Dr. Hongzhi Liu, Dr. Fei Yao, Mr. Birm June Kim, Dr. Dagang Liu, and Dr. Haiyun Liu, also helped me in my research in many different ways. Thanks. I also thank Dr. Craig M. Clemons, Materials Research Engineer in USDA Forest Service, for his revision on part of this dissertation.

My thanks also go to our host family, Virginia, Cheryl Elise, and Charles Grenier, and Lucille Price Parsons. They made us feel at home in this country. I also want to thank our friends, Hongyi Wu and Yingqin Zhang, and their host parents, Ronni and Richard DeBates, for their sincere friendship and help in my life and work. Mr. DeBates also edited this dissertation.

Finally, I owe my deepest gratitude to my wife, Xian Guan, for her love, care, and encouragement throughout our marriage. She is the most wonderful woman I have ever met in my life, and she is the one who should receive credit for each and every single achievement I made. I also thank our parents for their understanding and support.

TABLE OF CONTENTS

ACKNOWLEDGEMENTS	ii
LIST OF TABLES	vi
LIST OF FIGURES	viii
NOMENCLATURE	xi
ABSTRACT.....	xiii
CHAPTER 1 INTRODUCTION	1
1.1 BACKGROUND	1
1.2 OBJECTIVES.....	3
1.3 ORGANIZATION OF DISSERTATION	4
1.4 REFERENCES	4
CHAPTER 2 NATURAL FIBER REINFORCED POLY(VINYL CHLORIDE) COMPOSITES: EFFECT OF FIBER TYPE AND IMPACT MODIFIER	6
2.1 INTRODUCTION	6
2.2 EXPERIMENTAL.....	8
2.2.1 Raw Materials	8
2.2.2 Composite Preparation.....	9
2.2.3 Measurements	9
2.3 RESULTS AND DISCUSSION	12
2.3.1 Mechanical Properties.....	12
2.3.2 Glass Transition Temperature.....	15
2.3.3 Thermal Stability	16
2.3.4 Water Absorption (WA) and Thickness Swelling (TS).....	19
2.4 CONCLUSIONS.....	23
2.5 REFERENCES	24
CHAPTER 3 CREEP BEHAVIOR OF BAGASSE FIBER REINFORCED POLYMER COMPOSITES.....	26
3.1 INTRODUCTION	26
3.2 THEORETICAL BACKGROUND.....	27
3.2.1 Creep Models	27
3.2.2 Accelerated Testing	29
3.3 EXPERIMENTAL.....	30
3.3.1 Raw Material.....	30
3.3.2 Composite Preparation.....	31
3.3.3 Characterization	32
3.3.4 Creep Modeling	32
3.3.5 Recovery Analysis	33
3.3.6 Non-recoverable Deformation	34

3.4 RESULTS AND DISCUSSION	34
3.4.1 Stress-Strain Behavior	34
3.4.2 Temperature Effect	35
3.4.3 Time-Temperature Superposition	42
3.4.4 Creep Modeling	46
3.4.5 Recovery Analysis	53
3.5 CONCLUSIONS.....	53
3.6 REFERENCES	54
CHAPTER 4 THE EFFECT OF COUPLING AGENTS AND BAMBOO FLOUR LOADING ON CREEP PROPERTY OF HDPE-BASED COMPOSITES	55
4.1 INTRODUCTION	55
4.2 EXPERIMENTAL.....	57
4.2.1 Materials and Blend Design.....	57
4.2.2 Sample Preparation	57
4.2.3 Creep Characterization.....	58
4.2.4 Creep Modeling	58
4.2.5 Time-Temperature Superposition (TTS)	59
4.3 RESULTS AND DISCUSSION	59
4.3.1 Effect of Individual Modifier Type and Content	59
4.3.2 Effect of Combined Modifiers	65
4.3.3 Effect of BF Loading	66
4.3.4 Morphological Analysis on the Creep Mechanism of the Composites.....	66
4.3.5 Indexed Burgers Models	68
4.3.6 Creep Prediction.....	68
4.4 CONCLUSIONS.....	72
4.5 REFERENCES	73
CHAPTER 5 CREEP BEHAVIOR OF COMPOSITES ENHANCED WITH ENGINEERING PLASTIC MICROFIBRILS	75
5.1 INTRODUCTION	75
5.2. EXPERIMENTAL.....	76
5.2.1 Materials	76
5.2.2 Preparation of the Composites	77
5.2.3 Characterization	79
5.2.4 Creep Modeling	79
5.2.5 Time-Temperature Superposition (TTS)	80
5.3 RESULTS AND DISCUSSION	80
5.3.1 HDPE/PA6 Composites	80
5.3.2 HDPE/PET Composites	85
5.4 CONCLUSION.....	91
5.5 REFERENCES	91
CHAPTER 6 APPLICATION OF UHMWPE AND UV ABSORBER IN WOOD/HDPE COMPOSITE: MECHANICAL PROPERTIES AND CREEP BEHAVIOR.....	93
6.1 INTRODUCTION	93

6.2 EXPERIMENTAL	95
6.2.1 Materials	95
6.2.2 Composite Preparation.....	96
6.2.3 Weathering.....	97
6.2.4 Characterization	97
6.2.5 Creep Modeling	97
6.3 RESULTS AND DISCUSSION	98
6.3.1 Mechanical Properties.....	98
6.3.2 Creep Behavior	101
6.4 CONCLUSION.....	107
6.5 REFERENCES	107
 CHAPTER 7 CONCLUSIONS AND FUTURE WORK.....	 110
7.1 OVERALL CONCLUSIONS.....	110
7.2 FUTURE WORK.....	112
 APPENDIX: PERMISSION LETTER.....	 114
 VITA.....	 115

LIST OF TABLES

Table 2.1 Two-way ANOVA test on the influence of fiber type and SEBS level on tensile and impact strength of the composites.....	15
Table 2.2 Glass transition temperature (T_g) and degradation temperature (T_d) of PVC/natural fiber composites	16
Table 2.3 Thermal degradation kinetic parameters of PVC/natural fiber composites.....	20
Table 2.4 Water absorption rate (%) of PVC/natural fiber composites after being immersed in water for 4 weeks	23
Table 2.5 Two-way ANOVA test on the influence of natural fiber type and SEBS level on WA and TS after being immersed in water for four weeks.....	23
Table 3.1 Summary of parameters in Burgers model for thirty-minute creep of the composites.	41
Table 3.2 Summary of E_a calculated based on Arrhenius equation for the composites	44
Table 3.3 Summary of model parameters for three-day creep of the composites	48
Table 3.4 Instantaneous creep deformation obtained from the 4-element, 6-element, and 8-element Burgers models in comparison with real value	50
Table 4.1 Summary of parameters in Burgers model and recovery rate for one-day creep of the composites with individual modifiers.....	63
Table 4.2 Summary of parameters in Burgers model for one-day creep of the composites with combined modifiers	63
Table 4.3 Summary of parameters in Burgers model for one-day creep of the composites with different BF loading levels.....	64
Table 4.4 Summary of the parameters for the new models in comparison with the 4-element Burgers model for BF/HDPE/PE-g-MA composites.....	69
Table 5.1 Values of parameters for HDPE/PA6 composites obtained via fitting experimental data with Burgers model.....	82
Table 5.2 Values of parameters for HDPE/PET composites obtained via fitting experimental data with Burgers model.....	86
Table 6.1 Mechanical properties of samples with different UHMWPE and WF loading levels..	99

Table 6.2(a) Comparison of mechanical properties of samples with and without UV before weathering.....	100
Table 6.2(b) Comparison of mechanical properties of samples with and without UV after weathering.....	100
Table 6.3 Burgers parameters for samples with different UHMWPE and WF loading levels...	105
Table 6.4(a) Burgers parameters for samples with different UHMWPE, WF and UV loading levels before weathering	105
Table 6.4(b) Burgers parameters for samples with different UHMWPE, WF and UV loading levels after weathering	105

LIST OF FIGURES

Figure 2.1 Storage modulus (a), tensile strength (b), and impact strength (c) of four PVC/natural fiber composites with different levels (0%, 2.5%, and 5%) of SEBS. Error bar represents Standard Deviation.....	13
Figure 2.2 Dynamic TGA curves of four PVC/natural fiber composites without SEBS.	17
Figure 2.3 Isothermal TGA curves of four PVC/natural fiber composites without SEBS at 260 °C for 120 minutes (a) and for the first 20 minutes (b).....	18
Figure 2.4 Typical plot of $\ln t$ vs. $1/(RT)$ for PVC/bagasse composites without SEBS at different conversion rates.	20
Figure 2.5 Typical WA (a) and TS (b) data as a function of time for four PVC/natural fiber composites with 2.5% SEBS.....	21
Figure 2.6 TS as a function of WA for PVC/natural fiber composites. (a) PVC/bagasse, (b) PVC/rice straw, (c) PVC/rice husk, and (d) PVC/pine.....	22
Figure 3.1 A diagram of generalized Burgers model.....	28
Figure 3.2 Stress-strain curves of the composites at (a) 35 °C and (b) 65 °C.	36
Figure 3.3 Creep curves of the composites at (a) 35 °C and (b) 65 °C. Symbols represent experimental data and solid lines represent Burgers model simulation.....	37
Figure 3.4 Creep strain (a) and strain rate (b) of B/RPVC at different temperatures. Symbols represent experimental data and solid lines represent the 4-element Burgers model simulation.	38
Figure 3.5 Creep strain (a) and strain rate (b) of B/RHDPE at different temperatures. Symbols represent experimental data and solid lines represent the 4-element Burgers model simulation.	39
Figure 3.6 Log-scaled creep strain of (a) B/RPVC and (b) B/RHDPE.	43
Figure 3.7 TTS master curves of creep for the composites.	44
Figure 3.8 Comparison of TTS predicted creep with experimental data for the composites. Symbols represent experimental data; solid lines represent the 4-element Burgers model simulation; dash lines represent TTS predicted data. Two lines with the same circle are for the same composite.....	45
Figure 3.9 Residual plot of 4, 6, and 8-element Burgers models for bagasse/RPVC composites: (a) three days; (b) first 300 minutes.	49

Figure 3.10 Comparison of 4, 6, and 8-element Burgers models when using two-day creep data to predict the third day creep for bagasse/RPVC composites.	50
Figure 3.11 Creep (C), recovery (R), and non-recoverable deformation (NR) of B/VPVC (a), B/VHDPE (b), and W/HDPE (c).	52
Figure 4.1 Creep and recovery curves of BF/HDPE composites with individual modifier: a) PE-g-MA, b) sEPR-g-MA, and c) aEPR-g-MA.	61
Figure 4.2 Creep and recovery curves of BF/HDPE composites with combined modifier at 5.7% level: a) PE-g-MA/sEPR-g-MA and b) PE-g-MA/aEPR-g-MA.	62
Figure 4.3 Creep and recovery curves of HDPE, BF/HDPE without modifier, BF/HDPE composites at different BF loading levels with combined modifier of PE-g-MA/sEPR-g-MA at 15 wt% of the BF loading and PE-g-MA/sEPR-g-MA ratio of 2:1.....	64
Figure 4.4 Comparison of Burgers model, PIB and FIB models with fixed index, and power law model used to predict one-day creep of BF/HDPE composite without modifier based on three-hour creep data.	70
Figure 4.5 HDPE and BF/HDPE composite without modifier: a) TTS masters and b) Comparison of the TTS predicted creep curves with the experimental curves.	71
Figure 5.1 Creep and recovery behavior of different HDPE/PA6 composites.	81
Figure 5.2 SEM picture of HDPE/PA6 composite.	81
Figure 5.3 Creep strain as a function of time during creep experiment at 35°C, together with the fitted curves of Burgers model.....	82
Figure 5.4 The effect of temperature on the creep behavior of different composites in HDPE/PA6 system. The unit for temperature is °C.	83
Figure 5.5 TTS master curves in logarithmic scale (a) and normal scale (b) for HDPE/PA6 composites.....	84
Figure 5.6 Creep and recovery behavior of the HDPE/PET composites.....	87
Figure 5.7 SEM observation of HDPE/PET composite.....	87
Figure 5.8 The effect of temperature on the creep behavior of different composites in HDPE/PET system. The unit for temperature is °C.	88
Figure 5.9 TTS master curves in logarithmic scale (a) and normal scale (b) for HDPE/PET composites.....	89

Figure 6.1 Creep and recovery curves of the composites with different HDPE/UHMWPE ratio:
(a) without WF, (b) with WF. 102

Figure 6.2 Creep and recovery curves of the composites with and without UVA: (a) without WF,
(b) with WF. The HDPE/UHMWPE ratio is 80/20. 103

Figure 6.3 Creep and recovery curves of the composites before and after weathering (labeled
with *). The HDPE/UHMWPE ratio is 80/20. 104

NOMENCLATURE

ANOVA: analysis of variance

B: bagasse fiber

BF: bamboo Flour

DMA: dynamic mechanical analysis

E_a : Activation Energy

EPR-g-MA: ethylene propylene rubber-grafted- maleic anhydride

HDPE: high density polyethylene

MFC: microfibrillar composite

NF: natural fiber

NFPC: natural fiber/polymer composite

PA: polyamide

PE-g-MA: polyethylene-grafted-maleic anhydride

PET: polyethylene terephthalate

PP: polypropylene

PVC: poly (vinyl chloride)

SEBS: styrene-ethylene-butylene-styrene

T_d : degradation temperature

T_g : glass transition temperature

TGA: thermogravimetric analysis

TS: thickness swelling

TTS: time-temperature superposition

UHMWPE: ultra-high molecular weight polyethylene

UV: ultraviolet

UVA: UV absorber

WA: water absorption

WF: wood flour

WPC: wood/polymer composite

WSS: weighted sum of squares

α_T : horizontal shift factor in TTS

E_M : elastic modulus of the spring in Maxwell unit

η_M : viscosity of the dashpot in Maxwell unit

E_K : elastic modulus of the spring in Kelvin unit

η_K : viscosity of the dashpot in Kelvin unit

ABSTRACT

Creep behavior of natural fiber/polymer composites (NFPCs) was studied in response to the increasing application of this material as structural building products. Factors that influence creep behavior of the composites were investigated by analyzing creep curves of several different NFPC systems, which were designed for overall performance of the composites.

Among different models, the 4-element Burgers type was mostly used for quantitative characterization of the creep curves to compare the properties of different composites. The parameters from the 4-element Burgers model were easily interpretable due to their physical meanings. Generalized Burgers models provided better fit by introducing extra Kelvin units, but they are more complicated. Indexed Burgers models performed better for creep curves within the primary stage in terms of both characterization and prediction.

Creep prediction was attempted through two approaches: modeling and accelerated testing. Burgers models were proven unsuitable for long-term prediction if the creep test time was not long enough. Comparatively, the indexed Burgers and 2-parameter power law models performed better for prediction purposes. Accelerated creep tests were conducted at higher temperatures, and smooth curves were obtained based on the time-temperature superposition (TTS) principle. The accuracy of long-term prediction was unable to be evaluated due to the lack of long-term experimental data.

Several factors were shown to affect the creep resistance of NFPCs. These include polymer matrix type, natural fiber loading, additives, temperature, and weathering treatment. PVC had higher creep resistance than HDPE, and HDPE showed better creep resistance than ultra-high molecular weight polyethylene (UHMWPE). Introducing engineering plastics to form microfibrils in HDPE matrix improved its creep performance. Certain recycled plastics had

smaller creep deformation than the corresponding virgin resin. Adding natural fibers into polymer matrix greatly enhanced its creep resistance. The effect of a coupling agent on creep property of NFPCs was dependent on its modulus and coupling effect. UVA, an ultrafine titanium dioxide, slightly reduced the creep deformation of HDPE composites at a low loading level. Higher temperatures led to not only larger instantaneous deformations, but also to higher long-term creep rates. Weathering treatment also affected the creep properties of polymer and NFPCs.

CHAPTER 1 INTRODUCTION

1.1 BACKGROUND

Natural fiber/polymer composites (NFPCs) are experiencing dramatic growth in utilization because of low cost, low density, biodegradability, sound mechanical properties, water and rot resistance, dimensional stability, and processing ability (Bledzki et al. 1998, Clemons 2002). Moreover, NFPC can be made from recycled plastics and the waste part of natural products, thus it can reduce the use of non-biodegradable plastics and make efficient use of natural resources. The wood-like surface also makes this kind of material favorable for construction, decking, railing, and automobile parts.

The polymers used in NFPCs are mainly thermoplastics, such as high and low density polyethylene (HDPE and LDPE), polypropylene (PP), poly (vinyl chloride) (PVC), polystyrene (PS), and polymethylmethacrylate (PMMA) (Jiang and Kamdem 2004a). The natural fibers used to reinforce thermoplastics mainly include wood, cotton, flax, hemp, jute, sisal, and sugarcane fibers (Wollerdorfer and Bader 1998, Bledzki and Gassan 1999, Mohanty et al. 2000).

The application of NFPC in construction raised the requirements of their mechanical properties, especially their creep resistance under constant stress that commonly exists in structural building products. Creep is deformation of material under constant stress, dependent on time, stress, temperature, and material properties, etc. Creep deformation can exceed the creep limit and cause product failure, especially in applications with long-term loading. Understanding, evaluation and prediction of creep behavior of NFPC are thus of great importance for its application (Park and Balatinez 1998).

The creep process of polymeric material can be segregated into four stages: instantaneous deformation, primary creep, secondary creep, and tertiary creep. When a load is applied, the

instantaneous deformation results from the elastic deformation of the material. The instantaneous deformation is followed by the primary creep stage, during which the creep rate starts at a very high value and decreases gradually to a relatively low value. In the secondary creep stage, the viscous flow occurs, and the creep rate remains constant. Finally, the creep goes into the tertiary stage with an increasing creep rate until creep rupture occurs (Yang et al. 2006a).

Since creep measurement requires a relatively long time, creep properties have not been well studied for NFPCs. The limited research has been mainly focused on evaluating creep property and enhancing creep resistance (Sain et al. 2000, Marcovich and Villar 2003, Nunez et al. 2003, Bledzki and Faruk 2004, Acha et al. 2007). It was shown that increasing natural fiber content within an appropriate range enhanced the creep resistance of the composite (Sain et al. 2000, Nunez et al. 2004, Acha et al. 2007). The use of maleated polypropylene (MAPP), a coupling agent, reduced the creep deformation of natural fiber/PP composites by better dispersing natural fibers in PP and improving interfacial adhesion (Bledzki and Faruk 2004, Nunez et al. 2004, Acha et al. 2007). Sain et al. reported that maleated polypropylene modification of wood fiber decreased the creep rate of wood fiber/PP composite, although there was no obvious effect on the instantaneous deformation (Sain et al. 2000). However, Nunez et al. found that esterifying wood fiber with maleic anhydride (MAN) increased the creep of PP/wood composite (Nunez et al. 2003). Esterifying jute fiber with alkenyl succinic anhydride also increased the creep deformation in a jute/PP composite. (Acha et al. 2007).

Modeling techniques have been applied to analyze and evaluate the creep behavior of composites. Although recovery curves were presented in some research, no analysis has been made for this relaxation stage (Acha et al. 2007). Among the different models for the creep process, the 4-element Burgers model was widely adopted and the parameters of this model were

used to characterize the viscoelastic behavior of the materials (Marcovich and Villar 2003, Nunez et al. 2004, Acha et al. 2007). Other models, such as Findley's power law type (Jiang et al. 2007) and a simpler two-parameter power law type (Tajvidi et al. 2005), also attempted to simulate the creep curves of NFPCs. In these efforts, the 4-element Burgers model fitted the curves but the parameters failed to predict long-term creep deformation. Findley's model offered a better prediction though the parameters of this model are not as interpretable as those from Burgers model (Yang et al. 2006a). Time-temperature superposition (TTS) has been tried to predict long-term creep deformation of NFPCs from the short-term experimental data at different temperature levels (Acha et al. 2007). Though smooth master curves were obtained, various NFPCs have been shown to be thermorheologically complex and their long-term creep performance cannot be predicted by TTS through a single horizontal shift (Nunez et al. 2004, Tajvidi et al. 2005). Thus, a systematic study of creep behavior for NFPCs is highly needed.

1.2 OBJECTIVES

The objectives of the research described in this work were:

- 1) To evaluate creep models for different applications, i.e., comparison, characterization, and prediction;
- 2) To develop creep models suitable for comparison, characterization and prediction of creep in NFPCs;
- 3) To predict long-term creep behavior of NFPCs through accelerated testing; and
- 4) To apply the developed techniques to investigate creep behaviors of various systems aimed to improve the overall properties of NFPCs.

1.3 ORGANIZATION OF DISSERTATION

Chapter 1 provides an overall introduction of this research and the structure of this dissertation.

Chapter 2 presents investigation on several PVC composites enhanced with different natural fibers, including bagasse, rice straw, rice husk, and pine, in comparison with virgin PVC in terms of mechanical and thermal properties.

Chapter 3 shows the study on composites of different polymers (recycled PVC, virgin PVC, recycled PE, virgin PE) reinforced by bagasse fiber, with commercial wood/HDPE composite as a control. Creep analysis methods were developed in this chapter and applied in the later parts of this dissertation.

Chapter 4 discusses the effect of coupling agents and bamboo flour loading on creep property of HDPE/bamboo composite system.

Chapter 5 presents creep behavior of HDPE composites enhanced with engineering plastic microfibrils.

Chapter 6 shows the effect of ultra-high molecular weight polyethylene (UHMWPE) on the properties of wood/HDPE composite by combining superior impact strength of UHMWPE and satisfactory creep resistance from natural fibers. The effect of UVA on composite properties and weathering was also discussed in this chapter.

Chapter 7 provides overall conclusions of this dissertation.

1.4 REFERENCES

Acha, B. A., M. M. Reboledo, and N. E. Marcovich. 2007. Creep and dynamic mechanical behavior of PP-jute composites: Effect of the interfacial adhesion. *Composites Part a-Applied Science and Manufacturing* **38**:1507-1516.

- Bledzki, A. K. and O. Faruk. 2004. Creep and impact properties of wood fibre-polypropylene composites: influence of temperature and moisture content. *Composites Science and Technology* **64**:693-700.
- Bledzki, A. K. and J. Gassan. 1999. Composites reinforced with cellulose based fibres. *Progress in Polymer Science* **24**:221-274.
- Bledzki, A. K., S. Reihmane, and J. Gassan. 1998. Thermoplastics reinforced with wood fillers: A literature review. *Polymer-Plastics Technology and Engineering* **37**:451-468.
- Clemons, C. 2002. Wood-plastic composites in the United States - The interfacing of two industries. *Forest Products Journal* **52**:10-18.
- Jiang, H. and D. P. Kamdem. 2004. Development of poly(vinyl chloride)/wood composites. A literature review. *Journal of Vinyl and Additive Technology* **10**:59-69.
- Jiang, L., M. P. Wolcott, J. W. Zhang, and K. Englund. 2007. Flexural properties of surface reinforced wood/plastic deck board. *Polymer Engineering and Science* **47**:281-288.
- Marcovich, N. E. and M. A. Villar. 2003. Thermal and mechanical characterization of linear low density polyethylene/wood flour composites. *Journal of Applied Polymer Science* **90**:2775-2784.
- Mohanty, A. K., M. Misra, and G. Hinrichsen. 2000. Biofibres, biodegradable polymers and biocomposites: An overview. *Macromolecular Materials and Engineering* **276**:1-24.
- Nunez, A. J., N. E. Marcovich, and M. I. Aranguren. 2004. Analysis of the creep behavior of polypropylene-woodflour composites. *Polymer Engineering and Science* **44**:1594-1603.
- Nunez, A. J., P. C. Sturm, J. M. Kenny, M. I. Aranguren, N. E. Marcovich, and M. M. Reboredo. 2003. Mechanical characterization of polypropylene-wood flour composites. *Journal of Applied Polymer Science* **88**:1420-1428.
- Park, B. D. and J. J. Balatinecz. 1998. Short term flexural creep behavior of wood-fiber/polypropylene composites. *Polymer Composites* **19**:377-382.
- Sain, M. M., J. Balatinecz, and S. Law. 2000. Creep fatigue in engineered wood fiber and plastic compositions. *Journal of Applied Polymer Science* **77**:260-268.
- Tajvidi, M., R. H. Falk, and J. C. Hermanson. 2005. Time-temperature superposition principle applied to a kenaf-fiber/high-density polyethylene composite. *Journal of Applied Polymer Science* **97**:1995-2004.
- Wollerdorfer, M. and H. Bader. 1998. Influence of natural fibres on the mechanical properties of biodegradable polymers. *Industrial Crops and Products* **8**:105-112.
- Yang, J. L., Z. Zhang, A. K. Schlarb, and K. Friedrich. 2006. On the characterization of tensile creep resistance of polyamide 66 nanocomposites. Part I. Experimental results and general discussions. *Polymer* **47**:2791-2801.

CHAPTER 2 NATURAL FIBER REINFORCED POLY(VINYL CHLORIDE) COMPOSITES: EFFECT OF FIBER TYPE AND IMPACT MODIFIER¹

2.1 INTRODUCTION

Poly(vinyl chloride) (PVC) is one of the most commonly used plastics in our society. Its main applications include pipes, electric wires, window profiles, siding, etc. Recently, wood fiber reinforced PVC is becoming more popular because of its acceptable mechanical properties, moisture and fungus resistance, long lifetime, wood-like surface performance, and recyclability (Clemons 2002). Some weakness of this material including low impact strength and thermal stability imposes restriction on its application, which signals need for additional research on this important product.

Incorporation of wood fiber in a plastic matrix can enhance the modulus of the resulting composites, but decreases impact strength at the same time (Selke and Wichman 2004). Considering the relative low impact resistance of the neat PVC matrix, it is of more practical significance to improve the impact strength for PVC/natural fiber composites. Current research in this field has been mainly focused on adding impact modifiers and using coupling agents to improve composite properties. Coupling agents have been studied for PVC/natural fiber composites to improve their overall properties (Maldas and Kokta 1989, Jiang and Kamdem 2004b). Maleated polypropylene was shown to be able to improve shear strength of PVC/wood composites by 20% (Lu et al. 2002). Some organic acids were used to increase tensile modulus for PVC/wood fiber composites, but there was no effect on tensile strength and impact strength (Kokta et al. 1990). Coupling effectiveness of silane relied on both dispersion solvents and interfacial reaction initiators (Bledzki et al. 1998). Few of these coupling agents significantly

¹ Reprinted in part with permission from Journal of Polymers and the Environment. Xu, Y.; Wu, Q.; Lei, Y.; Yao, F.; Zhang, Q., Natural Fiber Reinforced Poly(vinyl chloride) Composites: Effect of Fiber Type and Impact Modifier. *Journal of Polymers and the Environment* **2008**, 16, (4), 250-257.

improved the impact strength of PVC composites. Using a coupling agent to reduce the hydrophilic property of wood fiber is not effective for enhancing the adhesion between PVC and wood fiber (Shah et al. 2005). Some commonly used impact modifiers for PVC, such as chlorinated polyethylene, ethylene vinyl acetate, methacrylate-butadiene-styrene, and all-acrylic elastomer, were proved to be also effective in PVC/wood composites (Mengeloglu et al. 2000). However, some other widespread impact modifiers for polymers and polymer blends, such as styrene-ethylene-butylene-styrene (SEBS), have not been used in PVC/natural fiber composites. SEBS proved to be able to improve the impact strength of the polymer blends (Schwarz et al. 1988, Hong and Jo 2000), but no work has been reported on its effect in PVC/natural fiber composites.

Beside mechanical properties, water resistance and thermal stability are also important for PVC/natural fiber composites. PVC resin shows relatively high water absorption compared with polyolefin. With the existence of hydrophilic natural fibers, PVC/ natural fiber composites tend to have higher water absorption rate than pure PVC, which further affects mechanical properties and structural stability of the composites (Sombatsompop and Chaochanchaikul 2004). As a weak point of both of PVC resin and natural fibers, their thermal stability and degradation mechanisms have been investigated with kinetic analysis of thermogravimetric data (Jimenez et al. 1993, Wu and Dollimore 1998). Combining the two components, thermal stability of PVC/natural fibers composites was investigated, but no kinetic analysis has been reported (Ge et al. 2004).

There are a large variety of natural fibers such as rice straw, rice husk, palm, bagasse, hemp, flax, and other agricultural residues (Ayora et al. 1997, Sombatsompop et al. 2003, Jiang and Kamdem 2004a). These cheap natural fibers are normally made from waste part of the

products. As different natural fibers have different chemical compositions, physical structures, and mechanical properties, variation of properties can be expected from the composites of different natural fibers (Bledzki and Gassan 1999). Little effort has been made so far to prepare non-wood fiber (e.g., agricultural fibers) reinforced PVC composites and to improve their properties. With increased wood costs and competition of wood resources from traditional wood sectors, developing alternative, cheap, and environmentally friendly natural fiber sources for plastic composite is highly needed.

In this study, three types of agricultural fibers (bagasse, rice straw, and rice husk) and one wood fiber (pine) were used to prepare PVC composites through compression molding. SEBS was used as an impact modifier. The objectives of this study were to investigate the influence of fiber type and SEBS loading level on mechanical properties, thermal stability, and water resistance of the composites.

2.2 EXPERIMENTAL

2.2.1 Raw Materials

PVC SE-450 was obtained from Shintech, Inc. (Plaquemine, LA), with a bulk density of 612.7 kg/m³ and inherent viscosity of 0.515. SEBS G1650M was obtained from Kraton Polymers LLC (Houston, TX), with a styrene/rubber ratio of 30/70 and specific gravity of 0.91. The thermal stabilizer used was Mark 1900, from Chemtura Corporation (Middlebury, CT), with specific gravity of 1.1768 and 19.5% Tin. Natural fibers included bagasse (sugarcane residue), rice straw, rice husk, and wood fiber (pine).

Pine fiber was purchased from American Wood Fibers Co. (Schofield, WI), with a nominal particle size of 20-mesh. Bagasse fiber was obtained from a local sugar mill in Louisiana. Rice husk and rice-straw were obtained from Louisiana State University (LSU)

AgCenter's Crowley Rice Research Station in Crowley, LA. These raw materials were oven-dried at 95 °C for 24 hours to reduce moisture content to the level of about 2%. The oven-dry material was ground with a Thomas-Wiley miller (Model 3383L10, Swedesboro, NJ) to pass through a 20-mesh screen, and the fibers were stored in sealed plastic bags prior to compounding.

2.2.2 Composite Preparation

Experimental design included four natural fibers (bagasse, rice straw, rice husk, and pine), one fiber/PVC loading rate (weight ratio=30/70), one thermal stabilizer/PVC loading rate (1.5%), and three levels of SEBS (0%, 2.5%, and 5%). Pure PVC blend was used as control. This gave a total of 13 blends.

The PVC/natural fiber composites were prepared as follows. Based on the formulations, weighed amount of neat PVC, thermal stabilizer and SEBS were first mixed with each of the four fibers in a K-mixer at 4800 rpm from room temperature to 196-202 °C. The blended material from K-mixing for each formulation was then cooled and granulated. Prior to sample manufacturing, each blend was re-mixed with a Haake rheometer (Rheomix 600) at 60 rpm and 180 °C for 10 minutes to provide more uniform fiber distribution.

The blends were then used to make test sample plates through compression molding (Wabash V200) at 190 °C with a pressure of 30 tons. The nominal thickness was 1 mm for tensile strength and dynamic mechanical analysis (DMA) samples; while the nominal thickness was 4 mm for impact strength, water absorption (WA), and thickness swelling (TS) test samples.

2.2.3 Measurements

- **Mechanical Properties.** Dynamic mechanical analysis (DMA) was carried out for all composites and neat PVC with a TA Q800 DMA system (New Castle, DE). Specimens with a nominal size of 60×12×1 mm were cut from the compression molded plates and two DMA

procedures were employed. One was with a dual cantilever mode at a frequency of 1 Hz at room temperature, from which the storage modulus of each specimen was measured. The second DMA was also with a dual cantilever mode at a frequency of 1 Hz, but with temperature ramped from 40 to 105 °C. From the second DMA, the relationship between modulus (storage modulus E' and loss modulus E'') and temperature for each specimen was determined. The peak temperature of loss modulus was taken as glass transition temperature (T_g) of these composites in this study.

The tensile strength was measured according to ASTM D 638-03, using a Model 1125 INSTRON machine (Boston, MA). Specimens with a nominal size of 60×12×1 mm were cut from the compression molded plates. For each treatment level, six replications were used.

Izod impact tests were done on a TINIUS OLSEN 892T impact tester (Testing Machine Company, Horsham, PA). Specimens with a nominal size of 60×12×4 mm were cut from the compression molded plates and were then notched on the center of one longitudinal side according to the ASTM D256. For each treatment level, six samples were tested.

- **Thermal Stability.** Thermogravimetric analysis (TGA) was employed to observe the thermal stability characteristics of composites with a TA Q50 Thermogravimetric Analyzer (New Castle, DE) under a nitrogen atmosphere. Two TGA methods were used for each treatment level: dynamic TGA at a scan rate of 10 °C/min from room temperature to 650 °C and isothermal TGA at different constant temperatures over a period of 120 to 300 minutes. Dynamic TGA mode was employed first to determine degradation temperature (T_d) of the composites based on the plot of sample weight versus temperature. Isothermal TGA mode was carried out at 4 different temperatures (240, 250, 260, and 270 °C) for the composites and 5 different temperatures (260, 265, 270, 275, and 280 °C) for the neat PVC. These temperatures were

slightly higher than their corresponding T_d and were kept constant during the experiment. For each run, 6-10 mg specimen was tested.

In dynamic TGA, weight change during temperature increase was recorded, and the values of T_d for each treatment level were determined. In isothermal TGA, the time for a certain percent of weight change was recorded. The data was modeled with a first order thermal kinetic model to determine the kinetic parameters (i.e., activation energy, E_a and pre-exponential factor, A) (Dollimore 1992, Vrandecic et al. 2005):

$$\ln t = E_a / RT + \ln[g(\alpha) / A] \quad (2.1)$$

where, t , E_a and T denote time, activation energy and temperature; α is degree of conversion; R is the gas constant. The first order model for thermal degradation, $g(\alpha)$, has the following form:

$$g(\alpha) = -\ln(1 - \alpha) \quad (2.2)$$

with conversion rate expressed as:

$$\alpha = \frac{(x_0 - x)}{(x_0 - x_1)} \quad (2.3)$$

where, x_0 , x , and x_1 denote initial, actual and final weight of specimen respectively. Based on Eq. (2.1), the dependence of $\ln t$ versus $1/RT$ was plotted, from which E_a at a given conversion rate was determined from the slope.

- Water absorption and thickness swelling. Water absorption (WA) and thickness swelling (TS) rates of the composite were tested by measuring the weight and thickness increase of specimens after being immersed in water for 1, 2, 3, and 4 weeks, respectively. Specimens with a nominal size of 60×12×4 mm were cut from the compression molded plates. The thickness and weight of these specimens were measured after initial drying to reach a constant weight at 80 °C.

They were then immersed in water for 4 weeks. The specimens were removed from water at the end of each week and conditioned for one hour. The thickness and weight of the conditioned specimens were measured. WA and TS were calculated as:

$$WA (\%) = \frac{WT - WT_o}{WT_o} \times 100 \% \quad (2.4)$$

$$TS (\%) = \frac{TK - TK_o}{TK_o} \times 100 \% \quad (2.5)$$

where WT (g) and TK (mm) are the weight and thickness at a given time, and WT_o (g) and TK_o (mm) are the initial weight and thickness, respectively.

- Data Analysis. Measured data on mechanical, thermal, and physical properties of composites were analyzed with a two-way analysis of variance (ANOVA) test in Statistical Analysis System (SAS) to determine treatment effect at the 5% significance level.

2.3 RESULTS AND DISCUSSION

2.3.1 Mechanical Properties

Storage moduli of the four types of PVC/natural fiber composites are shown in Figure 2.1(a). As shown, the addition of natural fibers increased storage modulus of PVC by up to 50% level. It is plausible that the stiff natural fibers contributed to overall stiffness of the composites. Among the composites, PVC/bagasse composite presented the highest storage modulus at 0% and 2.5% SEBS level. On the other hand, with the addition of SEBS, storage moduli of all four composites decreased, especially for PVC/bagasse composite, whose storage moduli decreased by more than 20% at the SEBS concentration of 5%. The existence of low-modulus SEBS might increase the flexibility of the composites under stress and reduce their moduli.

Tensile strengths of PVC/natural fiber composites are shown in Figure 2.1(b), and two-way ANOVA test results are shown in Table 2.1. As shown in Figure 2.1(b), the addition of four

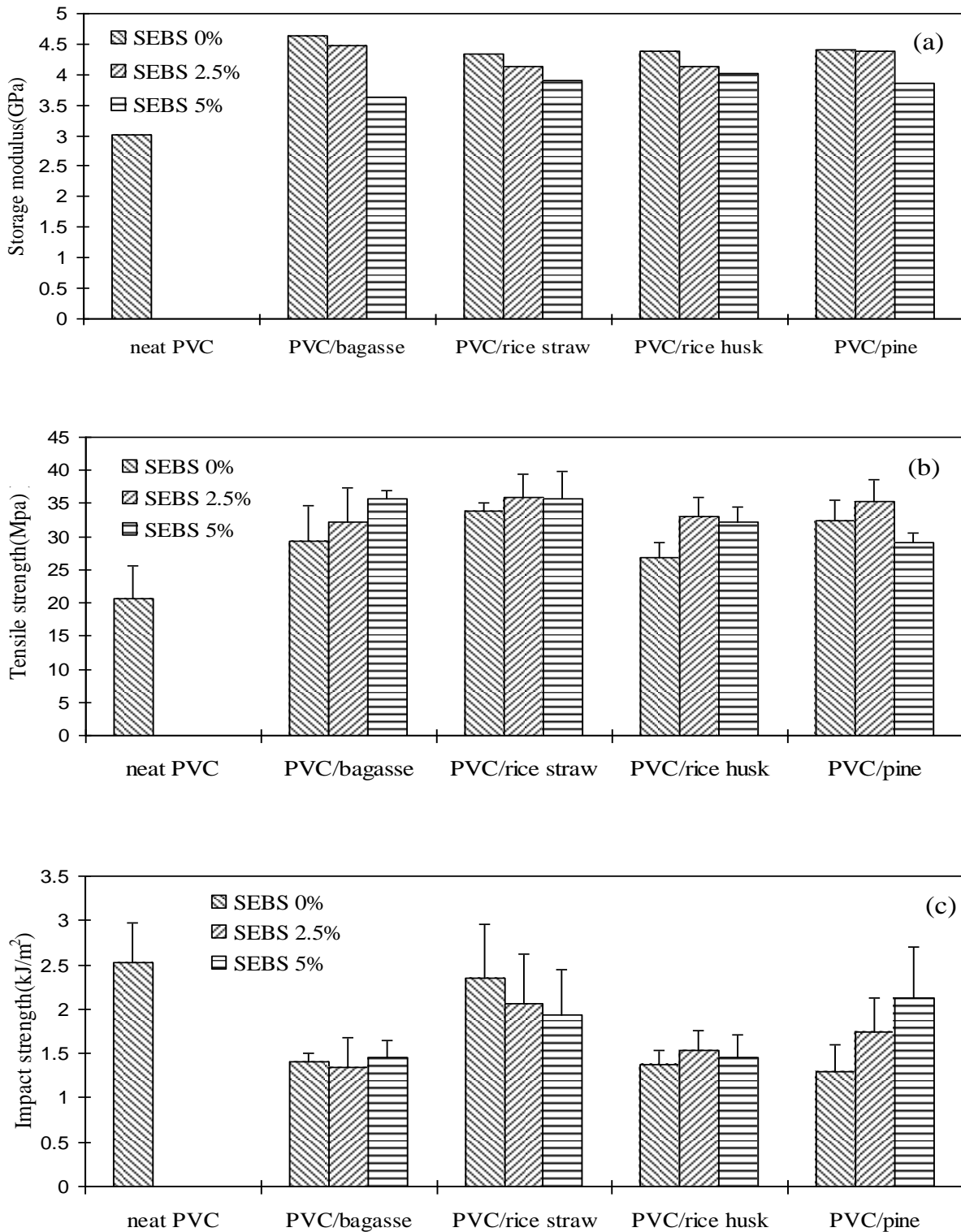


Figure 2.1 Storage modulus (a), tensile strength (b), and impact strength (c) of four PVC/natural fiber composites with different levels (0%, 2.5%, and 5%) of SEBS. Error bar represents Standard Deviation.

kinds of natural fibers increased the tensile strength of PVC by 30%-60%. During the tensile deformation of composites, the applied stress was partially transferred to strong natural fibers, especially those in the direction of elongation. Among the four composites, PVC/rice straw composites showed the highest tensile strength. The increase in the content of SEBS led to enhancement in tensile strength of most composites. For PVC/pine composites, tensile strength of the composites decreased as SEBS content increased from 2.5% to 5%. This difference suggests that for different PVC/natural fiber composites, the optimum SEBS contents are different. Higher content of SEBS may impair the tensile strength of the PVC matrix, so as to decrease the tensile strength of the composites. As indicated in Table 2.1, both fiber type and SEBS level had influence on the tensile strength of the composites.

Impact strengths of the four types of PVC/natural fiber composites are shown in Figure 2.1(c); and two-way ANOVA test results are shown in Table 2.1. Based on Table 2.1, natural fiber type showed significant influence on impact strength of the composites. As shown in Figure 2.1(c), the addition of all four types of natural fibers decreased the impact strength of the PVC matrix. This negative effect may be ascribed to the reduction of polymer matrix content and poor compatibility between the fiber and polymer matrix. Comparatively, rice straw offered superior impact property to the other three kinds of natural fibers. SEBS had no obvious effect on impact strength of PVC/bagasse composites and PVC/rice husk composites, as shown in Figure 2.1. For PVC/pine composites, impact strength increased as SEBS content increased from 0% up to 5%. However, for PVC/rice straw composites, addition of SEBS led to a slight decrease of impact strength. The different trends reflect the different interactions among the components of the four composites. A possible reason is the chemical composition of the natural fibers. Among the natural fibers, pine fiber has the highest content (26-34%) of lignin (Bledzki et al. 2002), which

is more hydrophobic than the other components (cellulose and hemicellulose) of natural fibers, so that SEBS is more compatible with pine fiber than with the other natural fibers. Contrastively, rice straw has the lowest lignin content (8-19%) (Jackson 1977). In general, SEBS with the content up to 5% showed little effect as an impact modifier for PVC/natural fiber composites.

Table 2.1 Two-way ANOVA test on the influence of fiber type and SEBS level on tensile and impact strength of the composites

Variable	Tensile strength	Impact strength
Fiber type	0.0016	<0.0001
SEBS level	0.0017	0.4971
Fiber type × SEBS level	0.0062	0.0223

The values shown in this table are p-values of the two-way ANOVA tests. A p-value smaller than 0.05 indicates significant influence of the corresponding treatment on the corresponding property at the 5% significance level.

2.3.2 Glass Transition Temperature

The influence of different natural fibers and different levels of SEBS on T_g of the PVC/natural fiber composites is presented in Table 2.2. The addition of natural fibers shifted T_g of PVC for up to 1.5 °C. This trend may be attributed to the fact that the presence of stiff natural fibers in PVC matrix made segments of PVC molecular chains more difficult to move and thus glass transition occurred at higher temperatures. Pine fiber showed less effect, and the reason may be related to the interface between PVC matrix and pine fiber, which will be investigated in the follow-up research on coupling agents.

As shown in Table 2.2, the addition of SEBS slightly increased T_g of all the four kinds of PVC/natural fiber composites. This may give evidence that SEBS had slight effect on the interface of PVC matrix and natural fibers, which corresponds to the aforementioned effect on tensile strength. However, these increments may not be significant considering the experimental errors resulting from the sample preparation and experimental tests.

Table 2.2 Glass transition temperature (T_g) and degradation temperature (T_d) of PVC/natural fiber composites

Composite type	0%SEBS		2.5%SEBS		5%SEBS	
	T_g (°C)	T_d (°C) ^a	T_g (°C)	T_d (°C)	T_g (°C)	T_d (°C)
Neat PVC	78.8	264.9	-	-	-	-
PVC/bagasse	79.8	209.1	80.5	213.1	80.8	212.2
PVC/rice straw	80.2	211.3	81.2	214.6	81.3	217.1
PVC/rice husk	80.2	217.5	80.7	211.5	80.7	216.9
PVC/pine	79.0	213.6	79.6	215.0	79.9	214.8

^a Onset temperature of derivative weight was taken as T_d .

2.3.3 Thermal Stability

The dynamic TGA curves for PVC/natural fiber composites and neat PVC without SEBS are plotted in Figure 2.2. From the curves, the onset temperature of degradation decreased when natural fibers were added to neat PVC. However, PVC/natural fiber composites reached the highest degradation speed at higher temperatures than neat PVC. Based on these phenomena, it might be concluded that natural fiber had a lower onset temperature of degradation, but a lower degradation speed than neat PVC. This difference corresponds to the sharp degradation peak of neat PVC and relatively broad degradation peak of PVC/natural fiber composites. It might be due to the different degradation mechanisms of neat PVC and natural fibers: HCl released from degradation (dehydrochlorination) of PVC can hasten this process by inducing further degradation and result in self-accelerating degradation (Marongiu et al. 2003); however, the degradation of natural fibers follows a different two-stage process with the low-temperature stage from degradation of hemicellulose and the high-temperature stage from degradation of lignin (Saheb and Jog 1999).

To better illustrate the dynamic TGA curves, onset temperatures of the derivative weight were taken as T_d and listed in Table 2.2. From the table, T_d of the composites were comparatively lower than that of neat PVC, but there was no obvious difference between different composites.

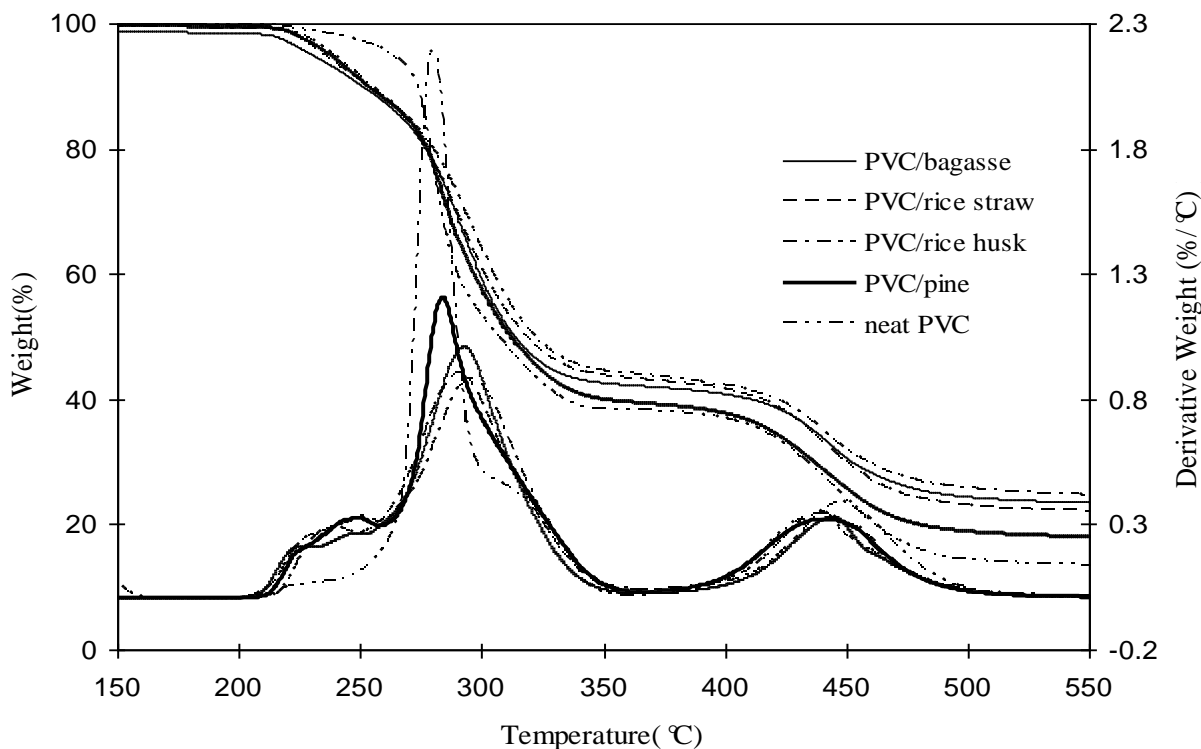


Figure 2.2 Dynamic TGA curves of four PVC/natural fiber composites without SEBS.

Figure 2.3 shows isothermal TGA curves of four PVC/natural fiber composites and neat PVC without the addition of SEBS at 260 °C for 120 minutes. As shown, there were two obvious degradation peaks for PVC/natural fiber composites. One was sharp and the other one was weak and broad. However, for neat PVC only one main degradation peak was observed. According to the dynamic TGA results, the first peak for PVC/natural fiber composites arose from degradation of natural fibers and the second one from degradation of PVC matrix. From the plot of weight versus time, PVC/natural fiber composites degraded prior to neat PVC at the beginning. After around 4 minutes, neat PVC began to degrade quickly showing a strong peak, which can be ascribed to the self-acceleration of PVC matrix. This peak is much broader and weaker than that of neat PVC. Presumably, the existence of natural fibers in PVC matrix weakened self-degradation of the PVC. This confirmed the results of dynamic TGA analysis.

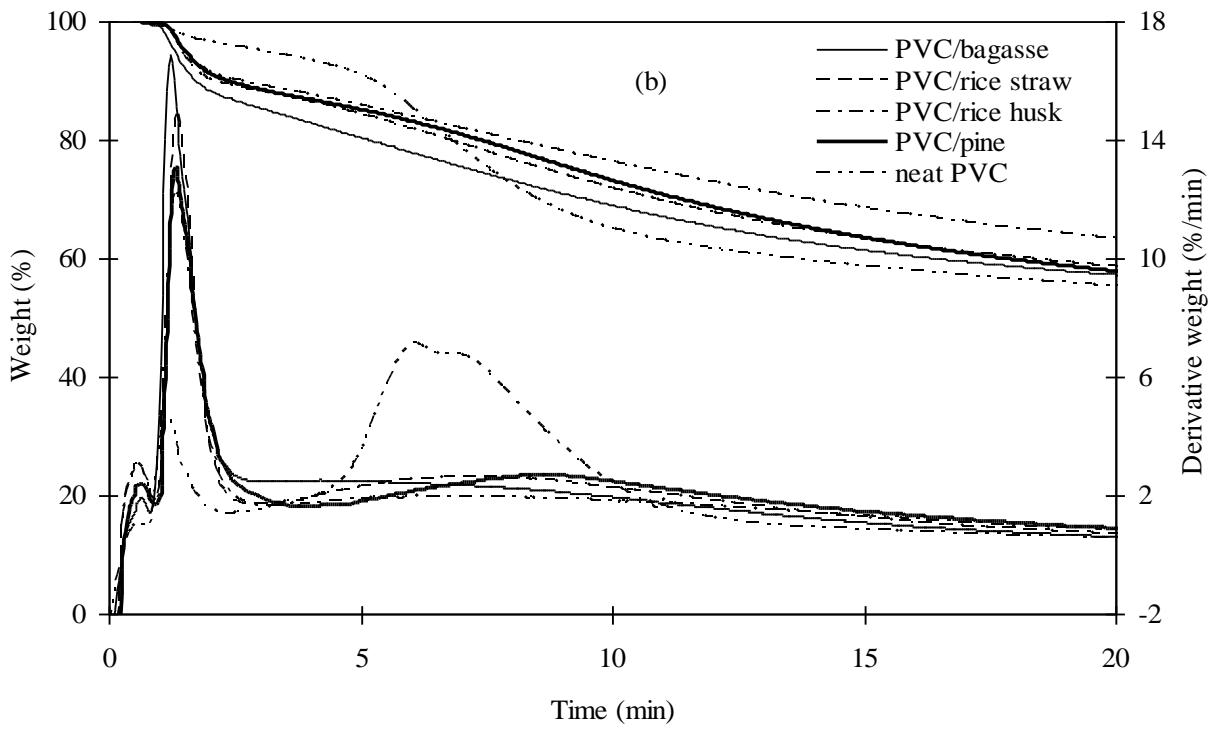
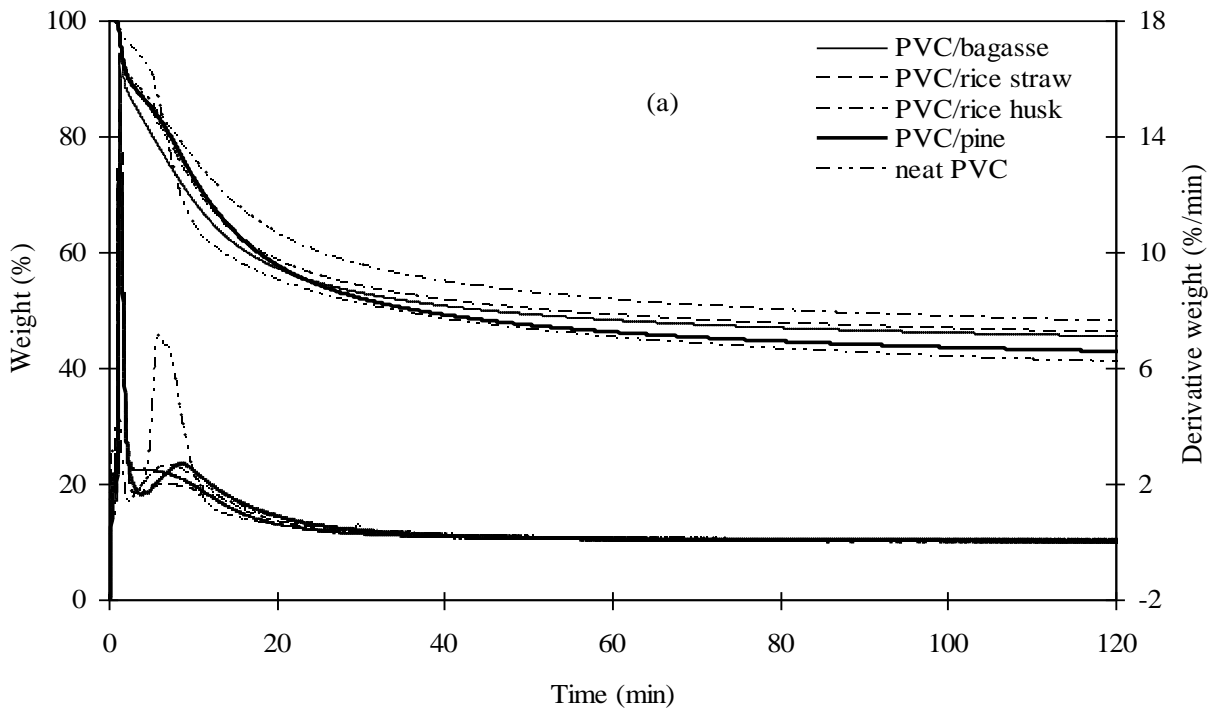


Figure 2.3 Isothermal TGA curves of four PVC/natural fiber composites without SEBS at 260 °C for 120 minutes (a) and for the first 20 minutes (b).

Figure 2.4 shows a typical plot of $[\ln t]$ versus $[1/RT]$ (Eq. (2.1)) for PVC/bagasse composite without SEBS, in which E_a and $\ln A$ were determined in a conversion rate range of 0.5-0.9. The average data are listed in Table 2.3. From the table, all the composites had much lower E_a than neat PVC. Incorporation of natural fibers lowered the thermal stability of PVC/natural fiber composites compared with neat PVC.

2.3.4 Water Absorption (WA) and Thickness Swelling (TS)

Typical WA and TS data as a function of time for all four composites at the 2.5% SEBS level is shown in Figure 2.5(a) and 5(b), respectively. Both WA and TS increased with increase of water soaking time in a nonlinear fashion. The rate of change in both WA and TS decreased as soaking time increased. The maximum TS for bagasse, rice husk, and wood fiber composites was attained after the samples being immersed in water for 2 weeks, but their WA increase continued beyond the first two weeks. Thus, for PVC/natural fiber composites, TS was not linearly proportional to the WA (Figure 2.6).

Test data on WA and TS at the end of the 4-week water soaking is summarized in Table 2.4, and two-way ANOVA test results are shown in Table 2.5. PVC/rice husk composites had the smallest WA and TS after being immersed in water for 4 weeks, as indicated in Table 2.4. On the contrary, PVC/rice straw showed the highest WA and TS. The addition of SEBS increased WA and TS of these composites in the water, but no proportional trends were observed. The ANOVA results (Table 2.5) showed that both fiber type and SEBS level showed significant influence on WA and TS of the composites. There is significant interaction of fiber type and SEBS level on WA, but not on TS.

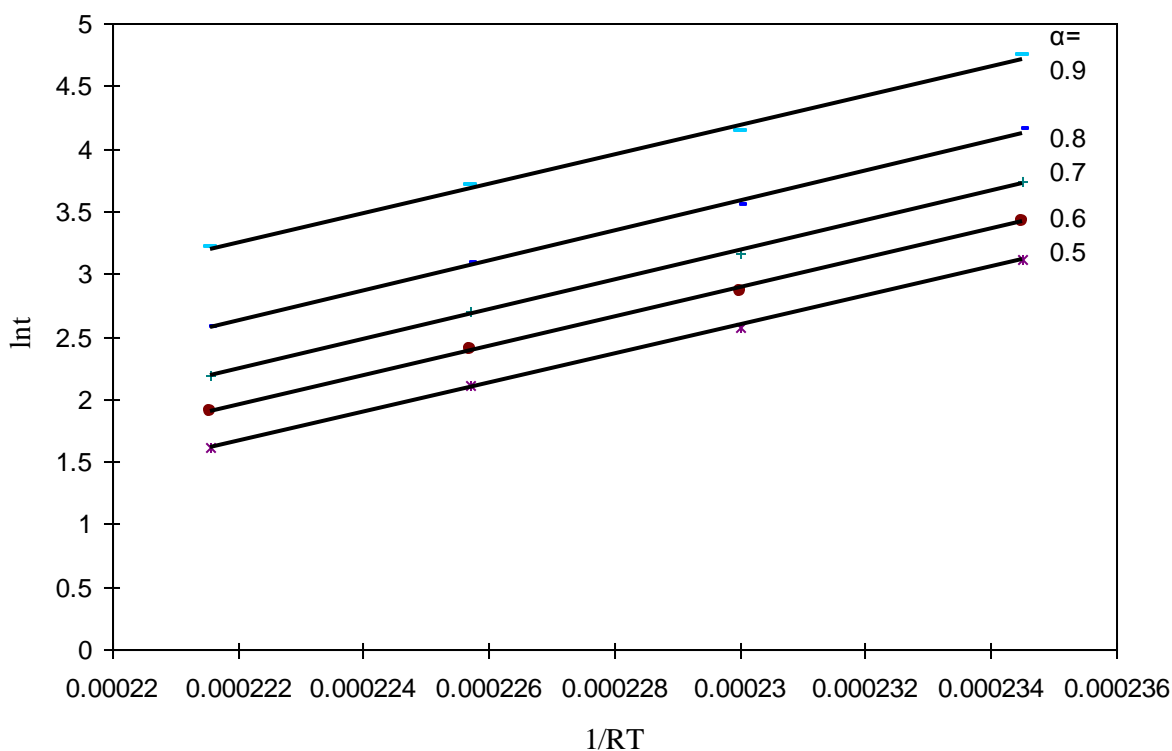


Figure 2.4 Typical plot of $\ln t$ vs. $1/(RT)$ for PVC/bagasse composites without SEBS at different conversion rates.

Table 2.3 Thermal degradation kinetic parameters of PVC/natural fiber composites

Composite Type	0%SEBS		2.5%SEBS		5%SEBS	
	E_a (KJ/mol)	$\ln A^a$	E_a (KJ/mol)	$\ln A$	E_a (KJ/mol)	$\ln A$
Neat PVC	133 (22) ^b	27.10 (4.66)	-	-	-	-
PVC/bagasse	118 (2)	24.00 (0.42)	114 (10)	23.15 (2.11)	122 (5)	25.12 (1.07)
PVC/rice straw	114 (5)	23.14 (1.06)	110 (7)	22.32 (1.42)	111 (9)	22.49 (1.87)
PVC/rice husk	113 (4)	22.60 (0.99)	110 (4)	22.08 (0.96)	122 (5)	24.79 (1.21)
PVC/pine	96 (7)	18.91 (1.41)	117 (6)	23.69 (1.31)	102 (2)	20.24 (0.48)

^a $\ln A$ was calculated based on the first order model.

^b The numbers in the brackets represent standard deviations.

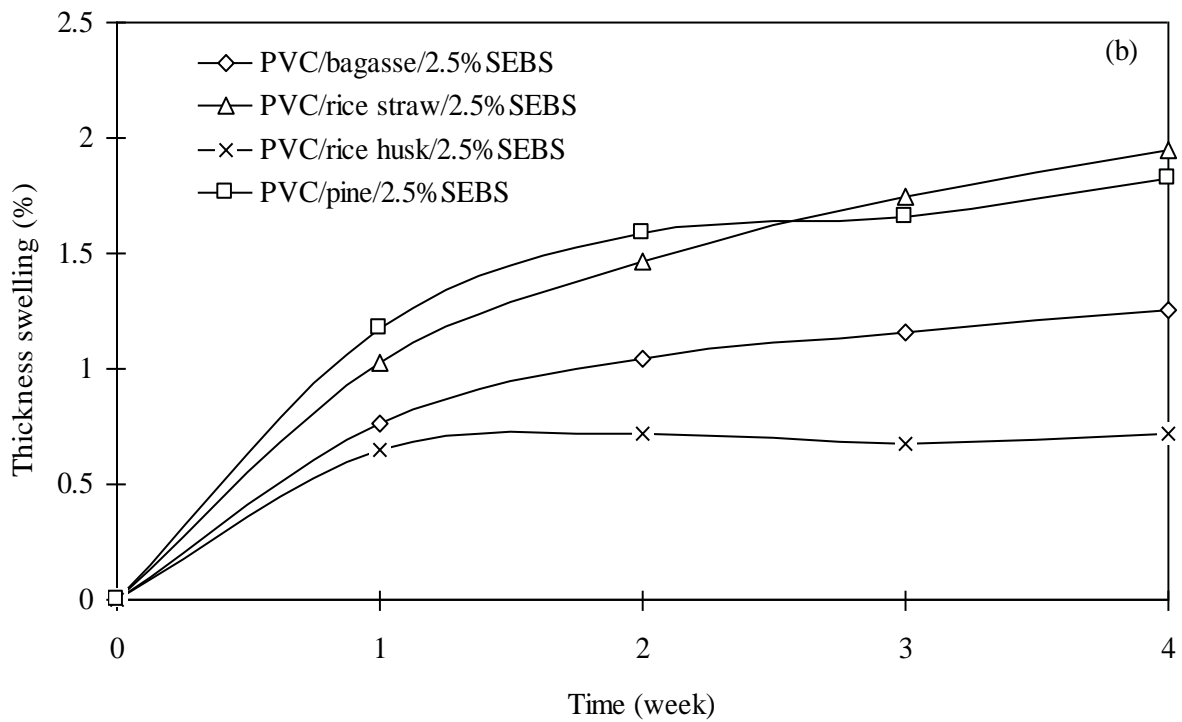
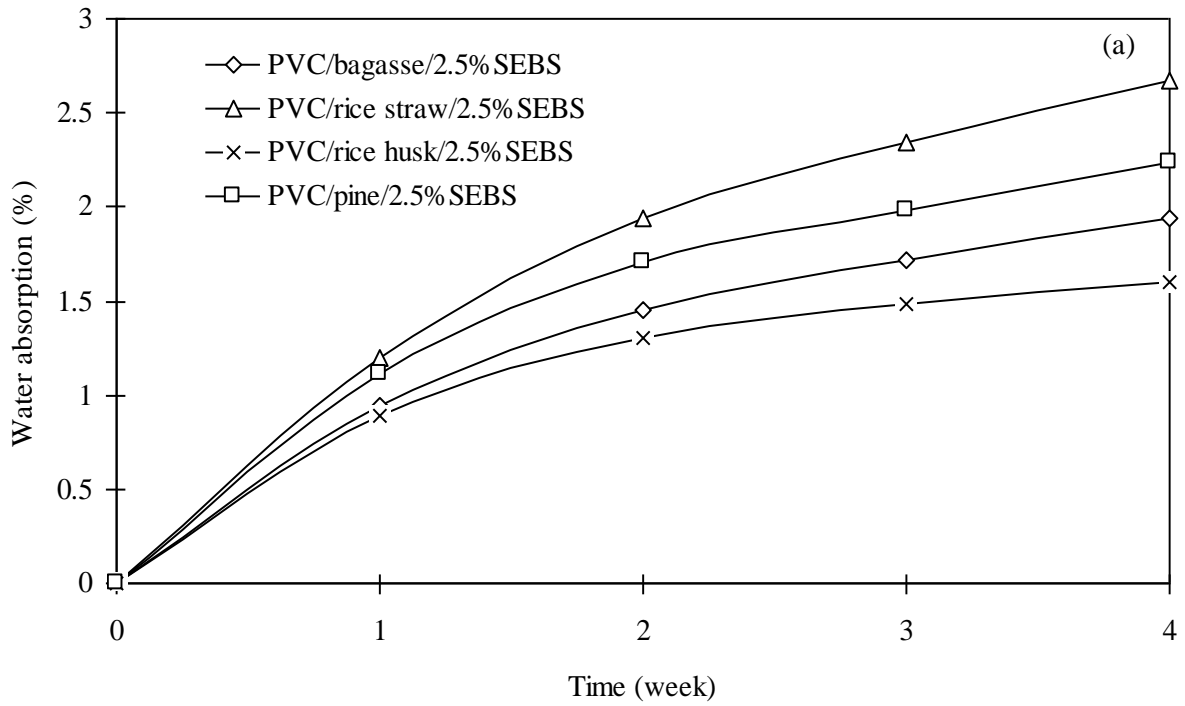


Figure 2.5 Typical WA (a) and TS (b) data as a function of time for four PVC/natural fiber composites with 2.5% SEBS.

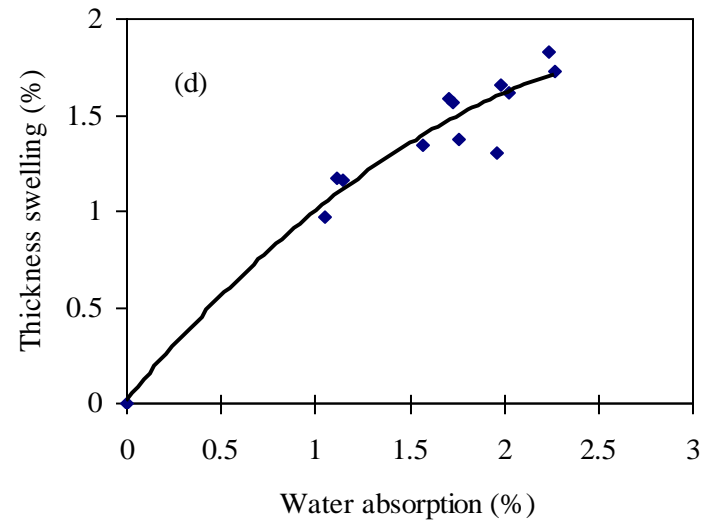
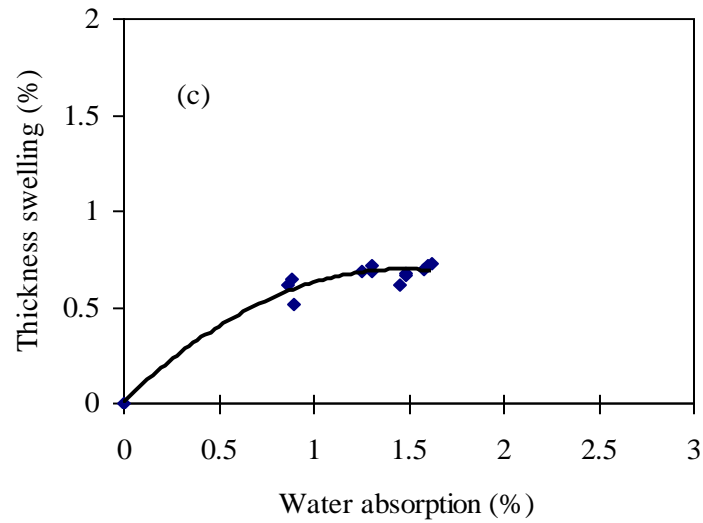
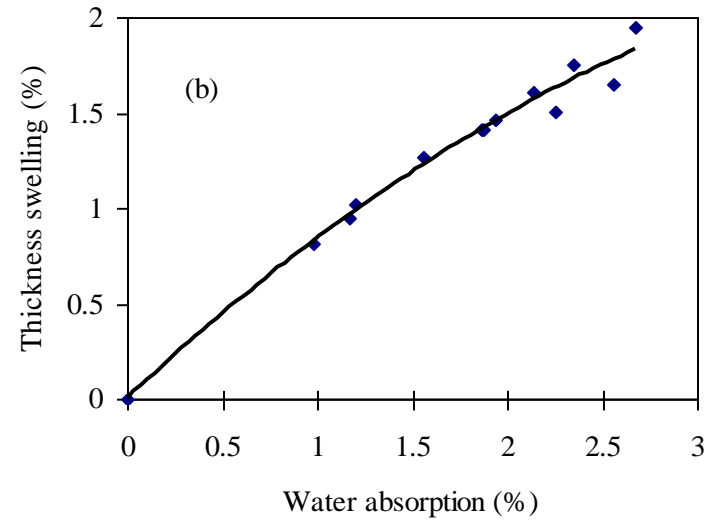
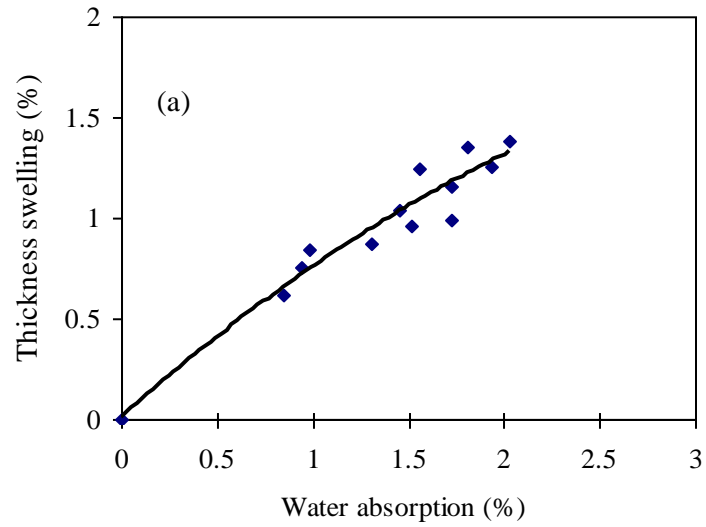


Figure 2.6 TS as a function of WA for PVC/natural fiber composites. (a) PVC/bagasse, (b) PVC/rice straw, (c) PVC/rice husk, and (d) PVC/pine.

Table 2.4 Water absorption rate (%) of PVC/natural fiber composites after being immersed in water for 4 weeks

Composite Type	0%SEBS		2.5%SEBS		5%SEBS	
	WA (%)	TS (%)	WA (%)	TS (%)	WA (%)	TS (%)
PVC/bagasse	1.73(0.03) ^a	0.99(0.09)	1.94(0.09)	1.25(0.23)	2.03(0.10)	1.38(0.29)
PVC/rice straw	2.14(0.09)	1.61(0.25)	2.67(0.10)	1.95(0.37)	2.55(0.14)	1.65(0.63)
PVC/rice husk	1.62(0.03)	0.73(0.13)	1.60(0.05)	0.72(0.21)	1.58(0.07)	0.69(0.18)
PVC/pine	1.97(0.20)	1.31(0.21)	2.23(0.12)	1.83(0.25)	2.27(0.12)	1.73(0.10)

^a The numbers in the brackets represent standard deviations.

Table 2.5 Two-way ANOVA test on the influence of natural fiber type and SEBS level on WA and TS after being immersed in water for four weeks

Variables	WA	TS
Fiber type	<0.0001	<0.0001
SEBS level	<0.0001	0.0034
Fiber type × SEBS level	<0.0001	0.1275

The values shown in this table are p-values of the two-way ANOVA tests. A p-value smaller than 0.05 indicates significant influence of the corresponding treatment on the corresponding property at the 5% significance level.

2.4 CONCLUSIONS

Among the four natural fibers used, rice straw offered better mechanical properties than bagasse, rice husk, or pine. SEBS showed a moderate effect on the tensile strength of PVC/natural fiber composites, but no obvious contributions to impact strength of the composites were observed. For different PVC/natural fiber systems, different SEBS levels should be employed to optimize mechanical properties.

The addition of natural fibers decreased the thermal stability of neat PVC, but also weakened the self-accelerating effect during degradation of PVC. SEBS had little effect on the thermal stability of the composites. PVC/rice husk composites showed lower water absorption rate and better dimensional stability in water than the other three types of composites. The addition of SEBS increased the water absorption rate of PVC/natural fiber composites. Thickness

swelling varied nonlinearly with water absorption rate. The results of the study demonstrate that PVC composites filled with agricultural fibers (i.e., bagasse, rice straw, and rice husk) had properties comparable with those of PVC/wood composite. Future work will deal with effective coupling agents for PVC (virgin and recycled) and natural fibers.

2.5 REFERENCES

Ayora, M., R. Rios, Jafet Quijano, and Alfredo Marquez. 1997. Evaluation by torque-rheometer of suspensions of semi-rigid and flexible natural fibers in a matrix of poly(vinyl chloride). *Polymer Composites* **18**:549-560.

Bledzki, A. K. and J. Gassan. 1999. Composites reinforced with cellulose based fibres. *Progress in Polymer Science* **24**:221-274.

Bledzki, A. K., S. Reihmane, and J. Gassan. 1998. Thermoplastics reinforced with wood fillers: A literature review. *Polymer-Plastics Technology and Engineering* **37**:451-468.

Bledzki, A. K., V. E. Sperber, and O. Faruk. 2002. Natural and Wood Fibre Reinforcement in Polymers. *Rapra Review Reports* **13**:10.

Clemons, C. 2002. Wood-plastic composites in the United States - The interfacing of two industries. *Forest Products Journal* **52**:10-18.

Dollimore, D. 1992. The application of thermal analysis in studying the thermal decomposition of solids. *Thermochimica Acta* **203**:7-23.

Ge, X. C., X. H. Li, and Y. Z. Meng. 2004. Tensile properties, morphology, and thermal behavior of PVC composites containing pine flour and bamboo flour. *Journal of Applied Polymer Science* **93**:1804-1811.

Hong, B. K. and W. H. Jo. 2000. Effects of molecular weight of SEBS triblock copolymer on the morphology, impact strength, and rheological property of syndiotactic polystyrene/ethylene-propylene rubber blends. *Polymer* **41**:2069-2079.

Jackson, M. G. 1977. Review article: The alkali treatment of straws. *Animal Feed Science and Technology* **2**:105-130.

Jiang, H. and D. P. Kamdem. 2004a. Development of poly(vinyl chloride)/wood composites. A literature review. *Journal of Vinyl and Additive Technology* **10**:59-69.

Jiang, H. and D. P. Kamdem. 2004b. Effects of copper amine treatment on mechanical properties of PVC/wood-flour composites. *Journal of Vinyl and Additive Technology* **10**:70-78.

- Jimenez, A., V. Berenguer, J. Lopez, and A. Sanchez. 1993. Thermal degradation study of poly(vinyl chloride): Kinetic analysis of thermogravimetric data. *Journal of Applied Polymer Science* **50**:1565-1573.
- Kokta, B. V., D. Maldas, C. Daneault, and P. Beland. 1990. Composites of poly(vinyl chloride) and wood fibers. Part II: Effect of chemical treatment. *Polymer Composites* **11**:84-89.
- Lu, J., Q. Wu, and I. Negulescu. 2002. The Influence of Maleation on Polymer Adsorption and Fixation, Wood Surface Wettability, and Interfacial Bonding Strength in Wood-PVC Composites. *Wood and Fiber Science* **34**:434-459.
- Maldas, D. and B. V. Kokta. 1989. Improving adhesion of wood fiber with polystyrene by the chemical treatment of fiber with a coupling agent and the influence on the mechanical properties of composites. *Journal of Adhesion Science and Technology* **3**:529-539.
- Marongiu, A., T. Faravelli, G. Bozzano, M. Dente, and E. Ranzi. 2003. Thermal degradation of poly(vinyl chloride). *Journal of Analytical and Applied Pyrolysis* **70**:519-553.
- Mengeloglu, F., L. M. Matuana, and J. A. King. 2000. Effects of impact modifiers on the properties of rigid PVC/wood-fiber composites. *Journal of Vinyl and Additive Technology* **6**:153-157.
- Saheb, D. N. and J. P. Jog. 1999. Natural fiber polymer composites: A review. *Advances in Polymer Technology* **18**:351-363.
- Schwarz, M. C., J. W. Barlow, and D. R. Paul. 1988. Mechanical properties of HDPE/(PEC/PS)/SEBS blends. *Journal of Applied Polymer Science* **35**:2053-2067.
- Selke, S. E. and I. Wichman. 2004. Wood fiber/polyolefin composites. *Composites Part A: Applied Science and Manufacturing* **35**:321-326.
- Shah, B. L., L. M. Matuana, and P. A. Heiden. 2005. Novel coupling agents for PVC/wood-flour composites. *Journal of Vinyl and Additive Technology* **11**:160-165.
- Sombatsompop, N. and K. Chaochanchaikul. 2004. Effect of moisture content on mechanical properties, thermal and structural stability and extrudate texture of poly(vinyl chloride)/wood sawdust composites. *Polymer International* **53**:1210-1218.
- Sombatsompop, N., K. Chaochanchaikul, C. Phromchirasuk, and S. Thongsang. 2003. Effect of wood sawdust content on rheological and structural changes, and thermo-mechanical properties of PVC/sawdust composites. *Polymer International* **52**:1847-1855.
- Vrandecic, S. N., B. Andricic, I. Klaric, and T. Kovacic. 2005. Kinetics of isothermal thermooxidative degradation of poly(vinyl chloride)/chlorinated polyethylene blends. *Polymer Degradation and Stability* **90**:455-460.
- Wu, Y. and D. Dollimore. 1998. Kinetic studies of thermal degradation of natural cellulosic materials. *Thermochimica Acta* **324**:49-57.

CHAPTER 3 CREEP BEHAVIOR OF BAGASSE FIBER REINFORCED POLYMER COMPOSITES

3.1 INTRODUCTION

Natural fiber/polymer composites (NFPCs) are being increasingly used in construction and their creep behaviors under constant stress are receiving more research interest. One of the main techniques for creep characterization is modeling. The 4-element Burgers model was widely adopted to characterize the viscoelastic behavior of the materials (Marcovich and Villar 2003, Nunez et al. 2004, Acha et al. 2007). Findley's power law model (Jiang et al. 2007) and a simpler two-parameter power law model (Tajvidi et al. 2005) were also attempted to simulate the creep curves of NFPCs. Although recovery curves were presented in some research work, no analysis has been made for this relaxation stage (Acha et al. 2007). Time-temperature superposition (TTS) was tried to predict long-term creep deformation of NFPCs from the accelerated testing data at different temperature levels and smooth master curves were obtained. Some NFPCs, however, have been shown to be thermorheologically complex and TTS cannot be applied to predict their long-term creep curves through a single horizontal shift (Nunez et al. 2004, Tajvidi et al. 2005).

Bagasse fibers are a by-product of sugar-cane processing. The composition of bagasse is approximately 50% cellulose, 25% hemicellulose, and 25% lignin (Pandey et al. 2000). In comparison with other agricultural residues, bagasse is regarded as a rich natural resource due to high yield and annual regeneration capacity (Pandey et al. 2000). With increased wood costs and competition of wood resources from traditional wood sectors, developing alternative, environmentally friendly resources for natural fiber plastic composites is greatly needed. Currently the main use of bagasse is for energy in the sugar-cane industry through burning, but

their caloric value is relatively low compared to other fuel resources (Vazquez et al. 1999). Thus, utilization of bagasse fiber in NFPCs can lead to more efficient use of this bioresource.

The objectives of this study were to: 1) study the effect of temperature and composite type on creep properties of bagasse fiber/polymer composites, 2) model the observed creep behavior of the composites, and 3) predict long-term creep behavior of the composites based on accelerated testing and the time-temperature superposition principle.

3.2 THEORETICAL BACKGROUND

3.2.1 Creep Models

Creep modeling is of considerable interest in creep analysis for NFPCs. Different models have been proposed for viscoelastic polymeric materials and they can be classified into physical models and empirical models based on the interpretation of the parameters.

Burgers model is the most commonly used physical model. A generalized Burgers model has one Maxwell unit and one or multiple Kelvin units connected in series, as shown in Figure 3.1. The Burgers model divides the creep strain of a polymeric material into three parts: instantaneous deformation resulting from the Maxwell spring; viscoelastic deformation resulting from Kelvin units; and viscous deformation resulting from the Maxwell dashpot. All these can be presented by the following mathematical equation:

$$\varepsilon(t) = \frac{\sigma}{E_M} + \sum_{j=1}^n \frac{\sigma}{E_{Kj}} [1 - \exp(-\frac{E_{Kj}}{\eta_{Kj}} t)] + \frac{\sigma}{\eta_M} t \quad (3.1)$$

where $\varepsilon(t)$ is the creep strain, σ is the stress, t is the time, E_M and η_M are the elastic modulus of the spring and viscosity of the dashpot in the Maxwell unit, and E_{Kj} and η_{Kj} are elastic modulus of the spring and viscosity of the dashpot in the j^{th} Kelvin unit.

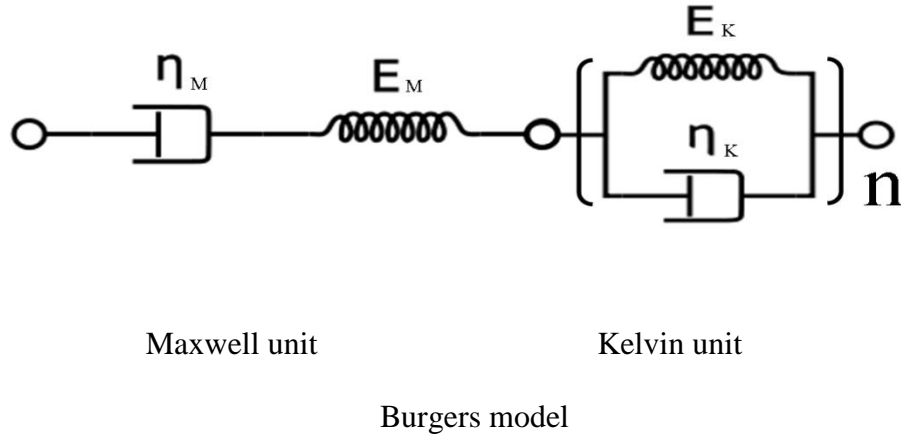


Figure 3.1 A diagram of generalized Burgers model

When there is only one Kelvin unit, i.e., $n=1$, the Burgers model can be simplified into the following 4-element Burgers model, which has been widely used in creep of NFPCs. (Marcovich and Villar 2003, Nunez et al. 2004, Acha et al. 2007).

$$\varepsilon(t) = \frac{\sigma}{E_M} + \frac{\sigma}{E_K} \left[1 - \exp\left(-\frac{E_K}{\eta_K} t\right) \right] + \frac{\sigma}{\eta_M} t \quad (3.2)$$

where $\varepsilon(t)$ is the creep strain, σ is the stress, t is the time, E_M and E_K are the elastic moduli of the springs, and η_M and η_K are viscosities of the dashpots in this model. The parameters E_M , E_K , η_M , and η_K can be obtained by fitting experimental data with the mathematical equation and be used for characterization of creep properties. In Eq. (3.2), the first term is a constant and does not change with time; the second term contributes to the early stage of creep, but reaches the maximum quickly; and the last term determines the long-term creep trend with a constant creep rate.

Based on the Burgers model, the creep rate of viscoelastic material can be obtained by taking derivative for Eq. (3.2) as follows:

$$\frac{d\varepsilon(t)}{dt} = \frac{\sigma}{\eta_K} \exp\left(-\frac{E_K}{\eta_K} t\right) + \frac{\sigma}{\eta_M} \quad (3.3)$$

Besides the Burgers model, several empirical models were proposed to simulate creep curves of polymeric material. One of the most commonly used empirical models is the Findley power law model (Jiang et al. 2007):

$$\varepsilon(t) = at^b + \varepsilon_0 \quad (3.4)$$

where ε_0 is the initial strain, which is dependent on stress; a is a parameter dependent on stress and b is one independent of stress.

A simpler 2-parameter power law model was also proposed and has been shown to be applicable for the creep modeling of kenaf fiber/HDPE composite (Tajvidi et al. 2005):

$$\varepsilon(t) = at^b \quad (3.5)$$

Although much work has been done on modeling of creep behavior of polymeric materials, no study has been reported on modeling of the recovery process, which is of importance for applications under non-constant stress. Understanding of the recovery process can also advance the modeling and prediction of creep behavior.

3.2.2 Accelerated Testing

Creep resistance is an important property for polymeric materials. However, it is often impractical to test long-term creep behavior directly with experiment because of the extremely long time required. Thus, predicting the creep behavior of polymers using short-term testing has gained considerable attention. One of the most useful extrapolation techniques is time-temperature superposition (TTS). It can be used to predict long-term creep behavior of certain polymers by shifting the curves from tests at different temperatures horizontally along a logarithmic time axis to generate a single curve known as the master curve (Ward 1971). Thus, a

long-term experiment can be replaced by shorter tests at higher temperatures. The shifting distance is called shift factor. The materials for which TTS holds are called thermorheologically simple materials and the rest are called thermorheologically complex materials (Tajvidi et al. 2005).

The shift factors of thermorheologically simple material can be related to temperature using either Williams–Landel–Ferry (WLF) or Arrhenius equations. The WLF equation is:

$$\log a_T = \frac{-C_1(T - T_0)}{C_2 + (T - T_0)} \quad (3.6)$$

where a_T is the horizontal (or time) shift factor, C_1 and C_2 are constants, T_0 is the reference temperature (K) and T is the temperature at which the test is performed (K).

The Arrhenius equation is given by:

$$\log a_T = \frac{E_a}{R} \left(\frac{1}{T} - \frac{1}{T_0} \right) \quad (3.7)$$

where E_a is the activation energy, R is the universal gas constant, T_0 is the reference temperature (K), and T is the temperature at which the test is performed (K). Regression analysis can be done using Eq. (3.7) to determine the activation energy for various materials from the experimental data.

3.3 EXPERIMENTAL

3.3.1 Raw Material

Polymers used in this work include recycled poly(vinyl chloride) (RPVC), virgin poly(vinyl chloride) (VPVC), recycled high density polyethylene (RHDPE), and virgin high density polyethylene (VHDPE). Both RPVC and RHDPE were obtained from Avangard Industries, Ltd. (Houston, TX). The VPVC was Shintech SE-450 from Shintech, Inc. (Plaquemine, LA), with an inherent viscosity of 0.515 (ASTM D 1243). VHDPE was Petrothene

LM 6007-00 with a MFI of 0.8 g/10min (190 °C and 2.16 kg) and a density of 960 kg/m³, from Equistar Chemicals, LP. (Houston, TX). The coupling agent used for the HDPE composites was Polybond 3009 (MAPE) from Chemtura Corporation (Middlebury, CT). The thermal stabilizer for PVC was Mark 1900, a mixture of methyltin tris(2-ethylhexyl thioglycolate and dimethyltin bis(2-ethylhexyl thioglycolate) from Chemtura Corporation (Middlebury, CT), with a specific gravity of 1.18 and 19.5% of Tin. The lubricant for PVC composite is TPW-012 from Struktol Company of America (Stow, OH), with a dropping point of 122-128 °C and a specific gravity of 0.98.

The raw bagasse fiber was obtained from a local sugar mill in Louisiana. The bagasse fiber was oven-dried at 95 °C for 24 hours to reduce the moisture content to below 2%. The dried fiber was hammer milled to pass through a 20-mesh screen, and then was stored in sealed plastic bags prior to compounding.

A commercial wood/HDPE composite decking material (W/HDPE) was used for comparative purpose in this study. However, the details of the composite formulation and processing conditions of the material were not known.

3.3.2 Composite Preparation

The plastic, bagasse fiber and additives were compounded in a 32-mm twin screw extruder (D-TEX extruder, Davis Standard). Compositions for the HDPE composites were 42% HDPE, 50% bagasse fiber, 2% MAPE, and 6% lubricant. For PVC composites, 41.2% PVC, 50% bagasse fiber, 2% SEBS, 6% lubricant, and 0.8% heat stabilizer were used. The extruder was then reconfigured for profiling and the compounded pellets were further processed into profiles of 65 × 6.5 mm cross section. Thin sections were cross-cut from the profiles and then sanded to yield 65 × 6.5 × 3 mm specimens.

3.3.3 Characterization

Three different tests were performed using a TA Q800 Dynamic Mechanical Analysis (DMA) instrument (TA Instrument Inc., New Castle, DE) using the dual-cantilever configuration. In each test, the sample was heated to the desired temperature and allowed to equilibrate for 5 minutes prior to beginning the test.

Strain sweep tests up to the maximum possible load level for the instrument (i.e., 18N) were performed at a frequency of 1 Hz and at temperatures of 35, 45, 55, and 65 °C.

Thirty-minute creep tests were performed at temperatures starting at 35 °C and increasing in 10 °C increments up to 65 °C for PVC composites and up to 85 °C for HDPE composites. After equilibrating at the desired temperature, 2 MPa of stress was applied and held constant for 30 minutes while the creep strain was measured. Three-day creep tests were also performed at a temperature of 35 °C with a stress level of 2 MPa. After 72 hours, the stress was released and the sample was allowed to recover for 24 hours.

3.3.4 Creep Modeling

Eq. (3.3) can be approximated by the following regression model:

$$\varepsilon(t_i) = \beta_{ME} + \sum_{j=1}^k \beta_{KEj} [1 - \exp(-\beta_{KVj} t_i)] + \beta_{MV} t_i + error \quad (3.8)$$

where: $\varepsilon(t_i)$ is the creep strain for the i^{th} observation at time t_i , β_{ME} and β_{MV} are estimates for σ/E_M and σ/η_M , respectively. β_{KEj} and β_{KVj} are estimates for σ/E_{Kj} and E_{Kj}/η_{Kj} , respectively, for the j^{th} Kelvin unit ($j = 1, 2, 3, \dots, k$). Nonlinear regression techniques were used to obtain estimates of the above parameters. Because the DMA instrument collected the data with increasing step size, resulting in more observations near time zero and fewer as time elapsed, each data point was weighted with the time interval from the previous point as follows:

$$w_i = t_i - t_{i-1} \quad (3.9)$$

Least-squares estimates of the regression parameters were computed by minimizing the following weighted Sum of Squares (WSS):

$$WSS = \sum_{i=1}^n w_i [\varepsilon(t_i) - \hat{\varepsilon}(t_i)]^2 \quad (3.10)$$

where $\varepsilon(t_i)$ represents creep strain observed at time t_i and $\hat{\varepsilon}(t_i)$ is the predicted creep strain for the i^{th} observation at time t_i . A smaller WSS value indicates better goodness-of-fit. When the parameters are determined, the goodness-of-fit can be visualized with a residual plot, defined as follows:

$$Resid(i) = \varepsilon(t_i) - \hat{\varepsilon}(t_i) \quad (3.11)$$

Statistical Analysis System (SAS) was employed to perform the nonlinear regression analysis on the creep curves. Gauss-Newton iterative method was implemented in this analysis to find least-square estimates for the nonlinear model. The similar numerical procedures were carried on the other models.

3.3.5 Recovery Analysis

When the stress was removed at time t_0 , test sample started the recovery process, which is a reverse process of creep. The maximum creep deformation was reached right before the stress was removed (at time t_0). Taking the maximum creep strain as the original state for the recovery process and the deformation reduction as recovery value, recovery curves were plotted in a way similar to creep curves. The recovery function can be expressed as follows:

$$R(t) = \varepsilon(t_0) - \varepsilon(t_0 + t) \quad (3.12)$$

where $R(t)$ stands for the recovery value at time t .

In Burgers model, the recovery function can be presented by the following mathematical equation:

$$R_B(t) = \frac{\sigma}{E_M} + \sum_{j=1}^n \frac{\sigma}{E_{Kj}} [1 - \exp(-t \frac{E_{Kj}}{\eta_{Kj}})] \quad (3.13)$$

3.3.6 Non-recoverable Deformation

With the introduction of recovery analysis, the creep deformation of the samples at time t can be divided into two parts: recoverable deformation and non-recoverable deformation. Denoting the non-recoverable deformation at time t as $NR(t)$, it can be calculated by the following equation:

$$NR(t) = \varepsilon(t) - R(t) \quad (3.14)$$

The non-recoverable deformation for Burgers model is this:

$$NR_B(t) = \frac{\sigma}{\eta_M} t \quad (3.15)$$

3.4 RESULTS AND DISCUSSION

3.4.1 Stress-Strain Behavior

Figure 3.2(a) shows the strain sweep test results for the composites at 35 °C. The stress and strain showed a good linear relationship in the testing region up to about 8 MPa at 35 °C, except for the composite made with virgin HDPE. The bagasse/PVC composites (B/PVC) showed higher stiffness than the bagasse/HDPE composites (B/HDPE) as a result of the stiffer PVC matrix. Moreover, the composites of recycled polymers (RPVC and RHDPE) had slightly higher moduli than the composites of virgin polymers (VPVC and VHDPE). At 35 °C, W/HDPE

had a stiffness between that of the bagasse/RHDPE composite (B/RHDPE) and the bagasse/VHDPE composite (B/VHDPE).

The linear viscoelastic regions were shortened to about 0-2 MPa when the temperature was increased to 65 °C (Figure 3.2(b)). This phenomenon indicates that viscous behavior was not apparent during the test at 35 °C, but a higher temperature (i.e., 65 °C) enhanced polymer mobility. For this reason, a stress of 2 MPa was used in the creep tests to ensure that the creep deformations were within the linear viscoelastic range. The composite stiffnesses at 65 °C differed from those at 35 °C, with W/HDPE being less affected by the temperature than B/HDPE and the bagasse/RPVC composite (B/RPVC) being more affected than the bagasse/VPVC composite (B/VPVC). The former can be caused by the difference in polymer matrix and fiber loading, which is unknown for W/HDPE; the latter may be due to possible thermal degradation of the recycled PVC.

3.4.2 Temperature Effect

Figure 3.3(a) shows the creep behavior of the five composites at 35 °C. At this temperature, B/PVC not only had lower instantaneous deformation, due to the higher stiffness of PVC compared to HDPE as indicated in Figure 3.2, but also showed a smaller creep rate than the HDPE composites. For the HDPE composites, their similar stiffness (Figure 3.2(a)) resulted in similar instantaneous deformations, but they differed much in creep rate, with B/VHDPE showing the highest creep rate and W/HDPE the lowest.

Figure 3.3(b) shows the creep behavior of the five composites at 65 °C. The creep strains of all composites increased at the higher temperature, but B/PVC were affected more than the HDPE composites. Although B/PVC had smaller instantaneous deformations than the HDPE composites, their long term creep was higher because of their high creep rates. This may be due

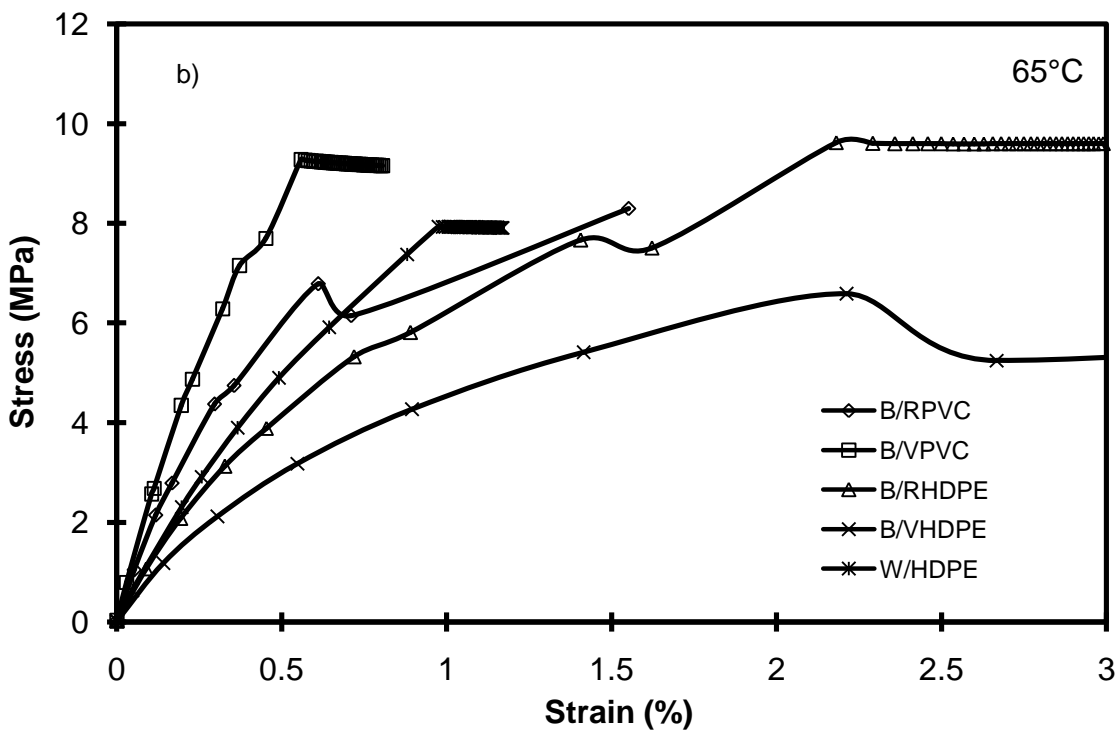
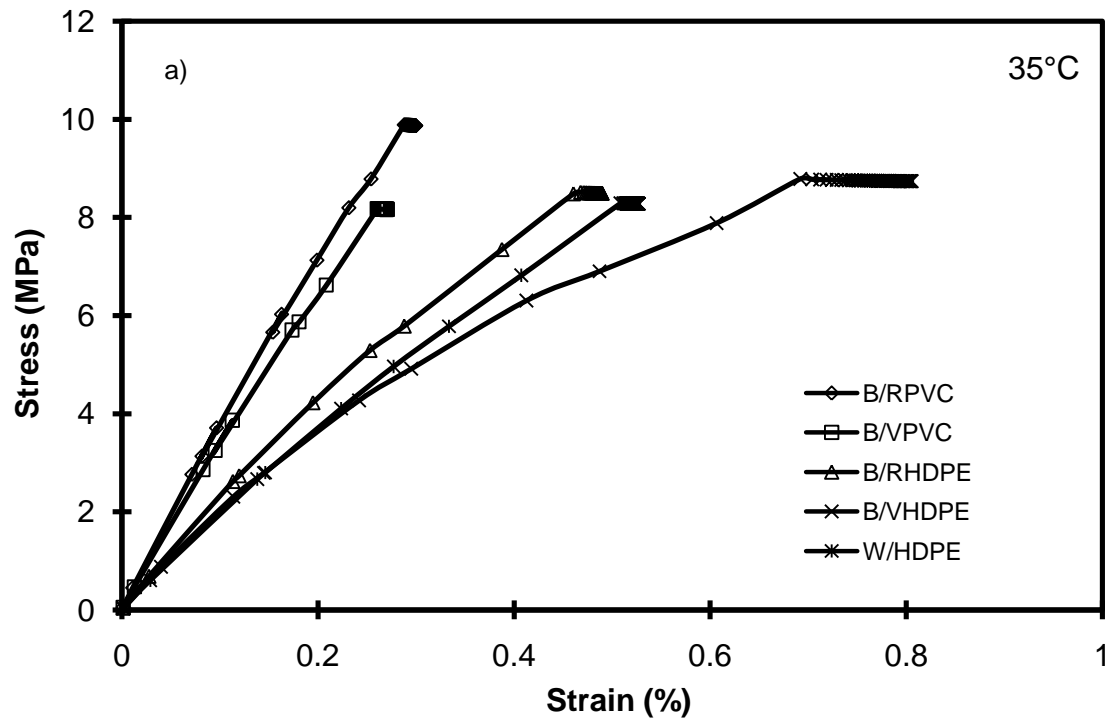


Figure 3.2 Stress-strain curves of the composites at (a) 35 °C and (b) 65 °C.

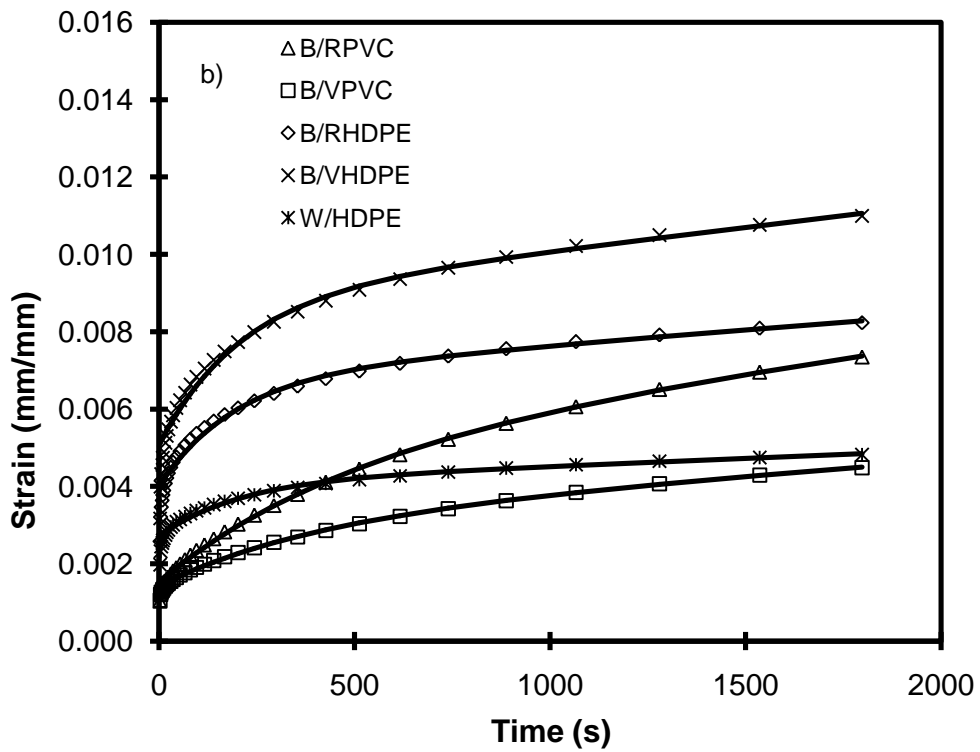
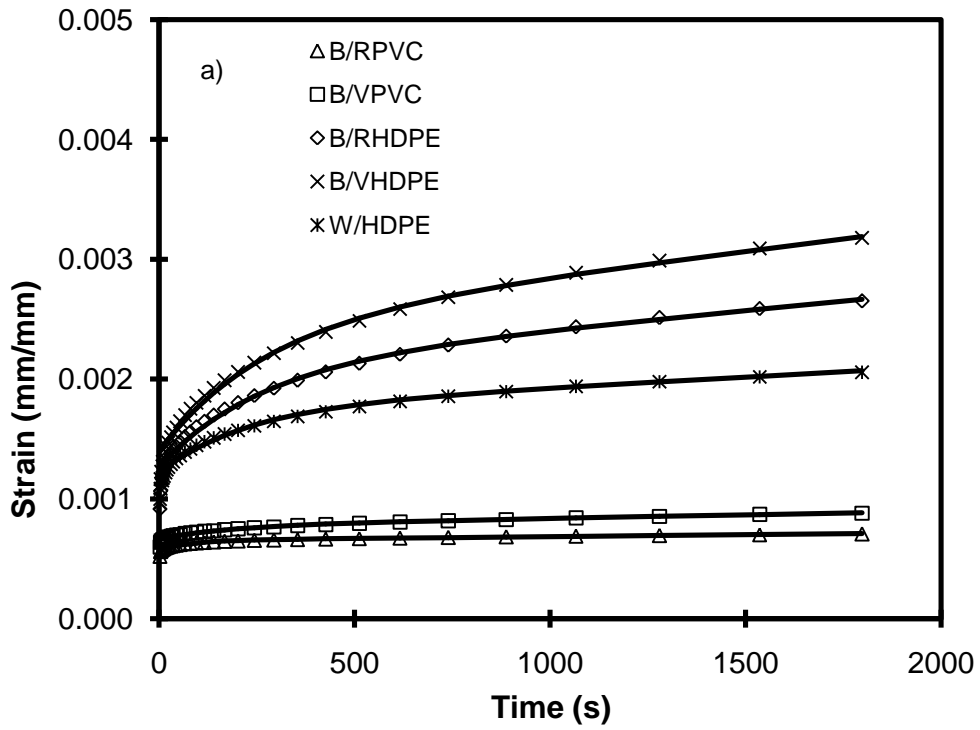


Figure 3.3 Creep curves of the composites at (a) 35 °C and (b) 65 °C. Symbols represent experimental data and solid lines represent Burgers model simulation.

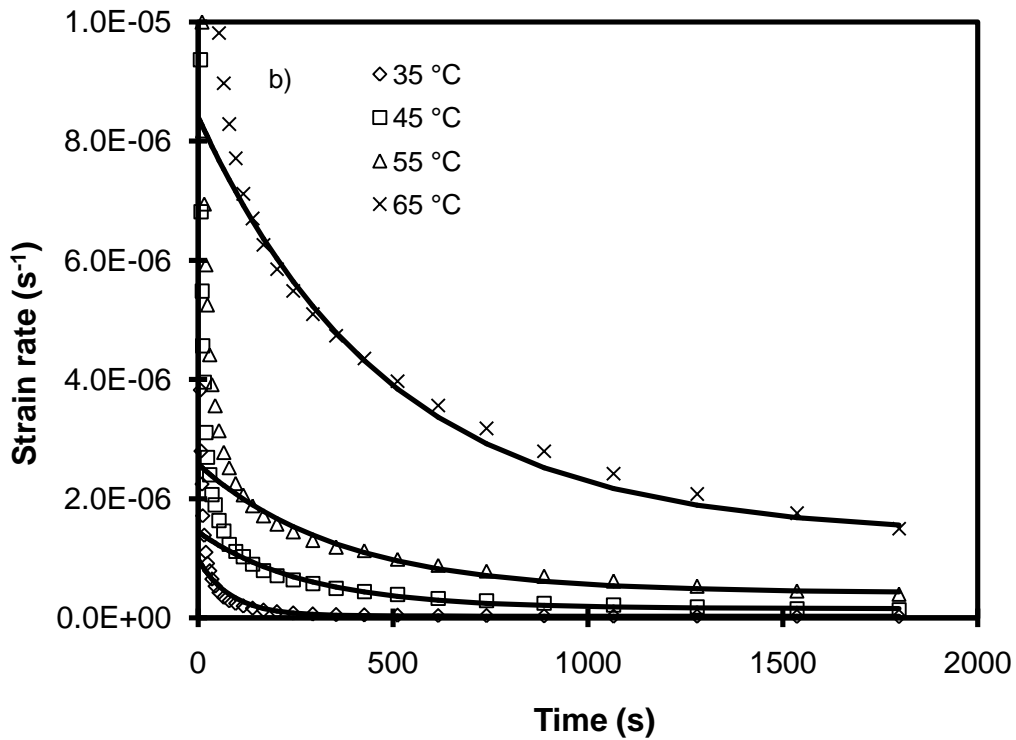
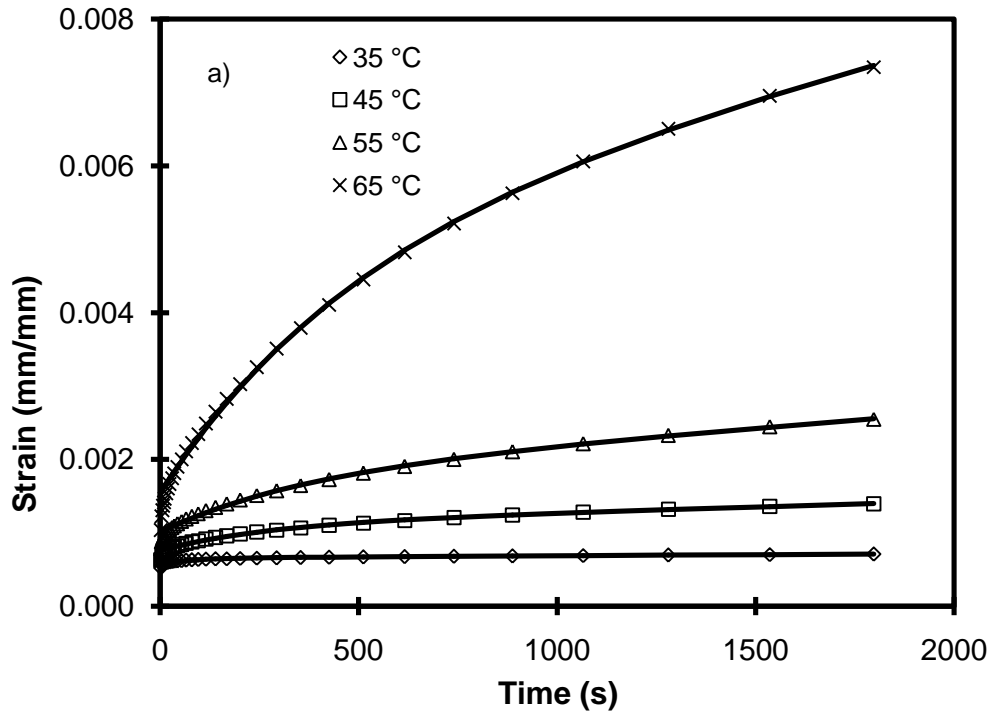


Figure 3.4 Creep strain (a) and strain rate (b) of B/RPVC at different temperatures. Symbols represent experimental data and solid lines represent the 4-element Burgers model simulation.

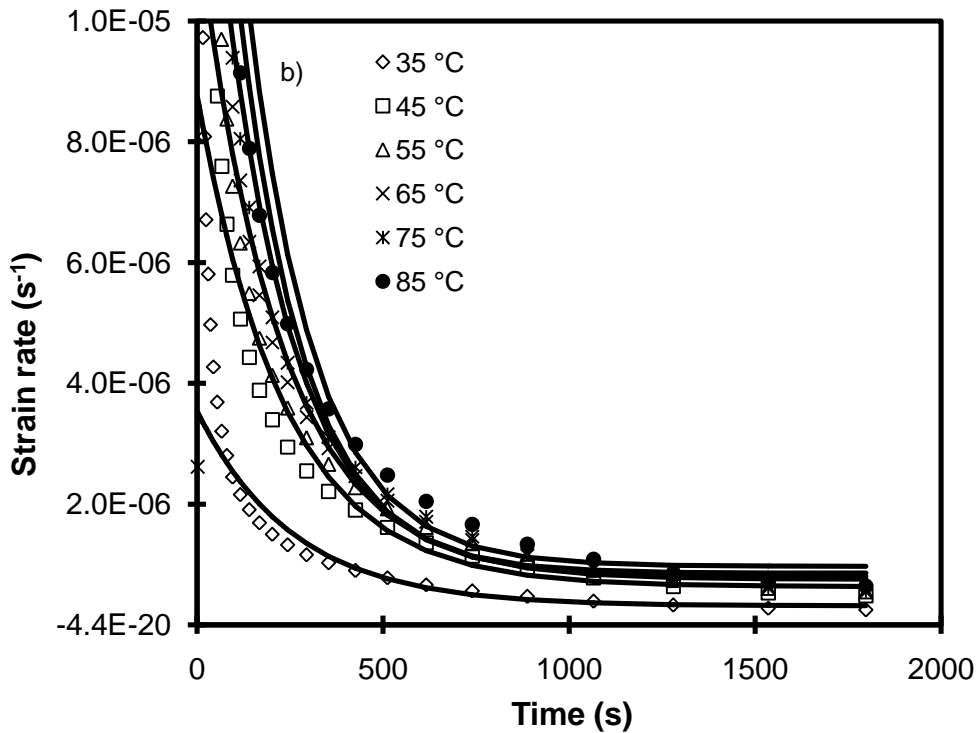
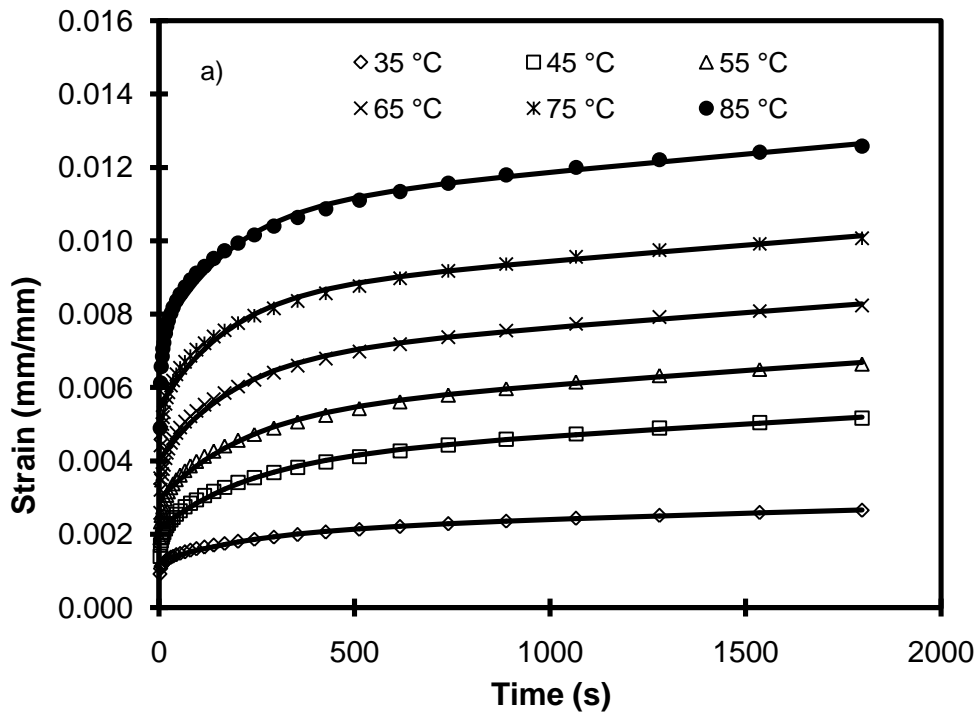


Figure 3.5 Creep strain (a) and strain rate (b) of B/RHDPE at different temperatures. Symbols represent experimental data and solid lines represent the 4-element Burgers model simulation.

to the morphological differences between the amorphous PVC and crystalline HDPE. Despite being less rigid and more prone to creep at 35°C, the increase in temperature had less effect on HDPE composites than on PVC composites because of the high crystalline content of HDPE composites since the temperatures investigated were well below the crystalline melting point of HDPE.

Figures 3.4 and 3.5 show the creep curves at 35 °C to 65 °C for B/RPVC and 35 °C to 85 °C for B/RHDPE. The increases were not only in instantaneous deformation but also in the creep rate. The mobility of the molecular chains was increased at higher temperatures. Comparatively, temperature had more influence on the creep of B/RPVC than that of B/RHDPE.

Table 3.1 shows the 4-element Burgers model parameters for the thirty-minute creep curves for the composites. All four parameters decreased for all composites as temperature increased. The decrease in E_M and E_K resulted from the increases in the instantaneous and the viscoelastic deformations as temperature increased. The decreases in η_K and η_M demonstrated higher mobility of molecular chains at higher temperature. The parameters for B/RPVC showed the largest decreases, especially on η_M , which is related to the long-term creep rate and demonstrates the large temperature-dependence of this composite, as can also be seen in Figure 3.4.

The sum of E_M and E_K , denoted as E , can be used to determine the total recoverable deformation during long-term creep and η_M reflects the non-recoverable long-term creep rate. Comparing the five composites, B/RPVC had the highest E and η_M values at low temperature, indicating the highest creep resistance for this composite, followed by B/VPVC. At higher temperature (e.g., 65 °C), W/HDPE showed the highest values for both E and η_M , indicating its good creep resistance at high temperature.

Table 3.1 Summary of parameters in Burgers model for thirty-minute creep of the composites

Composite	T(°C)	E_M (MPa)	E_K (MPa)	η_K (Pa s)	η_M (Pa s)	WSS
B/RPVC	35	3484.3	25000	2.08E+12	6.42E+13	1.45E-08
	45	2635.0	5586.6	1.55E+12	1.28E+13	1.20E-07
	55	1980.2	2528.46	9.26E+11	4.73E+12	4.10E-07
	65	1298.7	583.1	2.84E+11	1.45E+12	2.29E-06
B/VPVC	35	2994.0	18518.5	3.62E+12	3.28E+13	2.66E-08
	45	2475.2	7462.7	1.97E+12	1.62E+13	8.10E-08
	55	1960.8	4338.4	1.26E+12	6.86E+12	2.29E-07
	65	1398.6	1162.8	4.69E+11	2.63E+12	1.20E-06
B/RHDPE	35	1574.8	2389.5	6.19E+11	6.44E+12	9.00E-07
	45	934.6	1041.7	2.45E+11	3.16E+12	4.48E-06
	55	680.3	833.3	1.84E+11	2.67E+12	8.20E-06
	65	498.8	706.7	1.37E+11	2.49E+12	1.40E-05
	75	367.6	632.9	1.13E+11	2.34E+12	2.20E-05
	85	273.6	555.6	1.00E+11	2.06E+12	3.10E-05
B/VHDPE	35	1428.6	1886.8	5.10E+11	4.92E+12	1.19E-06
	45	781.3	847.5	1.95E+11	2.43E+12	7.22E-06
	55	558.7	668.9	1.53E+11	1.91E+12	1.30E-05
	65	394.5	526.3	1.08E+11	1.64E+12	3.50E-05
	75	274.7	427.4	7.96E+10	1.37E+12	4.60E-05
	85	198.0	374.5	5.88E+10	7.84E+11	6.50E-05
W/HDPE	35	1639.3	3766.5	8.43E+11	1.13E+13	4.11E-07
	45	1282.1	2469.1	5.54E+11	7.84E+12	9.30E-07
	55	975.6	1869.2	3.94E+11	6.03E+12	1.90E-06
	65	735.3	1428.6	2.90E+11	4.95E+12	3.58E-06
	75	539.1	1111.1	2.19E+11	3.95E+12	6.47E-06
	85	372.4	787.4	1.54E+11	2.89E+12	1.30E-05

The 4-element Burgers model parameters in Table 3.1 were used to simulate the thirty-minute creep curves, as shown by the solid lines in Figure 3.3-3.5. Generally speaking, the Burgers model simulation had good agreement with experimental data, demonstrating the applicability of Burgers model parameters in characterization of composite creep properties. However, some discrepancy existed at the beginning of creep process. The creep rate calculated with the Burgers parameters based on Eq. (3.2) are presented and compared to the real creep rate in Figure 3.4(b) and 3.5(b). Besides the deviation at short times, it also shows that the Burgers model may overestimate the long-term creep rate, so as to overestimate long-term creep.

3.4.3 Time-Temperature Superposition

To apply TTS, Figure 3.4 and 3.5 were replotted with logarithmic scales (see Figure 3.6). With horizontal shifts of the curves, smooth master curves over long time periods were obtained for the data at 35 °C (Figure 3.7). Based on these master curves, B/VHDPE showed the lowest creep resistance among the composites, followed by B/RHDPE. W/HDPE showed better creep resistance than B/HDPE, but not as good as B/PVC. However, the master curves show that B/PVC had larger creep rates than B/HDPE at long time frames and the creep strains eventually surpassed those of the HDPE composites. This resulted from the higher temperature-dependence of the PVC composites.

The shift factors used for generating the master curves were modeled using the Arrhenius equation (Eq. 3.7). The calculated activation energies (E_a) for the composites are summarized in Table 3.2. B/RPVC had the highest activation energy value, indicating that more energy is needed to mobilize the molecular chains of this composite during creep (Yang et al. 2006b). Comparatively, the HDPE composites had much lower activation energy values than the PVC composites.

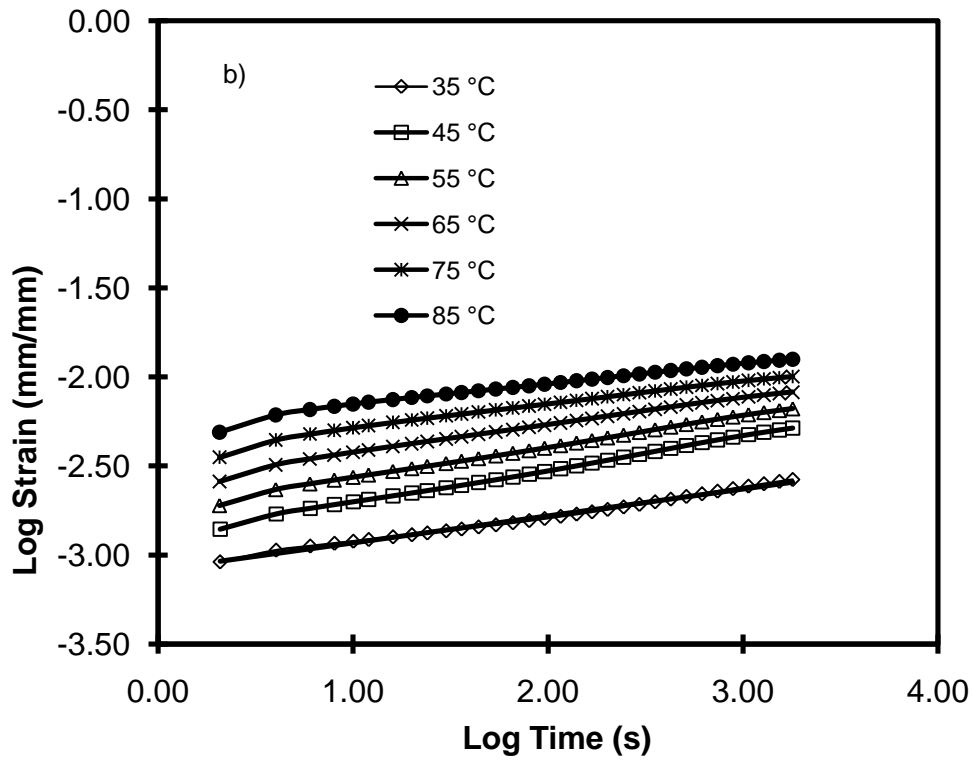
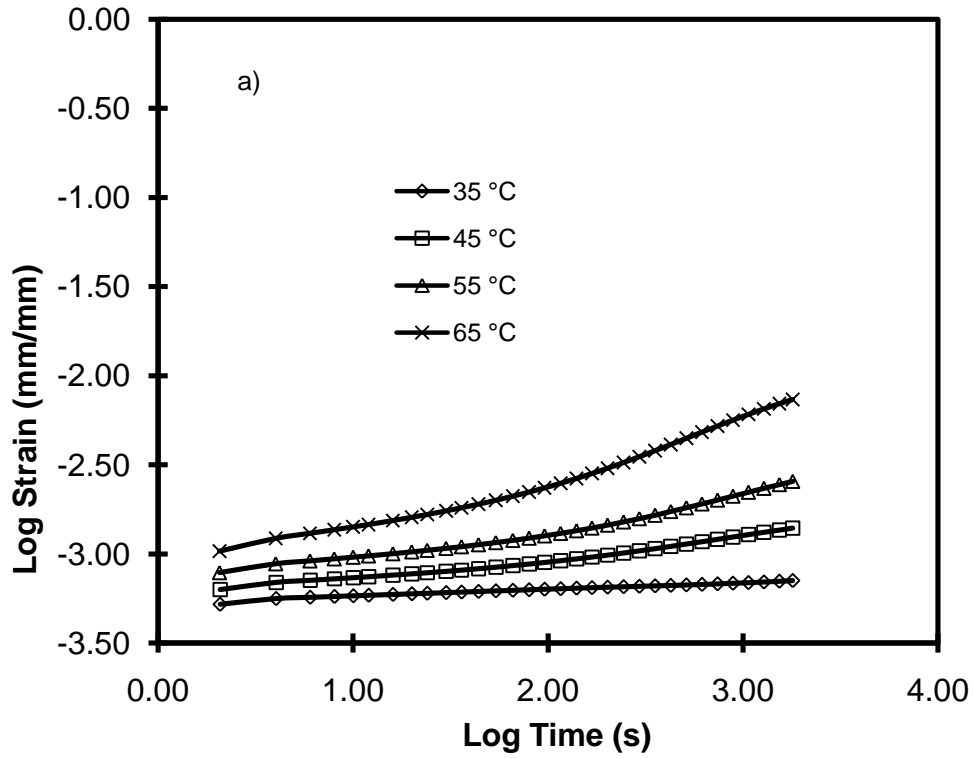


Figure 3.6 Log-scaled creep strain of (a) B/RPVC and (b) B/RHDPE.

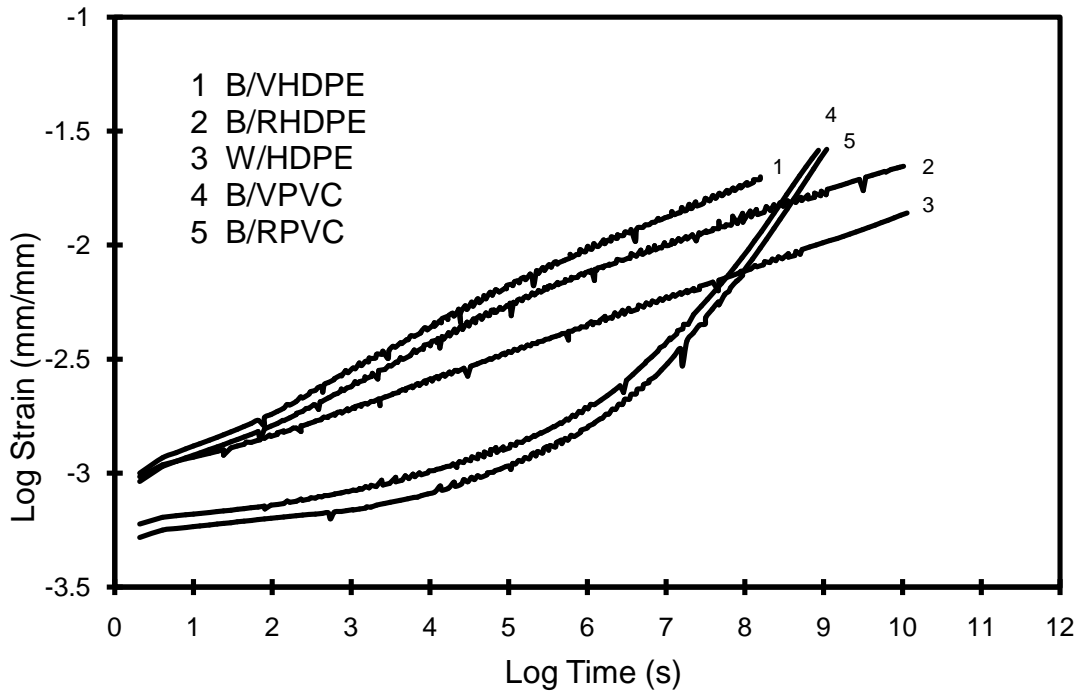


Figure 3.7 TTS master curves of creep for the composites.

Table 3.2 Summary of E_a calculated based on Arrhenius equation for the composites

Composites	E_a (kJ/mol)
B/RPVC	332.9
B/VPVC	271.3
B/RHDPE	202.3
B/VHDPE	213.5
W/HDPE	217.5

Although the master curves were successfully constructed, it is not a sufficient condition to validate the TTS principle. Figure 3.8 shows the comparison of the creep behavior predicted from the thirty-minute creep tests using TTS and the experimental creep data from the three-day creep tests. The TTS predicted the creep data well for B/PVC. However, for all of the HDPE composites, the predicted creep curves overestimated the experimental results. This inconsistency among the composites points out the necessity of evaluating TTS for different composites before its application.

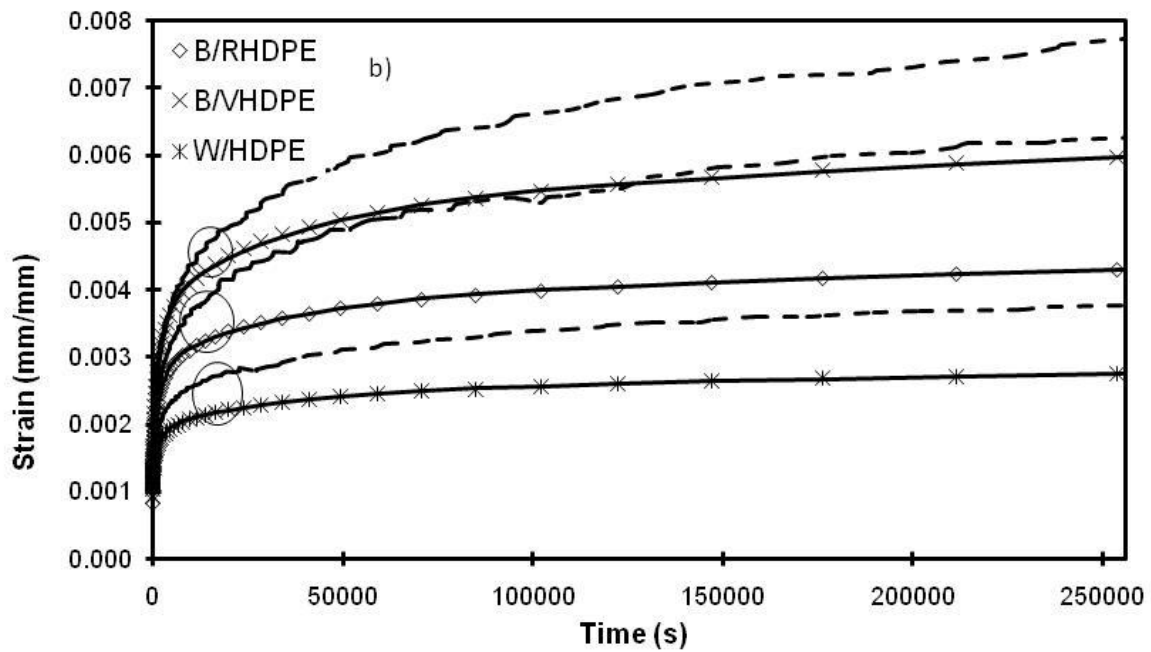
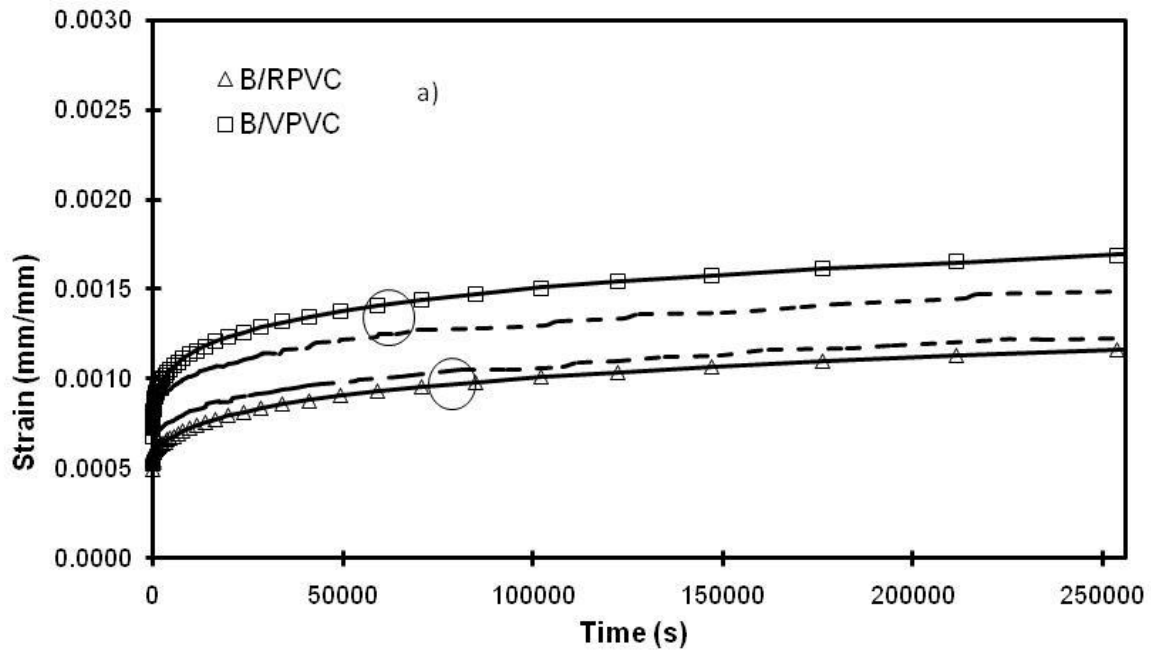


Figure 3.8 Comparison of TTS predicted creep with experimental data for the composites. Symbols represent experimental data; solid lines represent the 4-element Burgers model simulation; dash lines represent TTS predicted data. Two lines with the same circle are for the same composite.

3.4.4 Creep Modeling

The thirty-minute creep data was fitted only with the 4-element Burgers model, as described in Section 3.3.2. In this section several different models were evaluated on the three-day creep data.

3.4.4.1 Burgers Models

- Four-element Burgers model. As shown in Figure 3.8, the 4-element Burgers model offered a good fit on the three-day creep curves of all three composites. It was capable of representing the overall creep trend and predicting the creep for a longer time period. Table 3.3 shows that bagasse/VHDPE composite had the lowest E_M , which indicates the highest instantaneous deformation under stress. Comparatively, bagasse/RPVC had the highest E_M value and showed the smallest instantaneous strain at the beginning of the test. Parameter E_K showed the same order as E_M , indicating that B/VHDPE also had the highest viscoelastic deformation during the test. In Burgers model, the most important parameter for long-term creep is η_M , which determines long-term creep rate. Among the three composites, B/VHDPE had the lowest η_M , showing the highest long-term creep rate, while B/RPVC had the lowest long-term creep rate with the smallest η_M . Clearly, B/VHDPE composite had the worst creep resistance among the composites based on Burgers model, followed by B/RHDPE composite.

- Six-element Burgers model. A comparison of the Maxwell parameters E_M and η_M from the 4-element and 6-element Burgers models shows that they have the same trend for the 5 composites. E_M and η_M from 6-element Burgers model are larger than that from the 4-element Burgers model, indicating that 6-element Burgers model offers smaller instantaneous deformation value and smaller long-term creep rate prediction. This is because the extra Kelvin

unit introduced into this model accounted part of the instantaneous deformation and long-term creep. The smaller instantaneous deformation and lower creep rate were examined and proved to be more accurately later in this paper. Moreover, the WSS (Table 3.3) indicate that 6-element Burgers model offered a much better fit than the r-element Burgers model.

- Eight-element Burgers model. As shown in Table 3.3, 8-element Burgers model provided even larger Maxwell parameters E_M and η_M than 6-element Burgers model. This indicates that 8-element Burgers model results in smaller instantaneous deformation value and smaller long-term creep rate prediction with the introduction of another Kelvin unit. The WSS in Table 3.3 also show that 8-element Burgers model had a better fit than the 6-element and 4-element Burgers models.

- Residual plot. Although 4, 6, and 8-element Burgers models were all capable of fitting the creep curves of the composites, they had different fit accuracies, as shown by WSSs in Table 3.3. To illustrate the differences, the residuals of the models are plotted in Figure 3.9. It can be seen that the 4-element Burgers model shows a poor fit, especially at the beginning, which corresponds to the Kelvin unit of the physical model. The more complicated Burgers models offered a better fit due to added flexibility resulting from additional Kelvin units.

- Creep prediction. Figure 3.10 shows the comparison of the three models when being used to predict the third day creep based on two-day creep data. It can be found that 8-element Burgers model offered the best prediction and the 4-element Burgers model the worst. But all the three models overestimated the long-term creep deformation, or the long-term creep rate. A more complicated model might provide a smaller creep rate and offer better long-term prediction.

Table 3.3 Summary of model parameters for three-day creep of the composites

model	parameters	composites				
		B/ RPVC	B/VPVC	B/RHDPE	B/VHDPE	W/HDPE
4-element Burgers model	E_M (MPa)	3169.6	2036.7	836.8	668.9	1136.4
	E_K (MPa)	6756.8	4728.17	1481.5	956.9	2954.2
	η_{K1} (Pa s)	2.18E+14	1.31E+14	2.51E+13	1.71E+13	6.29E+13
	η_M (Pa s)	2.11E+15	1.75E+15	8.75E+14	5.46E+14	1.54E+15
	WSS	6.93E-06	0.000031	0.000679	0.00151	0.000142
6-element Burgers model	E_M (MPa)	3344.5	2247.2	1190.5	1010.1	1369.9
	E_{K1} (MPa)	15151.5	8928.6	1652.9	1123.6	3960.4
	η_{K1} (Pa s)	1.53E+14	5.10E+13	3.75E+12	2.83E+12	1.06E+13
	E_{K2} (MPa)	8000.0	5618.0	2059.7	1315.8	3745.3
	η_{K2} (Pa s)	5E+14	2.96E+14	6.87E+13	4.70E+13	1.39E+14
	η_M (Pa s)	2.69E+15	2.27E+15	1.16E+15	7.29E+14	1.97E+15
8-element Burgers model	WSS	3.70E-07	3.78E-06	0.000063	0.000134	0.000015
	E_M (MPa)	3669.7	2454.0	1526.7	1315.8	1587.3
	E_{K1} (MPa)	8032.1	5602.2	2515.7	1389.0	4228.3
	η_{K1} (Pa s)	5.02E+14	5.09E+14	1.61E+13	1.09E+12	2.11E+14
	E_{K2} (MPa)	14925.4	8403.4	2418.4	1550.4	5347.6
	η_{K2} (Pa s)	1.60E+14	1.12E+14	1.15E+14	8.16E+13	3.71E+13
	E_{K3} (MPa)	35714.3	12987.0	1980.2	1680.7	4545.5
	η_{K3} (Pa s)	2.73E+12	1.27E+13	1.25E+12	1.26E+13	2.44E+12
Findley's power law model	η_M (Pa s)	2.73E+15	3.45E+15	1.44E+15	9.39E+14	2.37E+15
	WSS	2.81E-07	6.24E-07	5.95E-06	0.00001	1.68E-06
	a	0.000027	0.000122	0.3554	0.5666	0.00305
	b	0.267	0.1843	0.001	0.001	0.0428
2-parameter power law model	ε_0	0.000424	0.000486	-0.356	-0.568	-0.0024
	WSS	4.45E-06	3.99E-06	4E-05	7E-05	7.11E-06
	a	0.00019	0.00038	0.0013	0.0014	0.00095
2-parameter power law model	b	0.1447	0.12	0.098	0.1155	0.0863
	WSS	3.90E-05	2.10E-05	4E-04	1E-03	2.3E-05

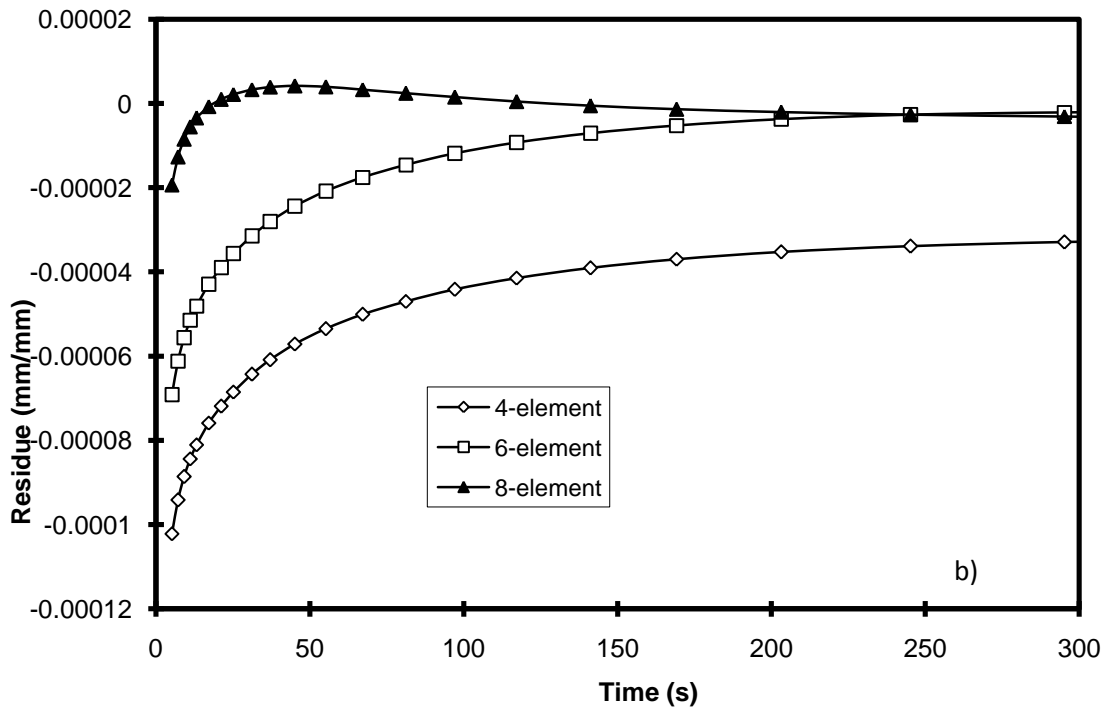
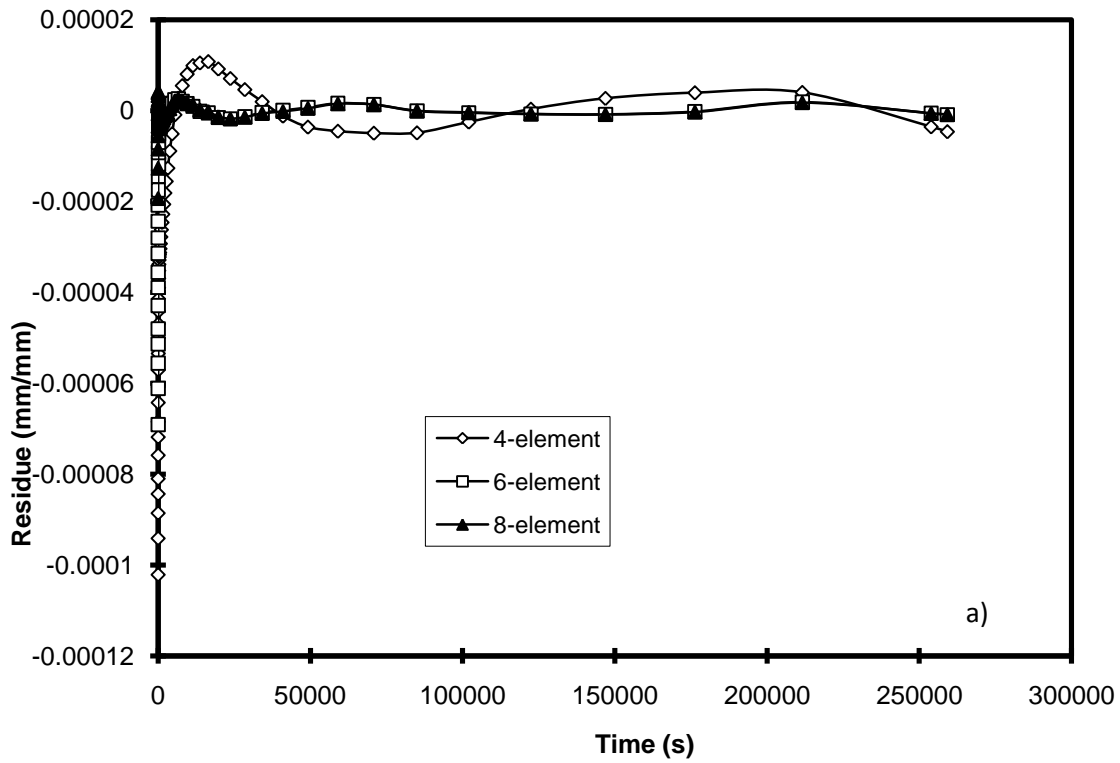


Figure 3.9 Residual plot of 4, 6, and 8-element Burgers models for bagasse/RPVC composites: (a) three days; (b) first 300 minutes.

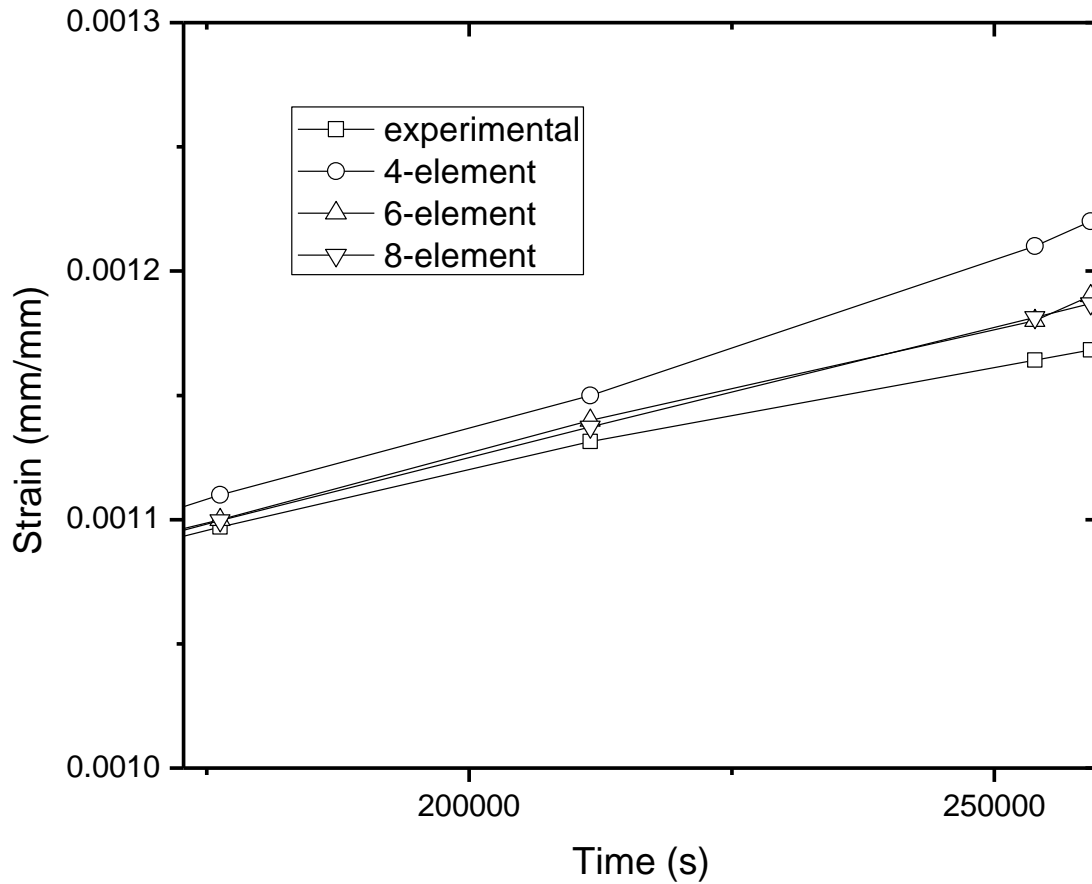


Figure 3.10 Comparison of 4, 6, and 8-element Burgers models when using two-day creep data to predict the third day creep for bagasse/RPVC composites.

Table 3.4 Instantaneous creep deformation obtained from the 4-element, 6-element, and 8-element Burgers models in comparison with real value

model	composites				
	B/ RPVC	B/VPVC	B/RHDPE	B/VHDPE	W/HDPE
4-element	0.000631	0.000982	0.00239	0.00299	0.00176
6-element	0.000598	0.00089	0.00168	0.00198	0.00146
8-element	0.000545	0.000815	0.00131	0.00152	0.00126
Experimental	0.000529	0.000726	0.000967	0.00109	0.00103

- Instantaneous creep deformation. Table 3.4 shows the comparison of the instantaneous deformation values obtained from the Burgers models with the real values. The fitted value approaches the real value when more complicated Burgers model is used. This again confirmed that the 8-element Burgers model offered the best fit among the three models.

3.4.4.2 Power law models

- Findley's power law model. The fitting results of the Findley's power law model on the three-day creep curves are summarized in Table 3.3. Based on the WSS, this model fit the data better than the Burgers model. However, comparing the results for B/VHDPE and W/HDPE, the parameters are very different. Although fitting the curves well, the 3 parameters seem very sensitive to different curve shapes and lack consistency needed for characterization and comparison purposes.

- Two-parameter power law model. The fitting results of the 2-parameter power law model on the three-day creep curves of the composites are also presented in Table 3.3. This model also showed good fit based on the WSS, although not as good as the Findley's power law model. Eliminating the parameter ε_0 made the remaining parameters more consistent, with parameter a mainly reflecting the short-term creep (including instantaneous deformation) and parameter b showing the long-term trend. Based on the result of this model, B/VPVC had the greatest creep resistance with the smallest value of a and largest value of b . This trend matches the general observations and the result of the Burgers model.

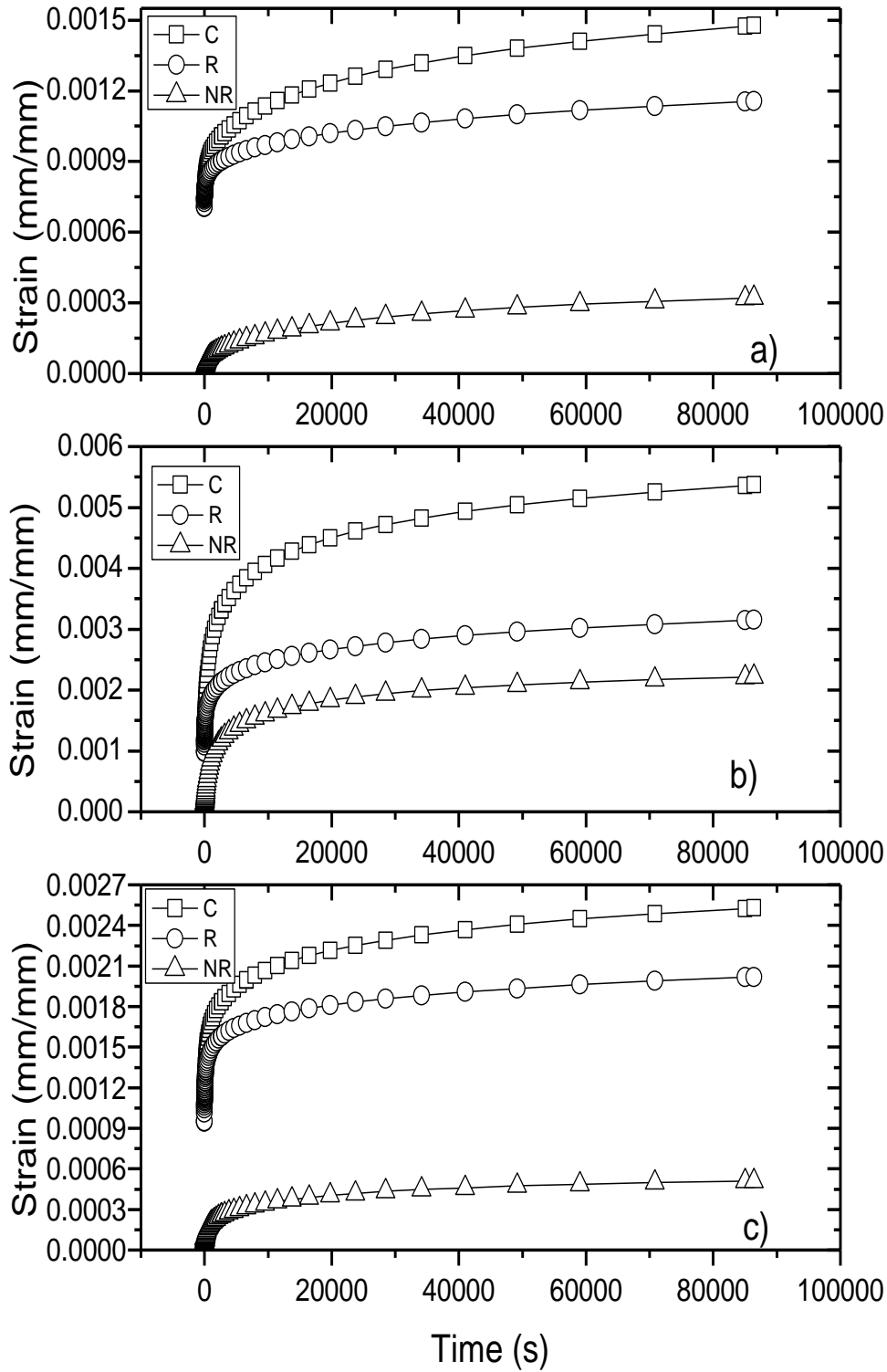


Figure 3.11 Creep (C), recovery (R), and non-recoverable deformation (NR) of B/VPVC (a), B/VHDPE (b), and W/HDPE (c).

3.4.5 Recovery Analysis

Figure 3.11 shows the curves for creep, recovery, and non-recoverable deformation of the composites. As shown, the non-recoverable deformation started from 0, indicating that instantaneous creep deformation was fully recovered. Based on the Burgers model, the dashpot in the Maxwell unit creates the non-recoverable deformation, which is proportional to creep time. However, the non-recoverable curves failed to follow a linear trend, suggesting that Burgers model cannot be directly applied for recovery prediction.

Comparatively, B/VHDPE had more non-recoverable deformation than bagasse/VPVC composite (B/VPVC) during the creep process. A possible explanation is that the high stiffness of PVC molecules provides high inner force during creep deformation and the inner force drives the recovery process. In HDPE composites, the flexibility of the HDPE molecules makes it easier to release the inner force during creep process so that less deformation can be recovered. The recoverability of creep deformation makes PVC composites more sustainable under discontinuous forces.

3.5 CONCLUSIONS

The creep behaviors of bagasse/PVC (recycled and virgin) composites, bagasse/HDPE (recycled and virgin) composites and a commercial wood/HDPE composite were investigated. Temperature showed a large impact on creep behavior of all composites. B/PVC had better creep resistance than B/HDPE at low temperature, but they showed higher temperature dependence. The Burgers models were capable of fitting the creep data and characterize the overall trend, but they failed to be used for prediction purpose. Comparatively, the more complicated 8-element Burgers model offered better fit than the other two. It can be concluded that more Kelvin units in the Burgers model can better describe the creep procedure for the composites. However, the

Burgers models are not directly applicable in recovery prediction. Comparatively, PVC composites are more likely to recover than the HDPE composites. Findley's power law model and 2-parameter power law model both fitted the creep data well, but the parameters in Findley's power law model were very sensitive to curve shape. The Burgers model and 2-parameter power law model yielded more consistent parameters between similar composites in three-day creep tests, so the parameters can be used to characterize the creep behavior of the composites at long time frames. The TTS principle was applied to these composites and smooth master curves were obtained. The TTS better predicted long-term creep behavior from short term creep tests for the PVC composites than the HDPE composites.

3.6 REFERENCES

- Acha, B. A., M. M. Reboredo, and N. E. Marcovich. 2007. Creep and dynamic mechanical behavior of PP-jute composites: Effect of the interfacial adhesion. *Composites Part a-Applied Science and Manufacturing* **38**:1507-1516.
- Jiang, L., M. P. Wolcott, J. W. Zhang, and K. Englund. 2007. Flexural properties of surface reinforced wood/plastic deck board. *Polymer Engineering and Science* **47**:281-288.
- Marcovich, N. E. and M. A. Villar. 2003. Thermal and mechanical characterization of linear low density polyethylene/wood flour composites. *Journal of Applied Polymer Science* **90**:2775-2784.
- Nunez, A. J., N. E. Marcovich, and M. I. Aranguren. 2004. Analysis of the creep behavior of polypropylene-woodflour composites. *Polymer Engineering and Science* **44**:1594-1603.
- Pandey, A., C. R. Soccol, P. Nigam, and V. T. Soccol. 2000. Biotechnological potential of agro-industrial residues. I: sugarcane bagasse. *Bioresource Technology* **74**:69-80.
- Tajvidi, M., R. H. Falk, and J. C. Hermanson. 2005. Time-temperature superposition principle applied to a kenaf-fiber/high-density polyethylene composite. *Journal of Applied Polymer Science* **97**:1995-2004.
- Vazquez, A., V. A. Dominguez, and J. M. Kenny. 1999. Bagasse fiber-polypropylene based composites. *Journal of Thermoplastic Composite Materials* **12**:477-497.
- Ward, I. M. 1971. *Mechanical Properties of Solid Polymers*. Wiley-interscience.
- Yang, J. L., Z. Zhang, A. K. Schlarb, and K. Friedrich. 2006. On the characterization of tensile creep resistance of polyamide 66 nanocomposites. Part II: Modeling and prediction of long-term performance. *Polymer* **47**:6745-6758.

CHAPTER 4 THE EFFECT OF COUPLING AGENTS AND BAMBOO FLOUR LOADING ON CREEP PROPERTY OF HDPE-BASED COMPOSITES

4.1 INTRODUCTION

Wood/polymer composites (WPCs) are being widely used in construction because of their natural appearance, sound mechanical properties, water resistance, and biodegradability. However, the polarity difference between hydrophilic wood and hydrophobic polymer matrix can lead to poor interfacial adhesion, and thus impair mechanical properties of final products. To promote the interaction between them, various coupling agents or compatibilizers (mainly functionalized polymers) have been used. The polymeric matrices used in WPCs are mainly polyolefin, i.e., polyethylene (PE) and polypropylene (PP), due to of low processing temperature that wood can sustain. Maleic anhydride-grafted PE or PP is commonly used as coupling agents for WPCs due to their compatibility with both hydrophobic polyolefin matrix and hydrophilic wood surfaces (Kazayawoko et al. 1997, Kazayawoko et al. 1999, Lai et al. 2003, Wang et al. 2003), leading to enhanced mechanical properties of the composites, such as flexural strength and tensile strength. However, low impact strength is still a critical problem for the application of WPCs and the toughening of this material has received much attention, mainly on polyolefin elastomers (Oksman and Clemons 1998, Hristova et al. 2002, Wang et al. 2003, Sombatsompop et al. 2005). To achieve superior overall mechanical properties, combinations of compatibilizers and impact modifiers have been examined (Oksman and Clemons 1998, Sombatsompop et al. 2005).

Bamboo is an important renewable natural resource, especially in the tropics and the sub-tropical areas, accounting for one quarter of the total biomass (Bansal and Zoolagud 2002). One advantage of this biomass is its rapid renewability compared with wood. In addition, bamboo

shows good overall mechanical properties. These advantages make bamboo a good alternative for wood in polymeric composites. Much work has been done in bamboo/polymer composites, with the emphasis on bamboo's reinforcing effect in polymer composites (Mi et al. 1997, Chen et al. 1998, Thwe and Liao 2000, 2003, Ge et al. 2004, Okubo et al. 2004), but there was little work on the coupling agents for the composites (Mi et al. 1997, Chen et al. 1998). In a previous work (Liu et al. 2008), various coupling agents were used for bamboo/HDPE composite. Among them, PE-g-MA was proven to be the most effective. In addition, two types of ethylene propylene rubber-grafted-maleic anhydride (EPR-g-MA) were used as impact modifiers for the bamboo/HDPE composites. It was found that semi-crystalline EPR-g-MA (sEPR-g-MA) showed better toughening effect than the amorphous EPR-g-MA (aEPR-g-MA). Two combined modifiers, PE-g-MA/sEPR-g-MA and PE-g-MA/aEPR-g-MA, were also examined and the combined PE-g-MA/sEPR-g-MA modifier achieved optimum strength/toughness balance at low percentage of sEPR-g-MA.

Creep behavior of WPC is critical for its application and the effect of coupling agents on creep behavior of WPC has been investigated with different results reported (Sain et al. 2000, Marcovich and Villar 2003, Nunez et al. 2003, Bledzki and Faruk 2004, Nunez et al. 2004, Acha et al. 2007). The published research is limited on PP composites and the results failed to show good agreement. In addition, no combined modifiers have been examined for their effect on creep property of the NFPCs. The work described in this chapter focuses on the effect of both individual and combined modifiers, and BF loading levels on the creep resistance of BF/HDPE composites. The objectives of this research were to: 1) study the effect of coupling agents, impact modifiers, combined modifiers, and BF loading rate on creep property of BF/HDPE

composites, 2) model the observed creep behavior of the composites, and 3) predict long-term creep behaviors of the composites through modeling and time-temperature superposition (TTS).

4.2 EXPERIMENTAL

4.2.1 Materials and Blend Design

HDPE6761 from ExxonMobil Chemical Co. (Houston, TX) was used as polymer matrix in this research. Coupling agent, PE-g-MA, is Epolene G2608 from Eastman Chemical Co. (Kingsport, TN). The two impact modifiers are Exxelor VA 1801 (sEPR-g-MA) and Exxelor VA 1803 (aEPR-g-MA), both from ExxonMobil Chemical Co. (Houston, TX). Bamboo flour was obtained by grinding bamboo flakes through a 28-mesh screen, and then oven-drying at 80 °C for 2 days.

Experimental design included three parts. The first one included 10 blends with three compatibilizers (PE-g-MA, sEPR-g-MA, and aEPR-g-MA), four loading rates (0, 2.9, 5.7 and 8.3wt% based on the total composite weight); and one HDPE/BF ratio (60/40 wt%). The second one consisted of nine blends covering two EPR-g-MAs (aEPR-g-MA, and sEPR-g-MA), five PE-g-MA to EPR ratios (0, 33.3, 50.0, 66.7, and 100 wt%), and one HDPE/BF ratio (60/40 wt%). The third one consisted of three blends with three HDPE/BF ratios (30, 40, and 50 wt%) and one combined modifier (PE-g-MA/sEPR-g-MA=2:1 by weight at 15% of the BF weight).

4.2.2 Sample Preparation

Composite pellets were obtained through extrusion with an intermesh, counter-rotating Brabender Intelli-Torque twin-screw extruder (Brabender Instruments Inc., Hackensack, NJ). The temperature profile of barrels ranged from 150 °C to 175 °C with a screw speed at 30 rpm. The pellets were oven-dried at 100 °C for 12 hours before being made into standard mechanical test specimens through injection molding (Batenfeld Plus 35, Batenfeld Inc, NJ) at 190 °C

injection temperature and 68 °C mold temperature. The impact test specimens with cross-section size of 3 mm × 12 mm were machined for creep tests.

4.2.3 Creep Characterization

Two different tests were performed using a TA Q800 Dynamic Mechanical Analysis (DMA) instrument (TA Instrument Inc., New Castle, DE) with a 3-point bending configuration. In each test, the sample was heated to the desired temperature and allowed to equilibrate for 5 minutes prior to the test.

Thirty-minute creep tests were performed at temperatures of 35, 45, 55, 65, 75, 85, and 95 °C. After equilibrating at the desired temperature, a stress of 2 MPa was applied and held constant for 30 minutes while the creep strain was measured.

One-day creep tests were performed at a temperature of 35 °C with a stress level of 2 MPa. After 24 hours, the stress was released and the sample was allowed to recover for 24 hours.

4.2.4 Creep Modeling

Several models were discussed in Chapter 3 and it was found that a more complicated Burgers model offered better fit of the data. Among them, the 8-element model fitted better than the 4-element model and Findley's power law model fitted the creep data better than the 2-parameter power law model. However, Findley's power law seemed not as stable as the 2-parameter power law model and more Kelvin's units in the generalized Burgers model made the model complicated. In this chapter, the Burgers model was used to characterize the creep curves. Two new models were developed by introducing power index to time t based on the 4-element Burgers model. The first one, denoted as Partially-Indexed Burgers (PIB) model, has the index only for the Kelvin unit, as shown in Eq. (4.1). The other one, denoted as Fully-Indexed Burgers

(FIB) model, has the index for both the Kelvin unit and the Maxwell unit, as shown in Eq. (4.2). Since these models are not directly related to the physical models, they are simplified as follows:

$$\varepsilon(t) = b_1 + b_2[1 - \exp(-b_3 t^n)] + b_4 t \quad (4.1)$$

$$\varepsilon(t) = b_1 + b_2[1 - \exp(-b_3 t^n)] + b_4 t^n \quad (4.2)$$

Statistical Analysis System (SAS) was employed to estimate the model parameters by performing nonlinear regression on the creep curves. The Gauss-Newton iterative method was implemented in this analysis to find the least-square estimates for the nonlinear model. Since the DMA instrument collected the data with an increasing step-size, every data point was weighted with the time interval of data collection.

4.2.5 Time-Temperature Superposition (TTS)

TTS was also applied in this chapter to obtain the long term creep curves for different composites. The details of TTS procedure were described in Chapter 3.

4.3 RESULTS AND DISCUSSION

4.3.1 Effect of Individual Modifier Type and Content

Figure 4.1(a) shows the one-day creep curves of the composites with different levels of PE-g-MA modifier. As shown, the addition of PE-g-MA improved the creep resistance of BF/HDPE composites, and different modifier loading levels led to different effects. The addition of PE-g-MA up to 5.7% decreased creep strain of the composite by improving interfacial adhesion between the fibers and the polymer matrix. However, further increase of PE-g-MA to 8.3% not only failed to offer better creep resistance, but also deteriorated it to the level obtained with 2.7% PE-g-MA. This trend suggests that PE-g-MA played two roles in the composite: one positive effect by improving interfacial adhesion between the fibers and the polymer matrix as coupling agent, and one negative effect by softening HDPE matrix because of its relative low

modulus. When the concentration of PE-g-MA was at a low level, the former effect outweighed the latter effect, improving the creep resistance of the composite. However, as PE-g-MA content increased, the positive effect reached the maximum and the negative effect continued to increase, exceeding the positive effect at a certain PE-g-MA level.

The addition of sEPR-g-MA or aEPR-g-MA increased the creep strain of BF/HDPE composites and higher modifier loading levels resulted in larger creep strains, as shown in Figure 4.1(b) and (c). Based on the aforementioned mechanism, the deteriorating effect of sEPR-g-MA and aEPR-g-MA were more obvious than the enhancing effect even at a low loading level, due to their lower modulus compared with HDPE matrix. Comparatively, aEPR-g-MA led to worse creep resistance property than sEPR-g-MA because of the lower modulus arising from its amorphous structure.

Table 4.1 shows the Burgers parameters for the composites with individual modifiers. The addition of PE-g-MA improved the creep property of BF/HDPE by increasing both instantaneous modulus E_M and long-term viscosity η_M . The PE-g-MA loading level of 5.7% resulted in the best effect based on the two parameters, which is in agreement with Figure 4.1. The use of PE-g-MA slightly improved the recoverability of the composite.

Both E_M and η_M of the composites were reduced with the addition of sEPR-g-MA or aEPR-g-MA, but there was some quantitative difference. For sEPR-g-MA, the major effect was observed on E_M when its content increased from 5.7% to 8.3%. For aEPR-g-MA, the major effect was observed on η_M when its content increased from 2.9% to 5.7%. Moreover, sEPR-g-MA increased the creep recoverability of the composite, but aEPR-g-MA slightly decreased the recoverability of the composite. Comparatively, the addition of aEPR-g-MA resulted in smaller values for both E_M and η_M compared with sEPR-g-MA at the same level.

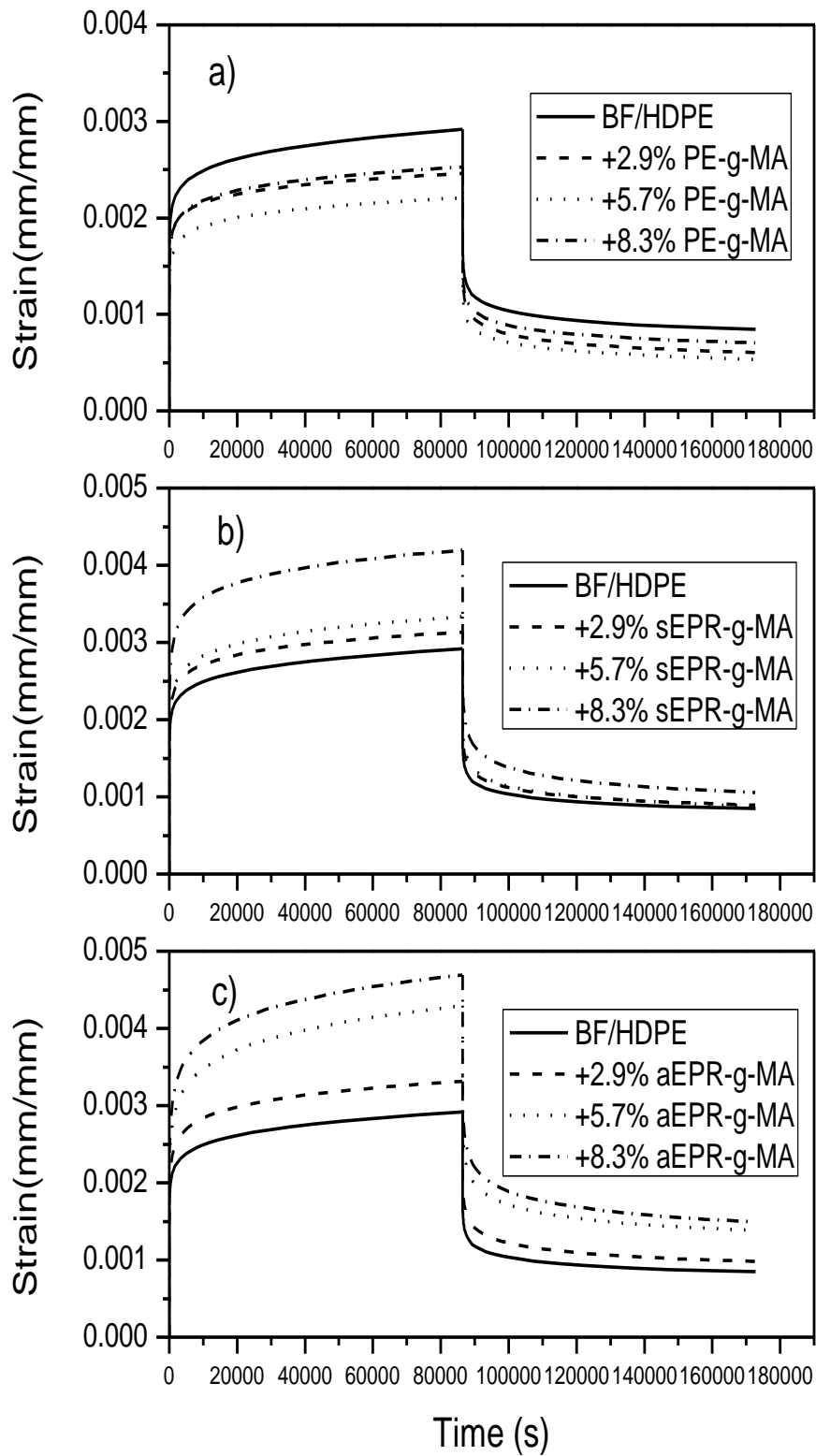


Figure 4.1 Creep and recovery curves of BF/HDPE composites with individual modifier: a) PE-g-MA, b) sEPR-g-MA, and c) aEPR-g-MA.

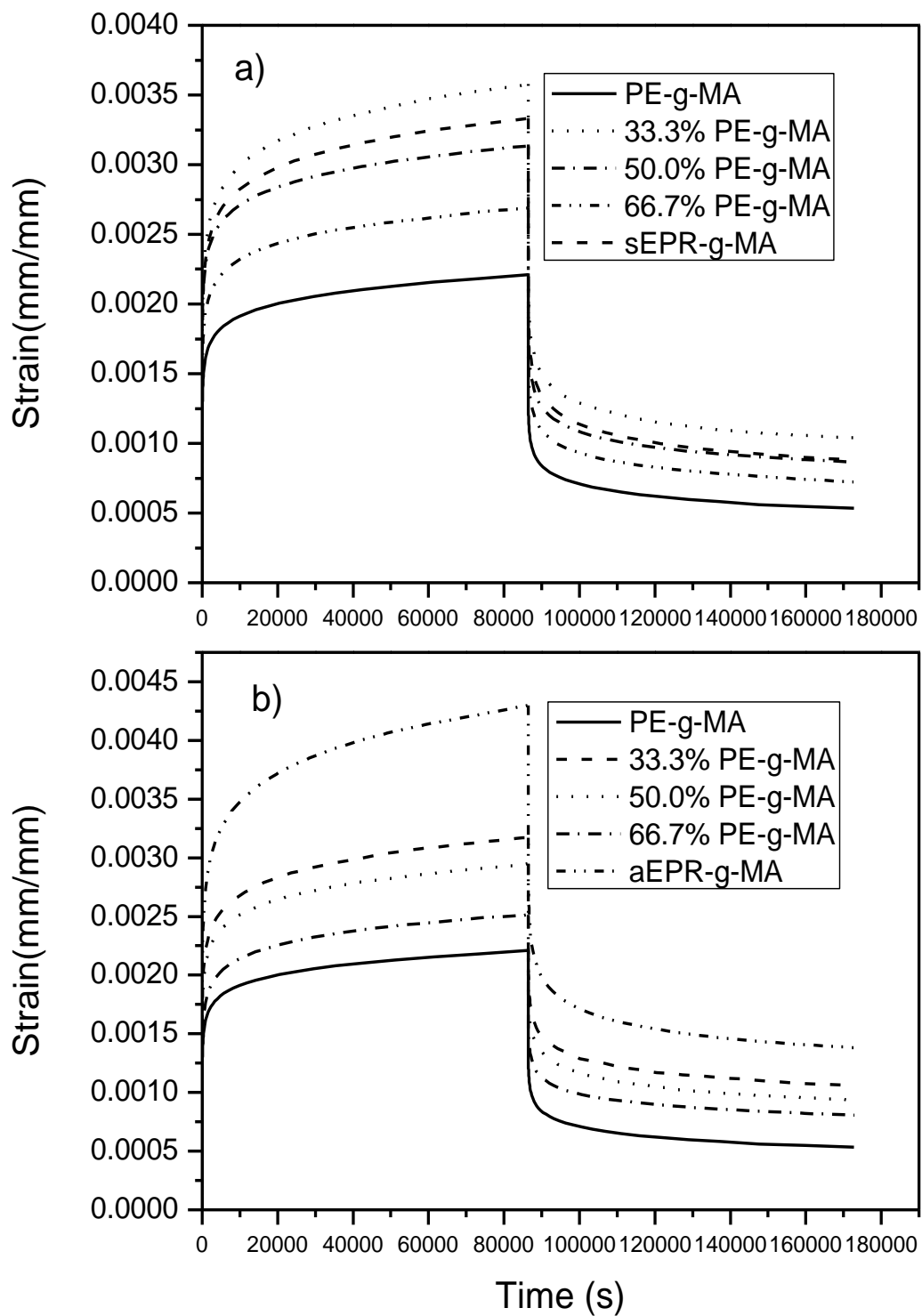


Figure 4.2 Creep and recovery curves of BF/HDPE composites with combined modifier at 5.7% level: a) PE-g-MA/sEPR-g-MA and b) PE-g-MA/aEPR-g-MA.

Table 4.1 Summary of parameters in Burgers model and recovery rate for one-day creep of the composites with individual modifiers

Composite	Modifier content (%)	E_M (MPa)	E_K (MPa)	η_k (10^{13} Pa s)	η_M (10^{14} Pa s)	WSS	Recovery rate (%)
HDPE	-	334.5	751.9	0.39	1.43	0.000814	73.32
BF/HDPE	0	975.6	3816.8	2.58	4.90	0.000035	71.01
BF/HDPE/ PE-g-MA	2.9	1129.9	4504.5	2.56	6.70	0.000035	75.47
	5.7	1298.7	4662.0	2.68	6.99	0.000022	75.88
	8.3	1136.4	4081.6	2.43	6.02	0.00003	72.08
BF/HDPE/ sEPR-g-MA	2.9	917.4	3262.6	1.83	4.83	0.000049	71.44
	5.7	900.9	2770.1	1.74	4.24	0.000066	73.61
	8.3	714.3	2169.2	1.32	3.51	0.000101	74.84
BF/HDPE/ aEPR-g-MA	2.9	885.0	2911.2	1.82	4.46	0.000055	70.36
	5.7	760.5	1923.1	1.36	2.65	0.00011	67.83
	8.3	689.7	1739.1	1.20	2.60	0.000147	68.21

Table 4.2 Summary of parameters in Burgers model for one-day creep of the composites with combined modifiers

Composite	PE-g-MA percentage (%)	E_M (MPa)	E_K (MPa)	η_k (10^{13} Pa s)	η_M (10^{14} Pa s)	WSS	Recovery rate (%)
HDPE	-	334.5	751.9	0.39	1.43	0.000814	73.32
BF/HDPE	-	975.6	3816.8	2.58	4.90	0.000035	71.01
BF/HDPE/ PE-g-MA/	33.3	869.57	2448	1.54	3.62	0.000077	71.01
PE-g-MA/ sEPR-g-MA	50.0	909.09	3294.9	2.01	4.99	0.000046	72.38
PE-g-MA/ aEPR-g-MA	66.7	1075.3	3683.2	2.19	5.75	0.00003	73.05
BF/HDPE/ PE-g-MA/	33.3	934.58	3016.6	2.05	4.44	0.000047	66.51
PE-g-MA/ aEPR-g-MA	50.0	990.1	3401.4	2.19	4.98	0.00004	68.22
PE-g-MA/ aEPR-g-MA	66.7	1183.4	3745.3	2.36	5.76	0.000034	67.86

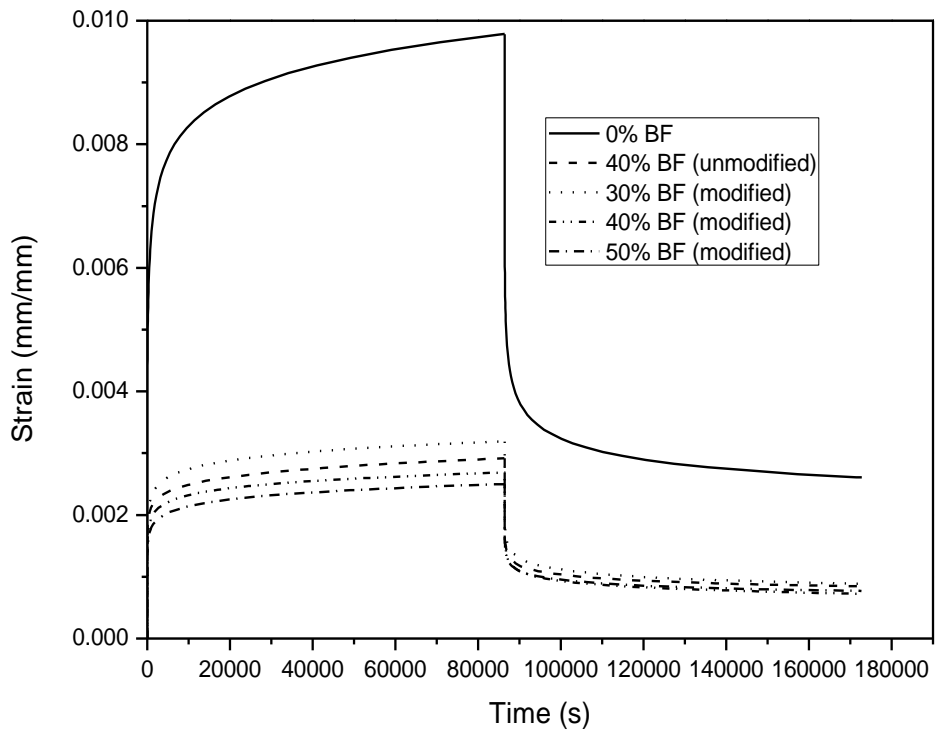


Figure 4.3 Creep and recovery curves of HDPE, BF/HDPE without modifier, BF/HDPE composites at different BF loading levels with combined modifier of PE-g-MA/sEPR-g-MA at 15 wt% of the BF loading and PE-g-MA/sEPR-g-MA ratio of 2:1.

Table 4.3 Summary of parameters in Burgers model for one-day creep of the composites with different BF loading levels

Composite	BF loading (%)	E_M (MPa)	E_K (MPa)	η_k (10^{13} Pa s)	η_M (10^{14} Pa s)	WSS	Recovery rate (%)
HDPE	-	334.5	751.9	0.39	1.43	0.000814	73.32
Uncompatibilized	40	975.6	3816.8	2.58	4.90	0.000035	71.01
	30	917.43	3030.3	1.84	4.71	0.000052	72.20
Compatibilized	40	1075.3	3683.2	2.19	5.75	0.000003	73.05
	50	1169.6	3891.1	2.49	5.91	0.000029	69.20

4.3.2 Effect of Combined Modifiers

The creep curves of the samples with 5.7% combined modifier of PE-g-MA/sEPR-g-MA are shown in Figure 4.2(a). The smallest creep strain was observed for the sample with only PE-g-MA. As the percentage of PE-g-MA was reduced, the creep strain increased gradually. However, 5.7% combined modifier of PE-g-MA and sEPR-g-MA at 1:2 ratio resulted in larger creep strain than either 5.7% of sEPR-g-MA or 5.7% PE-g-MA, suggesting that combined modifiers may have a worse effect than either of its components presumably due to the incompatibility between the two components.

Figure 4.2(b) shows the creep curves of the samples with 5.7% combined modifier of PE-g-MA/aEPR-g-MA. Again, the smallest creep strain was observed for the sample with PE-g-MA as the individual modifier. The creep strain increased as the percentage of PE-g-MA decreased in the combined modifier. It should be noted that although aEPR-g-MA individually increased creep strains of the samples more than sEPR-g-MA, it resulted in relatively better creep resistance when being used together with PE-g-MA.

The Burgers parameters for the composites with the two combined modifiers are listed in Table 4.2. As shown, the addition of the combined modifiers showed different effects on the creep property of BF/HDPE with different PE-g-MA/EPR-g-MA ratios. Higher PE-g-MA contents in the combined modifier resulted in larger E_M and η_M . For PE-g-MA/sEPR-g-MA, a positive effect on creep resistance was achieved at PE-g-MA/sEPR-g-MA ratio of 2:1. However, for PE-g-MA/aEPR-g-MA, the enhancing effect was obtained at PE-g-MA/aEPR-g-MA ratio of 1:1 and higher.

Comparing PE-g-MA/sEPR-g-MA and PE-g-MA/aEPR-g-MA, the former had higher values of all four Burgers parameters at PE-g-MA/EPR-g-MA ratio of 1:2. As the ratio increased,

the difference on η_M became negligible. Again, the PE-g-MA/sEPR-g-MA combined modifier improved the recoverability of the composite but the PE-g-MA/aEPR-g-MA combined modifier decreased it.

4.3.3 Effect of BF Loading

Figure 4.3 shows the creep and recovery curves of HDPE, BF/HDPE without modifier, BF/HDPE composites at different BF loading levels with combined modifier of PE-g-MA/sEPR-g-MA at 15 wt% of the BF loading and PE-g-MA/sEPR-g-MA ratio of 2:1. The addition of BF dramatically improved the creep resistance of HDPE due to its high modulus. With BF loading increased from 30% to 50% at the presence of combined modifier, the creep strain of the composite decreased. There was a clear trend that the increase of BF loading rate led to better creep resistance of the composites. However, the recovery process was more complicated. Although 50% BF loading resulted in smaller creep strain than 40% BF loading, it showed slightly higher strain residual after a one-day recovery. Table 4.3 shows that the sample with 40% BF loading had the highest recovery percentage. The recoverability of the samples failed to show a clear trend with different BF loading levels.

4.3.4 Morphological Analysis on the Creep Mechanism of the Composites

Four additives were applied in the HDPE matrix in this study: BF, PE-g-MA, sEPR-g-MA, and aEPR-g-MA, with their modulus in a decreasing order. With the observation and discussion above, three roles of the additives on creep resistance of the composites can be proposed to explain the experimental observations. The first is the volume effect, where the additives reduced the relative volume of viscoelastic polymer matrix, which is prone to creep. The second is the bridging effect, where the additives sustained part of the stress by connecting to each other. The third is the blocking effect, where the additives interacted with the molecular

chains of polymer matrix and blocked them from moving under stress. BF alone showed significant enhancing effect on the HDPE matrix by exhibiting the first two effects. Adding a high percentage of the stiff BF largely decreased the relative volume of HDPE matrix, leaving less material to creep under stress and improving the overall creep resistance of the composite. Also, the high percentage of BF distributed in the HDPE matrix made part of them connected to each other, so that the stress tended to be sustained by the high stiff additive network. Due to the poor interfacial adhesion between BF and HDPE matrix, BF had little effect in stabilizing the HDPE molecular chains movement.

Adding PE-g-MA into BF/HDPE composite increased the relative volume of the polymeric material which tends to creep more. However, it improved the interfacial adhesion between BF and HDPE matrix at the same time. The volume effect and blocking effect introduced by PE-g-MA are contradictive and the overall effect varied as the PE-g-MA content increased. The maximum blocking effect was achieved at a certain PE-g-MA level but the volume effect kept increasing, resulting in optimum creep resistance at the 5.7% PE-g-MA level. Addition of sEPR-g-MA or aEPR-g-MA had the similar effect, but the low moduli of the two modifiers made its volume effect dominant over the blocking effect, leading to increased creep strain even at low EPR-g-MA level.

The effect of combined modifier of PE-g-MA and EPR-g-MA was similar to the individual modifier of EPR-g-MA, but more complicated due to the compatibility between the two components. The addition of the combined modifier showed negative effect on creep resistance of the composite because of its low modulus. The relatively higher creep resistance of the composites modified with PE-g-MA/aEPR-g-MA might be obtained through a better compatibility between the two components because of the amorphous structure of aPER-g-MA.

PE-g-MA is more compatible with HDPE matrix than EPR-g-MA. Combination of PE-g-MA and aEPR-g-MA led to superior interfacial adhesion between BF and the HDPE matrix, so as to enhance the blocking effect of BF on creep of the composites.

4.3.5 Indexed Burgers Models

As shown in Table 4.4, both PIB and FIB models (i.e., Equations 4.1 and 4.2) offered better fit than the 4-element Burgers model based on WSS. This is because the power index for time extended the functioning region of the units and made them more flexible. However, the flexibility increased the variability of the parameters and made it hard to use them for comparison purposes. To solve this problem, the index was fixed at a reasonable value both the two Indexed Burgers Models. The parameters presented an order in agreement with Figure 4.1(a) with fixed index value.

4.3.6 Creep Prediction

4.3.6.1 Prediction Through Modeling

The Burgers model parameters were used to characterize the creep curves and showed good agreement with the curves. This modeling technique can only be used for characterization purposes within the test period. Attempt to use the Burgers model for the prediction of long-term creep behavior led to large error, as shown in Figure 4.4, in which the one-day creep was predicted with the parameters obtained from the creep data for the first three hours.

The PIB model (i.e., Equation 4.1) offered much better prediction than the 4-element Burgers model, but it still over-predicted the creep deformation. The FIB model (i.e., Equation 4.2) and the power law model performed better in terms of prediction. The one-day creep, predicted with the parameters obtained from the first three hour data, showed good agreement with the experimental curve, as shown in Figure 4.4.

Table 4.4 Summary of the parameters for the new models in comparison with the 4-element Burgers model for BF/HDPE/PE-g-MA composites

Model	PE-g-MA (%)	$b1$	$b2$	$b3$	$b4$	n	WSS
4-element	0	0.00205	0.000524	0.000148	4.08E-09	1	0.000035
	2.9	0.00177	0.000444	0.000176	2.98E-09	1	0.000027
	5.7	0.00154	0.000429	0.000174	2.86E-09	1	0.000022
	8.3	0.00176	0.00049	0.000168	3.32E-09	1	0.00003
PIB model	0	-0.00022	0.00563	0.3088	1.20E-09	0.081	2.55E-07
	2.9	-0.00048	0.00384	0.5051	5.54E-10	0.090	2.13E-07
	5.7	0.00058	0.00183	0.2398	8.10E-10	0.183	5.42E-08
	8.3	0.000407	0.00268	0.2872	6.65E-10	0.144	1.17E-07
PIB with fixed index	0	0.00111	0.00213	0.1641	1.38E-09	0.2	5.76E-07
	2.9	0.00084	0.00175	0.2192	9.88E-10	0.2	3.43E-07
	5.7	0.00067	0.00168	0.2102	8.93E-10	0.2	5.85E-08
	8.3	0.00081	0.00193	0.1953	9.53E-10	0.2	1.62E-07
FIB model	0	0.00097	0.00097	0.3641	0.000063	0.242	2.68E-07
	2.9	0.00082	0.00101	0.3143	0.00004	0.244	1.41E-07
	5.7	0.00086	0.000827	0.1926	0.000021	0.285	4.58E-08
	8.3	0.00090	0.00097	0.2386	0.000034	0.260	6.28E-08
FIB with fixed index	0	0.00103	0.000945	0.3286	0.000056	0.25	2.70E-07
	2.9	0.00085	0.000992	0.2953	0.000036	0.25	1.41E-07
	5.7	0.00073	0.000901	0.2713	0.000034	0.25	6.81E-08
	8.3	0.00086	0.000994	0.2643	0.00004	0.25	6.50E-08

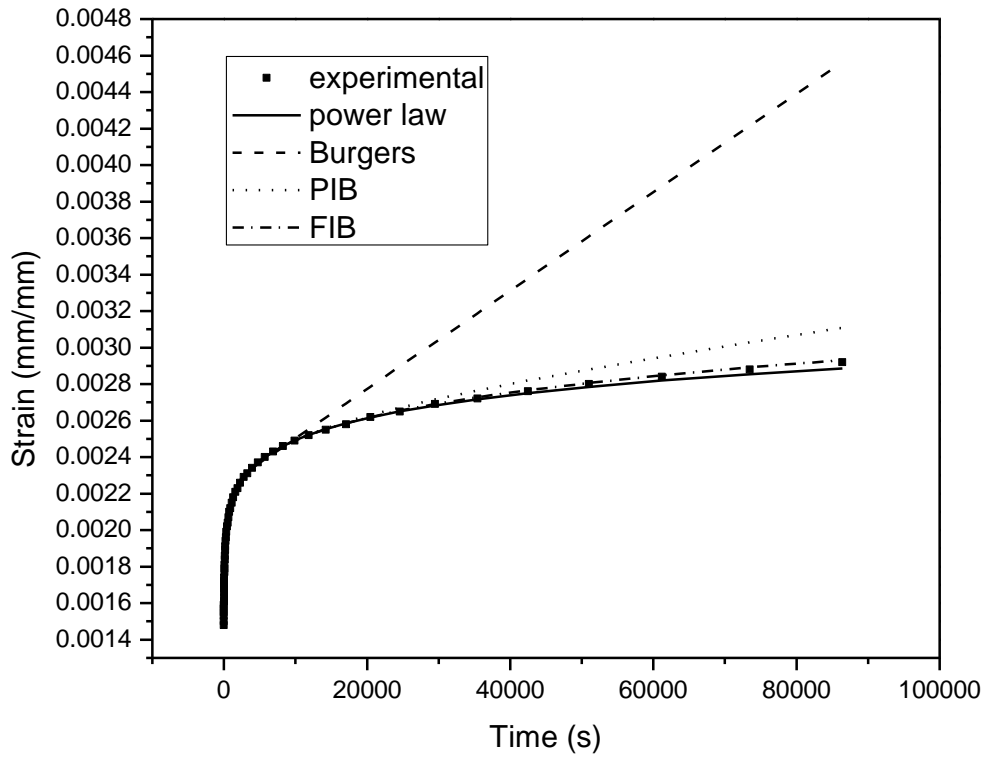


Figure 4.4 Comparison of Burgers model, PIB and FIB models with fixed index, and power law model used to predict one-day creep of BF/HDPE composite without modifier based on three-hour creep data.

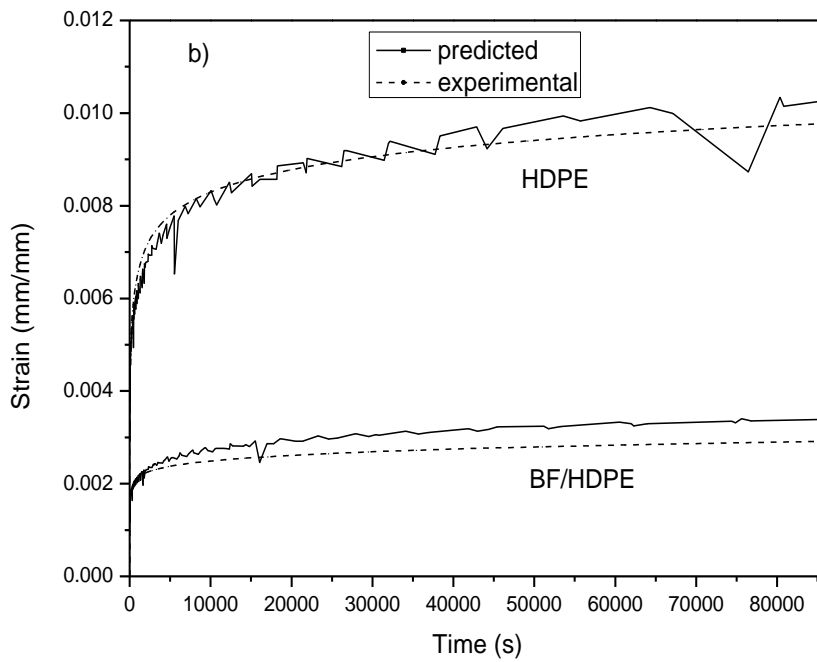
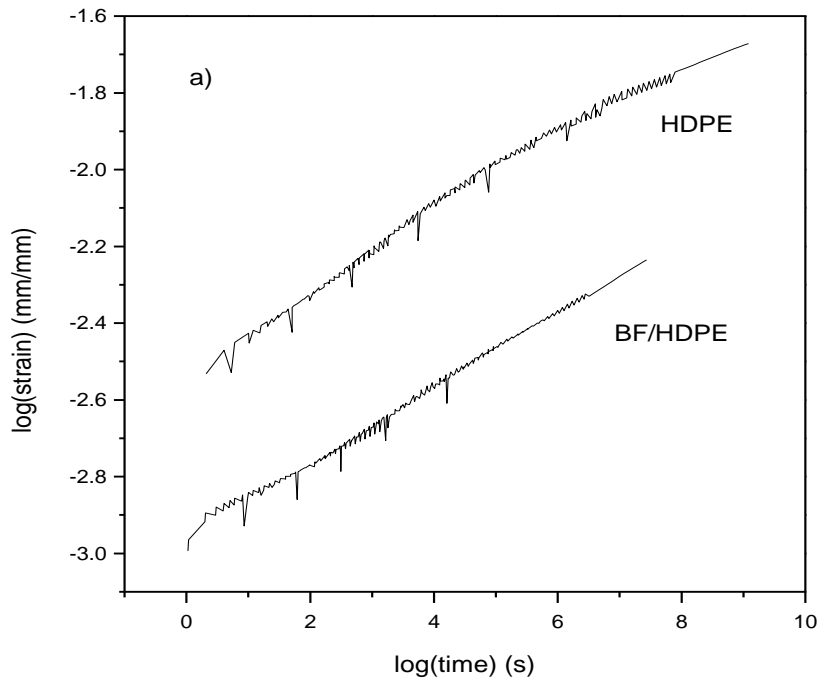


Figure 4.5 HDPE and BF/HDPE composite without modifier: a) TTS masters and b) Comparison of the TTS predicted creep curves with the experimental curves.

4.3.6.2 Prediction Through TTS

Smooth master curves were obtained through horizontal shifts of the short-term creep curves in logarithmic scales. Typical curves can be seen in Figure 4.5(a). To verify these master curves, they were transferred to regular time scale and compared with the long-term creep curves, as shown in Figure 4.5(b). For pure HDPE, TTS prediction had a good agreement with the experimental curve. However, TTS slightly over-predicted the creep strain of BF/HDPE composite. The same trend was observed for the BF/HDPE composites with modifiers.

4.4 CONCLUSIONS

The creep behaviors of bamboo flour (BF)/HDPE composites were investigated to examine the effect of coupling agents on creep property of the composites. The addition of PE-g-MA enhanced the creep resistance of BF/HDPE composites at different loading levels and achieved the optimum effect at the concentration of 5.7%. The incorporation of either sEPR-g-MA or aEPR-g-MA decreased the creep resistance of BF/HDPE composites. Comparatively, the composites with sEPR-g-MA showed better creep resistance than those with aEPR-g-MA. However, when being combined with PE-g-MA, aEPR-g-MA resulted in better creep property than sEPR-g-MA. In the combined modifiers, higher percentage of PE-g-MA led to better creep resistance. Physical model (i.e., Burgers model) was able to characterize creep property of the composites, but it was not applicable for long-term prediction purposes. Power index for *time* was introduced to the 4-element burgers model and it was found that both PIB model and FIB model can be applied for characterization/comparison purposes when the index was fixed. The FIB model, as well as the power law model, offered better long-term prediction based on the short-term data. Time-temperature superposition (TTS) produced smooth master curves through

horizontal shifts, but they slightly over-predicted the long-term creep for most of the BF/HDPE composites.

4.5 REFERENCES

Acha, B. A., M. M. Reboredo, and N. E. Marcovich. 2007. Creep and dynamic mechanical behavior of PP-jute composites: Effect of the interfacial adhesion. *Composites Part a-Applied Science and Manufacturing* **38**:1507-1516.

Bansal, A. K. and S. S. Zoolagud. 2002. Bamboo composites: Material of the future. *Journal of Bamboo and Rattan* **1**:119-130.

Bledzki, A. K. and O. Faruk. 2004. Creep and impact properties of wood fibre-polypropylene composites: influence of temperature and moisture content. *Composites Science and Technology* **64**:693-700.

Chen, X., Q. Guo, and Y. Mi. 1998. Bamboo fiber-reinforced polypropylene composites: A study of the mechanical properties. *Journal of Applied Polymer Science* **69**:1891-1899.

Ge, X. C., X. H. Li, and Y. Z. Meng. 2004. Tensile properties, morphology, and thermal behavior of PVC composites containing pine flour and bamboo flour. *Journal of Applied Polymer Science* **93**:1804-1811.

Hristova, J., V. Valeva, and J. Ivanova. 2002. Aging and filler effects on the creep model parameters of thermoset composites. *Composites Science and Technology* **62**:1097-1103.

Kazayawoko, M., J. J. Balatinecz, and R. N. S. Sodhi. 1999. X-ray photoelectron spectroscopy of maleated polypropylene treated wood fibers in a high-intensity thermokinetic mixer. *Wood Science and Technology* **33**:359-372.

Kazayawoko, M., J. J. Balatinecz, and R. T. Woodhams. 1997. Diffuse reflectance Fourier transform infrared spectra of wood fibers treated with maleated polypropylenes. *Journal of Applied Polymer Science* **66**:1163-1173.

Lai, S.-M., F.-C. Yeh, Y. Wang, H.-C. Chan, and H.-F. Shen. 2003. Comparative study of maleated polyolefins as compatibilizers for polyethylene/wood flour composites. *Journal of Applied Polymer Science* **87**:487-496.

Liu, H., Q. Wu, G. Han, F. Yao, Y. Kojima, and S. Suzuki. 2008. Compatibilizing and toughening bamboo flour-filled HDPE composites: Mechanical properties and morphologies. *Composites Part A: Applied Science and Manufacturing* **39**:1891-1900.

Marcovich, N. E. and M. A. Villar. 2003. Thermal and mechanical characterization of linear low density polyethylene/wood flour composites. *Journal of Applied Polymer Science* **90**:2775-2784.

Mi, Y., X. Chen, and Q. Guo. 1997. Bamboo fiber-reinforced polypropylene composites: Crystallization and interfacial morphology. *Journal of Applied Polymer Science* **64**:1267-1273.

Nunez, A. J., N. E. Marcovich, and M. I. Aranguren. 2004. Analysis of the creep behavior of polypropylene-woodflour composites. *Polymer Engineering and Science* **44**:1594-1603.

Nunez, A. J., P. C. Sturm, J. M. Kenny, M. I. Aranguren, N. E. Marcovich, and M. M. Reboredo. 2003. Mechanical characterization of polypropylene-wood flour composites. *Journal of Applied Polymer Science* **88**:1420-1428.

Oksman, K. and C. Clemons. 1998. Mechanical properties and morphology of impact modified polypropylene-wood flour composites. *Journal of Applied Polymer Science* **67**:1503-1513.

Okubo, K., T. Fujii, and Y. Yamamoto. 2004. Development of bamboo-based polymer composites and their mechanical properties. *Composites Part A: Applied Science and Manufacturing* **35**:377-383.

Sain, M. M., J. Balatinecz, and S. Law. 2000. Creep fatigue in engineered wood fiber and plastic compositions. *Journal of Applied Polymer Science* **77**:260-268.

Sombatsompop, N., C. Yotinwattanakumtorn, and C. Thongpin. 2005. Influence of type and concentration of maleic anhydride grafted polypropylene and impact modifiers on mechanical properties of PP/wood sawdust composites. *Journal of Applied Polymer Science* **97**:475-484.

Thwe, M. M. and K. Liao. 2000. Characterization of bamboo-glass fiber reinforced polymer matrix hybrid composite. *Journal of Materials Science Letters* **19**:1873-1876.

Thwe, M. M. and K. Liao. 2003. Durability of bamboo-glass fiber reinforced polymer matrix hybrid composites. *Composites Science and Technology* **63**:375-387.

Wang, Y., F.-C. Yeh, S.-M. Lai, H.-C. Chan, and H.-F. Shen. 2003. Effectiveness of functionalized polyolefins as compatibilizers for polyethylene/wood flour composites. *Polymer Engineering & Science* **43**:933-945.

CHAPTER 5 CREEP BEHAVIOR OF COMPOSITES ENHANCED WITH ENGINEERING PLASTIC MICROFIBRILS

5.1 INTRODUCTION

Wood plastic composites (WPCs) have been mainly based on polyolefin (i.e., PE and PP) and PVC resins due to the poor thermal stability of wood fibers. The properties of these composites are often not sufficient for structural applications. Different ways have been attempted to enhance the properties of WPCs. For example, structural WPCs with high flexural toughness were made through cross-linking (Bengtsson et al. 2007). However, these kinds of products are not easily recyclable and lose one of the main advantages of WPCs. Engineering plastics were used as polymer matrices for WPCs in order to obtain better mechanical properties (Klason et al. 1984), but high processing temperatures needed for engineering plastics caused thermal degradation for the cellulose fibers (Caufield et al. 2001).

By incorporating microfibrils of high-melting temperature engineering plastics into low-melting thermoplastic matrices, new kinds of polymer blends, known as microfibrillar composites (MFCs), were obtained (Fakirov et al. 1993, Friedrich et al. 2005). With better mechanical properties than the single-phase thermoplastic matrix and the same processing temperature, this blend offers a good choice as the matrix for WPCs. Some work was done on the application of MFCs in WPCs but no examination on their creep properties was reported (Lei et al. 2009b). Due to the common existence of stress in structural building products, creep resistance is essential to the application of this new product aimed for structural applications.

Previous creep research on WPCs were focused on the effect of wood flour, including loading levels and wood flour treatment (Sain et al. 2000, Nunez et al. 2004), and additives, such as coupling agents (Bledzki and Faruk 2004, Nunez et al. 2004), on creep resistance of WPCs.

Modeling techniques have been applied to analyze and evaluate the creep behavior of the composites (Marcovich and Villar 2003, Nunez et al. 2004). Time-temperature superposition (TTS) has also been tried to predict long-term creep deformation of NFPCs from the accelerated tests at higher temperature levels (Nunez et al. 2004). However, little research has been done on enhancing the creep resistance of WPCs through the modification of polymer matrix.

In this research, wood flour was successfully mixed into two pre-mixed MFCs, i.e., high density polyethylene (HDPE)/polyamide 6 (PA6) blend and HDPE/ polyethylene terephthalate (PET) blend, under the processing temperature of HDPE (Lei et al. 2009a, Liu et al. 2009). The creep properties of these WPCs were investigated and analyzed. The objective of this study was to evaluate the effect of engineering plastic microfibrils on polymer and WPC in terms of creep resistance.

5.2. EXPERIMENTAL

5.2.1 Materials

5.2.1.1 HDPE/PA6 System

The HDPE was HD6706.17 from Exxon-Mobil Chemical Co, with a melt flow index of 6.1 g/10min (190 °C, 2.16 kg) and a density of 0.952 g/cm³. An injection-molding grade PA6 (Aegis H8202NLB) was provided by Honeywell Co., with a density of 1.13 g/cm³ and a melting temperature (T_m) of 220 °C. A maleated polyethylene (*PE-g-MA*) (Fusabond MB100D) was supplied by Dupont Co., with a MA grafting ratio of about 1 wt% and a melt flow index of 2 g/10min (190 °C, 2.16 kg). Wood flour (WF) was provided by American Wood Fibers Inc. (Madison, MI), with a 40-mesh particle size. Both PA6 and WF were dried at 90 °C for 24 hours in an oven prior to use.

5.2.1.2 HDPE/PET System

The PET pellets were provided by Avangard Industries, Ltd. (Houston, TX) with a melting peak temperature of 237.6 °C (10 °C/min) and a density of 1.33 kg/m³. HDPE (HGB-0760) pellets were from Channel Prime Alliance (Des Moines, IA), with a density of 960 kg/m³ and a melt index of 0.70 g/10min (190 °C). An ethylene-glycidyl methacrylate copolymer (E-GMA) (LOTADER[®] AX 8840) was provided by Arkema Inc. (Philadelphia, PA), with a melt index of 5 g/10min (190 °C, 2.16 kg) and a glycidyl methacrylate content of 8%. A PE-g-MA (G-2608) was purchased from Eastman Chemical Company (Kingsport, TN), with a melt index of 8 g/10min (190 °C, 2.16 kg) and an acid number of 8 mg KOH/g. WF was from American Wood Fiber Co. (Madison, MI), with a 40-mesh particle size.

5.2.2 Preparation of the Composites

5.2.2.1 HDPE/PA6 System

HDPE, PA6 and PE-g-MA were fed in an intermesh, counter-rotating Brabender twin-screw extruder (Brabender Instruments Inc., Hackensack, NJ) with a weight ratio of 70/30/3. The extruding speed was 40 rpm and the extruding temperature was between 220 - 235°C to melt PA6 during extrusion. The extruded strands passed through a water bath before being drawn and cut into pellets with a diameter of around 1 mm.

The HDPE/PA6 pellets were then extruded to make WPC with WF and PE-g-MA at a weight ratio of 70/30/1.1, an extruding speed of 40 rpm and a temperature profile between 170 - 175°C. As a comparison, a composite with pure HDPE, WF and PE-g-MA was also extruded into WPC with the same weight ration and processing condition.

Standard mechanical test samples were prepared through injection molding on Battenfeld Plus 35 (Battenfeld of American Inc. South Elgin, IL) at 190 °C with four formulations: pure

HDPE, HDPE/PA6 composite, HDPE/WF composite, and HDPE/PA6/WF composite. The impact test specimens with cross-section size of around 3 mm × 12 mm were further machined for creep tests.

5.2.2.2 HDPE/PET System

HDPE and PET at a weight ratio of 75/25 were first extruded through a co-rotating twin screw extruder MIC27/GL-400 (Leistritz Corporation, Allendale, NJ) with a screw length/diameter of 40:1. The extrusion temperature was between 260 - 270 °C to melt PET and the screw rotating speed was fixed at 150 rpm. The extruded strands were directly stretched with a PV212 Puller (Al-Be Industries, Inc, Paramount, CA) without passing the water bath, and then further stretched and pelletized with a BT 25 Strand Pelletizer (Scheer Bay Co., Bay City, MI). E-GMA at 2.5 % of the total weight of PET/HDPE was used as compatibilizer for PET and HDPE.

The MFC pellets were then melt blended with dried wood flour on the same extruder with extrusion temperatures between 180 - 190 °C. Wood flour was fed by a side stuffer; the fiber to plastic weight ratio was 40/60. The loading level of PE-g-MA was 1% based on the total weight of dry wood flour and plastic matrix. The extrudates were cut into pellets after cooling in a water bath and were dried before injection molding.

The test samples for mechanical properties were made through injection molding, using a PLUS 35 injection molding machine from Battenfeld of American Inc. (South Elgin, IL). The WPC pellets were injection molded at 190 °C with a mold temperature of 85 °C. The impact test specimens with cross-section size of around 3 mm × 12 mm were further machined for creep tests.

5.2.3 Characterization

TA Q800 Dynamic Mechanical Analysis (DMA) instrument (New Castle, DE) was used for short-term creep tests with a 3-point bending mode. The test samples with approximate cross-section size of 3×12 mm were used for creep tests. In each test, the sample was heated to $35\text{ }^{\circ}\text{C}$ and allowed to equilibrate for 5 minutes. A static stress level of 4 MPa was then applied for 12 hours, and the stress was released afterward to allow the sample to recover for 12 hours. The sample deformation was measured during this process.

Accelerated creep tests were performed for 30 minutes at temperature levels starting at $35\text{ }^{\circ}\text{C}$ and increasing $10\text{ }^{\circ}\text{C}$ at a time up to $95\text{ }^{\circ}\text{C}$. After equilibrating at the desired temperature for 5 minutes, 4 MPa of stress was applied and held constant for 30 minutes while the creep strain was measured.

Morphological observations were done for the injection-molding samples using a Hitachi S-3600N VP SEM (Hitachi, Japan) as described by Lei et al. and Liu et al. (Lei et al. 2009a, Liu et al. 2009).

5.2.4 Creep Modeling

The four-element Burgers model was used to fit the creep curves.

$$\varepsilon(t) = \frac{\sigma}{E_M} + \frac{\sigma}{E_K} \left[1 - \exp\left(-t \frac{E_K}{\eta_K}\right) \right] + \frac{\sigma}{\eta_M} t \quad (5.1)$$

where $\varepsilon(t)$ is the creep strain as a function of time (t) and σ is the applied stress; E_M and E_K represent elastic moduli of the springs in this model; η_M and η_K represent viscosities of the dashpots.

Statistical Analysis System (SAS) was employed to estimate the model parameters by performing nonlinear regression on the creep curves. The Gauss-Newton iterative method was implemented in this analysis to find the least-square estimates for the nonlinear model. Since the

DMA instrument collected the data with an increasing step-size, every data point was weighted with the time interval of data collection.

5.2.5 Time-Temperature Superposition (TTS)

TTS was also applied to obtain the long term creep curves based on the accelerated testing data for different composites, as introduced in Chapter 3.

5.3 RESULTS AND DISCUSSION

5.3.1 HDPE/PA6 Composites

As shown in Figure 5.1, both the addition of 30 % WF and the introduction of 30% PA6 remarkably reduced the creep response of the HDPE matrix. In the discussion shown in Chapter 4, it was proposed that the additives played three roles on creep resistance of the composites: reducing the volume of polymer matrix (volume effect), connecting to each other to sustain part of the stress (bridging effect), and reducing the mobility of polymer molecule chains by blocking them from moving under stress (blocking effect). As shown in Figure 5.2, PA6 microfibrils were successfully obtained during the stretching process and the diameter of the microfibrils is around 2 μm (Liu et al. 2009). These microfibrils were entangled into a three dimensional network which provided good bridging effect during the creep process. Comparatively, HDPE/WF composite had better creep resistance than HDPE/PA6 composite. Besides the property differences between WF and PA6, one possible reason is that the low density of WF led to higher volume percentage than PA6 at the same weight percentage, resulting in more volume effect and bridging effect. Introducing PA6 microfibrils further decreased the creep of the HDPE/WF composite, but this improvement was less pronounced in the HDPE/PA6/WF composite than in the HDPE/PA6 composite. This phenomenon suggests that 30% WF played a dominant role in creep resistance enhancement of HDPE/PA6/WF composite.

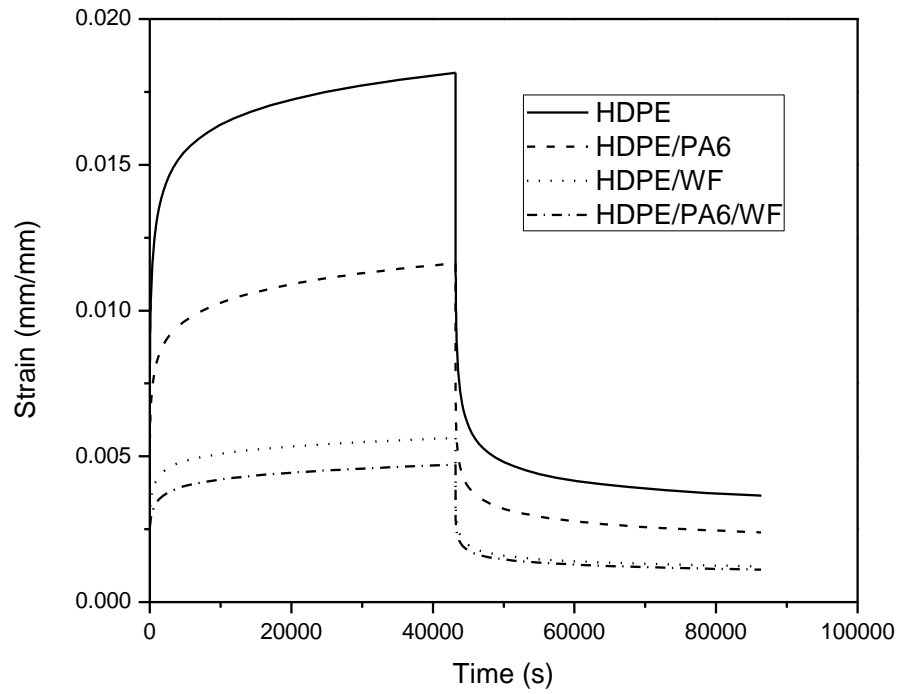


Figure 5.1 Creep and recovery behavior of different HDPE/PA6 composites.



Figure 5.2 SEM picture of HDPE/PA6 composite.

Figure 5.3 shows the curves fitted with Burgers model. The Burgers model offered a good characterization for the creep curves of the composites and the corresponding model parameters are listed in Table 5.1. The parameters showed a good agreement with what was observed in Figure 5.1. Quantitatively, the addition of WF greatly increased the elasticity and viscosity of the Maxwell unit, indicating much lower instantaneous deformation and long-term creep rate, while PA6 microfibrils only led to slight improvement on the two parameters.

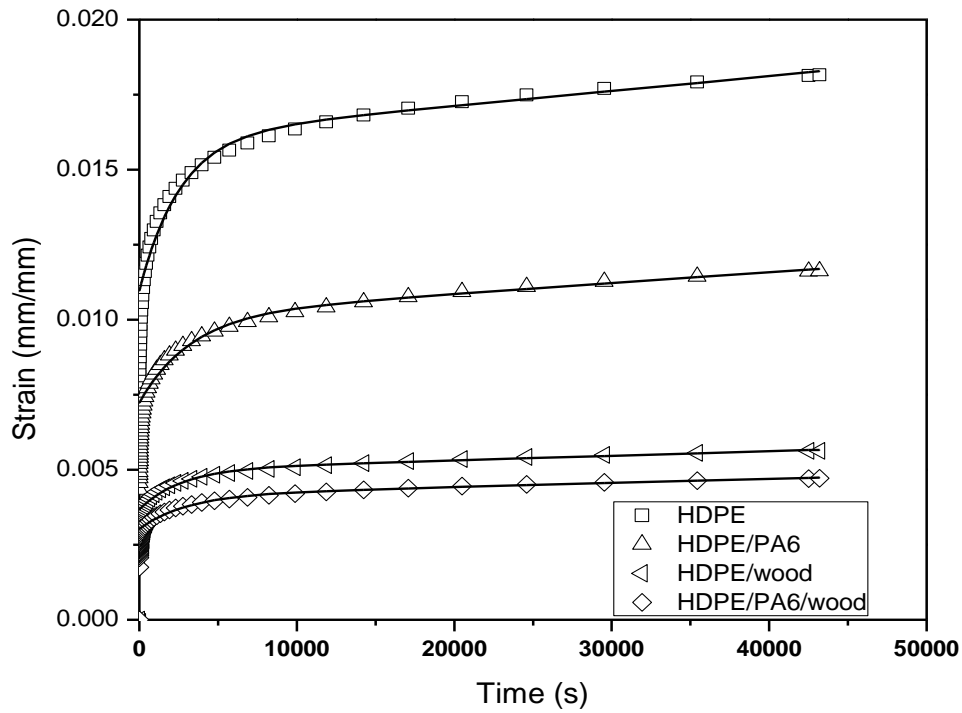


Figure 5.3 Creep strain as a function of time during creep experiment at 35°C, together with the fitted curves of Burgers model.

Table 5.1 Values of parameters for HDPE/PA6 composites obtained via fitting experimental data with Burgers model

Composite	E_M (MPa)	E_K (MPa)	η_k (Pa s)	η_M (Pa s)
HDPE	363.64	773.69	1.98E+12	8.03E+13
HDPE/PA6	553.25	1374.6	4.42E+12	1.11E+14
HDPE/WF	1087	3007.5	7.89E+12	2.63E+14
HDPE/PA6/WF	1320.1	3571.4	1.08E+13	2.92E+14

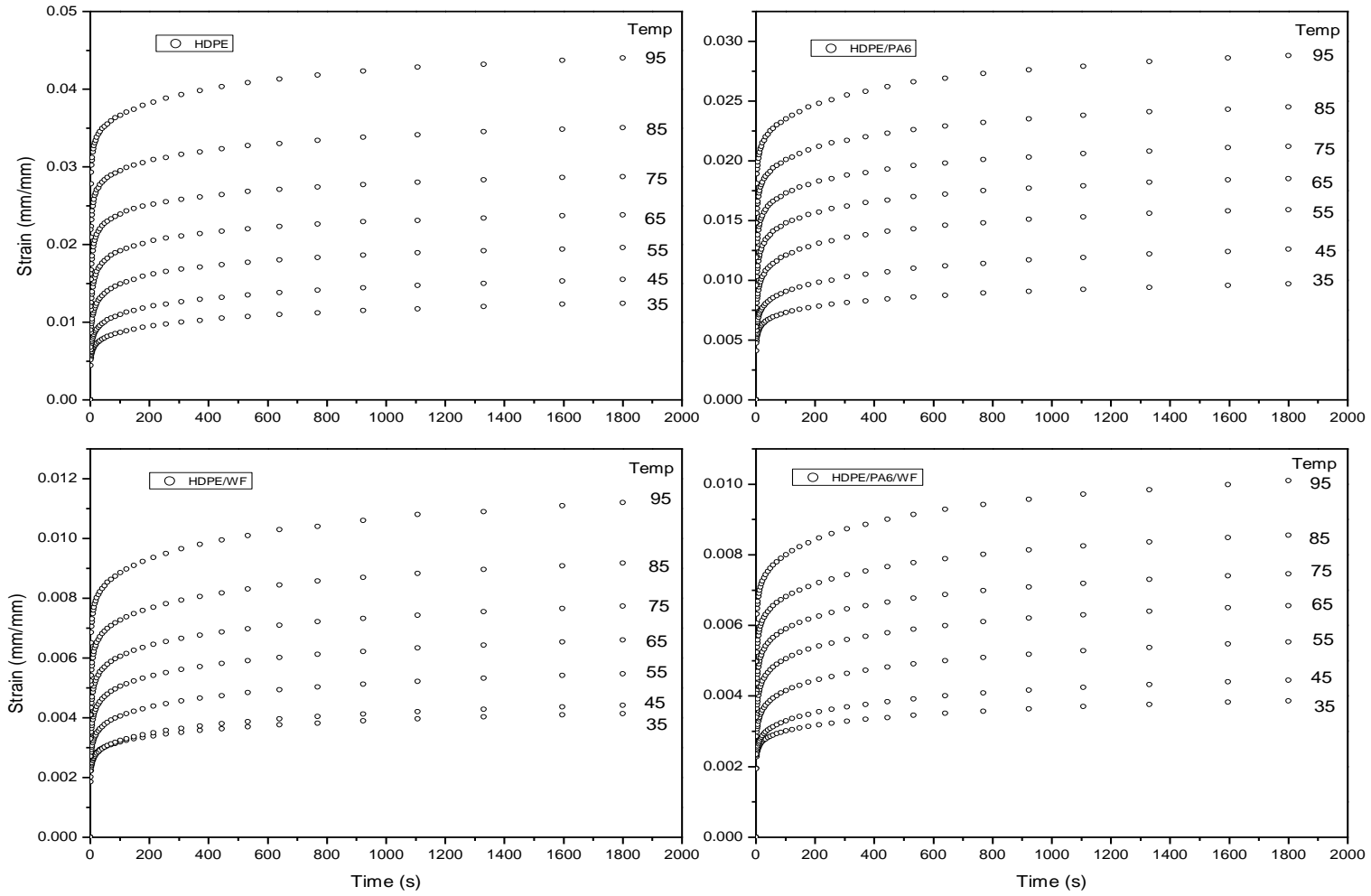


Figure 5.4 The effect of temperature on the creep behavior of different composites in HDPE/PA6 system. The unit for temperature is °C.

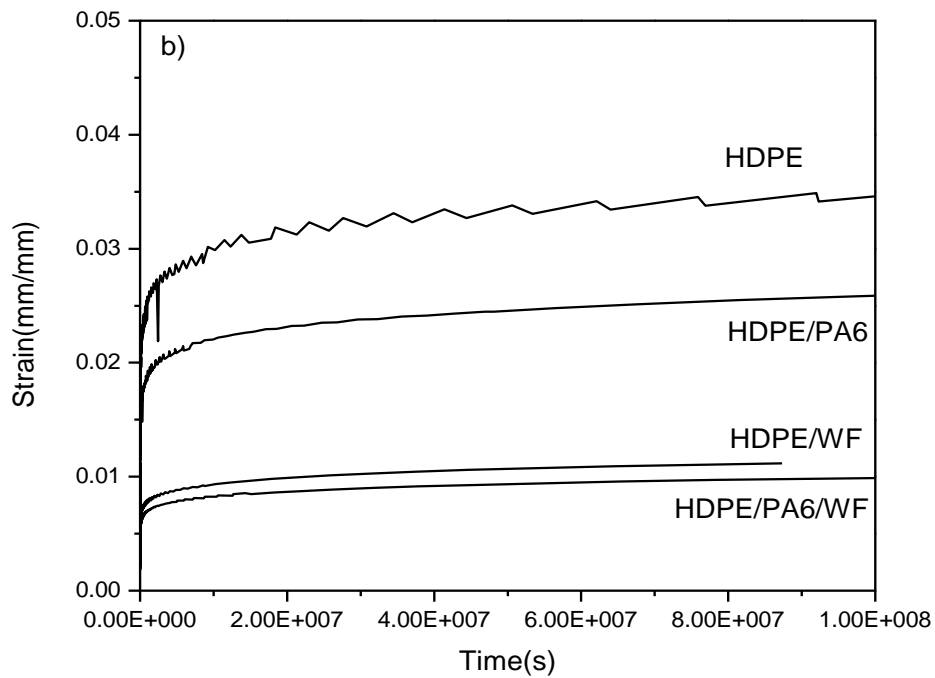
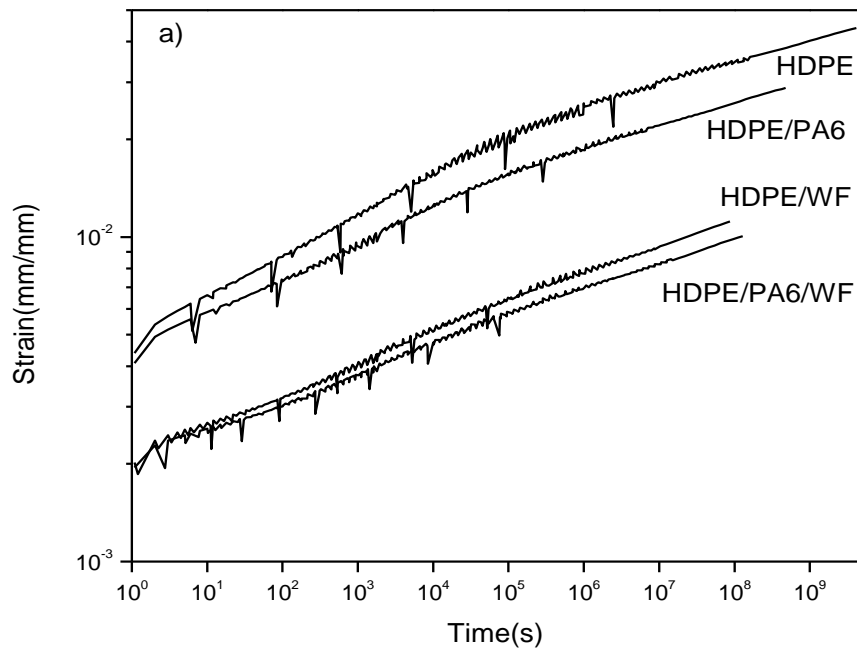


Figure 5.5 TTS master curves in logarithmic scale (a) and normal scale (b) for HDPE/PA6 composites.

Figure 5.4 shows the effect of temperature on the creep behavior of the four materials in the HDPE/PA6 system. As shown, higher temperature resulted in larger creep deformation and this effect became more evident when temperatures were high enough. Adding PA6 reduced the creep of HDPE at each temperature level, but the temperature effect remained. WF was more effective in the creep enhancement of HDPE and seemed to reduce the temperature dependence of creep of HDPE when it increased from 35 °C to 45 °C, but this effect disappeared when temperature kept increasing. Similar trend was observed for HDPE/PA6/WF composite.

Figure 5.5 shows the TTS master curves of the HDPE/PA6 composites both in logarithmic scale and in normal scale. The long-term creep deformation was predicted through horizontal shifting of the accelerated testing curves and the overall trend of the master curves were consistent with what was observed during the creep-recovery process. It is hard to examine the accuracy of TTS prediction through experiments for years. The master curves, however, offered plausible results based on which the material can be evaluated for structural applications.

5.3.2 HDPE/PET Composites

Figure 5.6 shows the creep and recovery behaviors of HDPE/PET composites in comparison with HDPE and HDPE/wood composite. As expected, both the addition of 40% wood flour and 25% PET greatly enhanced the creep resistance of PE matrix due to the high modulus of the additive. Similar to what was observed and discussed in HDPE/PA6 system, the 40% WF showed a stronger enhancing effect on creep property of HDPE than the 25% PET, possibly because of its higher volume percentage. However, it should be noted that adding 25% of PET resulted in more improvement than 30% of PA6. Except for the difference between the properties of PET and PA6, a possible explanation is the difference on their stretching ratio. Different from the HDPE/PA6 composite, no cooling process was applied during the stretching

of the HDPE/PET composite (Lei et al. 2009a). It was observed that the hot-stretching process provided higher stretching ratio, leading to finer PET microfibrils (0.5 ~ 1 μm) than PA6 microfibrils (~2 μm), as shown in Figure 5.7. Thus, the PET microfibrils were more entangled, providing higher bridging effect, and had more specific surface area which resulted in greater blocking effect together with E-GMA as coupling agent for PET and HDPE. In addition, the synergizing effect of PET and WF was better than that of PA6 and WF. The finer PET microfibrils were more prone to wind and crosslink with WF, a state in which PET fibers tended to undertake more stress. The recovery curves show that although HDPE/PET composite had higher creep deformation than HDPE/WF composite, it is more likely to recover after the stress was removed, differing from what was observed in HDPE/PA6 system. This may be attributed to both the difference in the stretching ratio and the use of E-GMA as compatibilizer for the HDPE and PET. The more entangled network of PET microfibrils prevented the composite from further non-recoverable viscous deformation after the instantaneous elastic deformation, and the improved compatibilization between the HDPE matrix and PET network enhanced this effect. This effect was also revealed in Table 5.2. Though the contribution of PET microfibrils on the elasticity of Maxwell unit (i.e., instantaneous deformation) was less profound than that of WF, the two were comparable in terms of the viscosity of Maxwell unit (i.e., long-term creep rate).

Table 5.2 Values of parameters for HDPE/PET composites obtained via fitting experimental data with Burgers model

Composite	E_M (MPa)	E_K (MPa)	η_k (Pa s)	η_M (Pa s)
HDPE	483.09	900.9	2.25E+12	8.91E+13
HDPE/PET	753.3	2197.8	5E+12	2.03E+14
HDPE/WF	1169.6	2816.9	8.67E+12	2.23E+14
HDPE/PET/WF	1785.7	4993.8	1.55E+13	3.56E+14

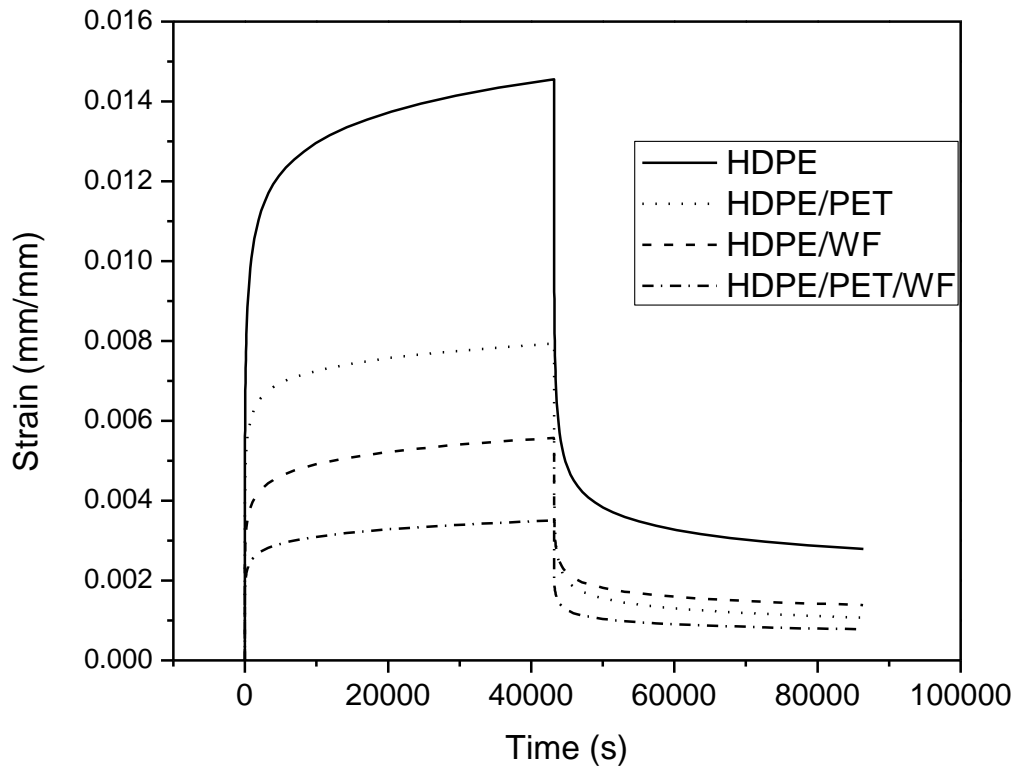


Figure 5.6 Creep and recovery behavior of the HDPE/PET composites.



Figure 5.7 SEM observation of HDPE/PET composite.

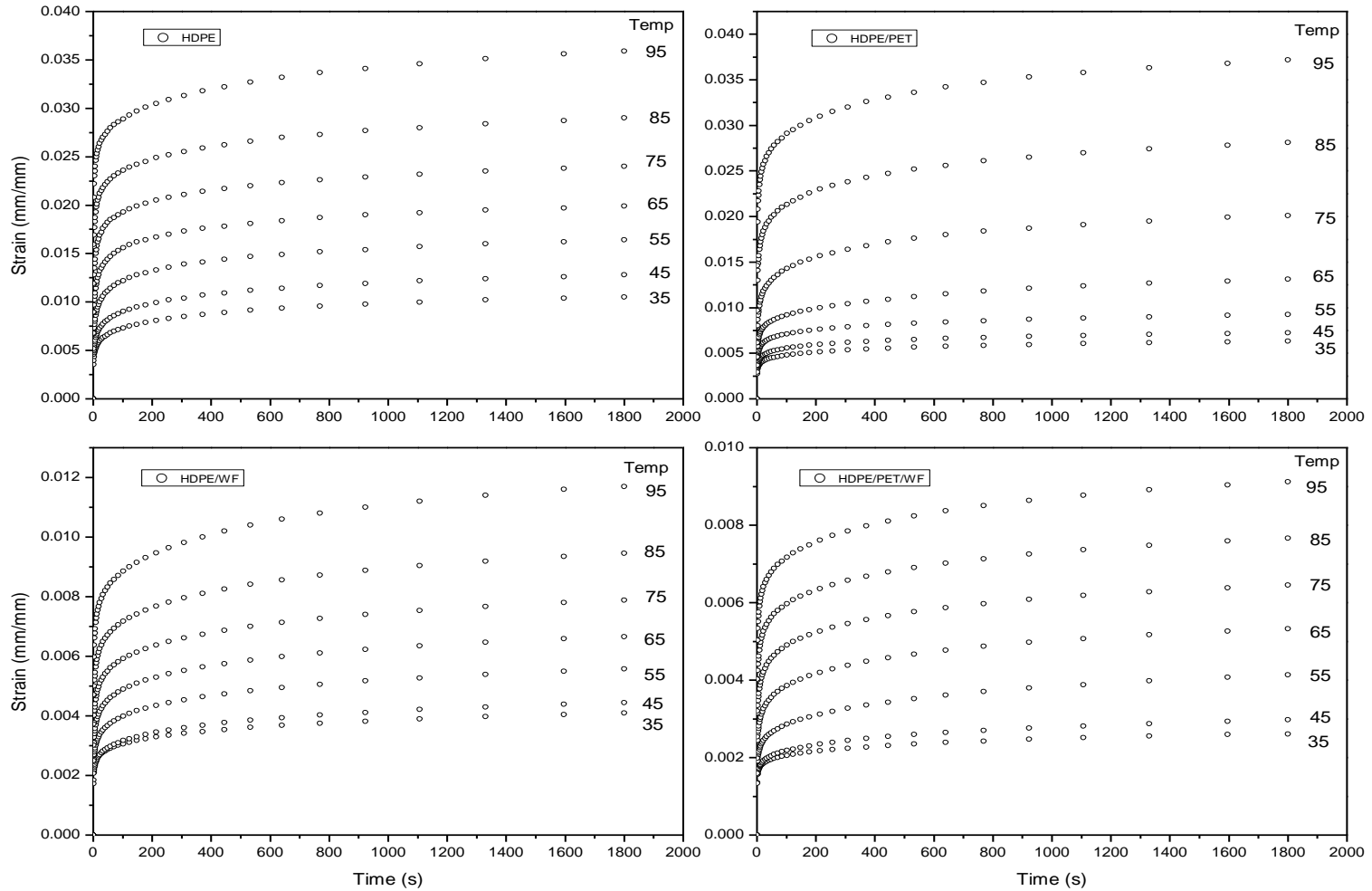


Figure 5.8 The effect of temperature on the creep behavior of different composites in HDPE/PET system. The unit for temperature is °C.

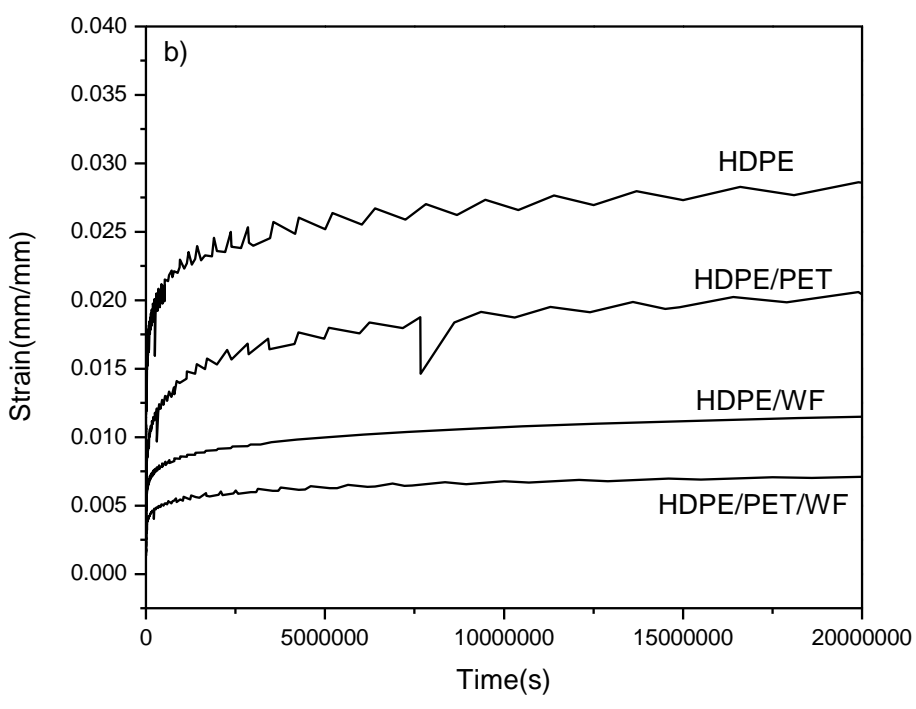
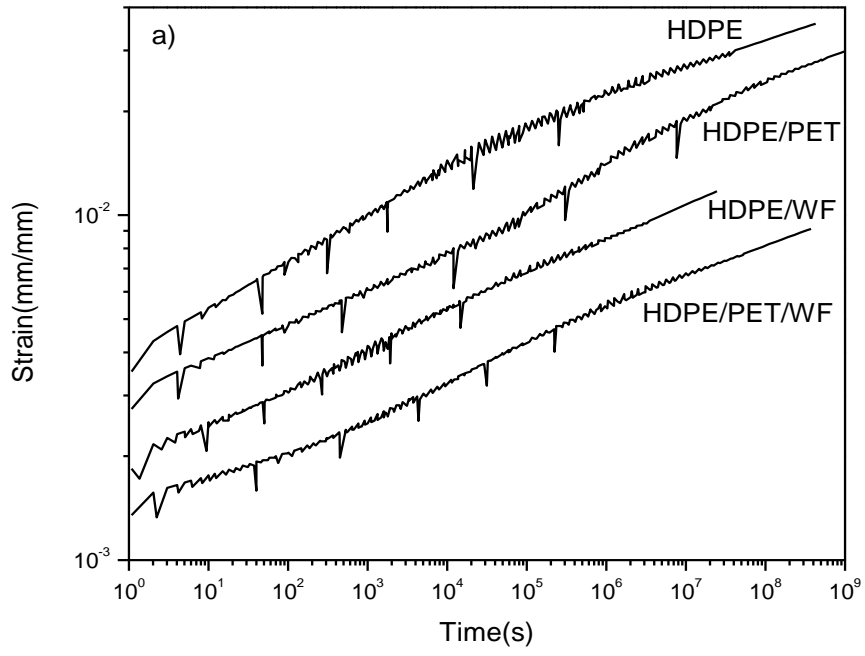


Figure 5.9 TTS master curves in logarithmic scale (a) and normal scale (b) for HDPE/PET composites.

Figure 5.8 shows the effect of temperature on the creep behavior of the four materials in the HDPE/PET system. Similar to what was observed above in HDPE/PA6 system, creep deformation of HDPE increased as temperature increased, and the increment was larger at higher temperatures. Adding WF also reduced the temperature effect on creep of HDPE when it increased from 35°C to 45°C. However, though introducing PET microfibrils reduced the creep of HDPE at low temperature, it showed much larger temperature dependence, especially starting from 65°C. As the temperature reached 95°C, the HDPE/PET composite had almost the same creep deformation as HDPE, suggesting that the PET microfibril network failed to function against creep under that temperature. This is possibly because the fine PET microfibrils network had limited strength and started to break when the stress and strain increased to a certain value. At low temperature, the strain was small and HDPE matrix sustained part of the stress. As temperature increased, the strain approached the limitation of the PET microfibril network and the stress was mainly transferred to this network due to the increased relaxation of HDPE matrix, causing the network to fail. The criteria value of the strain is around 0.01 for the PET microfibril network in the HDPE/PET composite, as shown in Figure 5.8. For the HDPE/PET/WF composites, the maximum strain at all temperature levels was within 0.01, so no increase on temperature dependence was observed.

TTS master curves of the HDPE/PET composites both in logarithmic scale and in normal scale are shown in Figure 5.9. Similar to the HDPE/PA6 system, TTS provided long-term creep prediction based on the accelerated testing results. These predictions were in good agreement with the short-term data, but further verification would be needed if it is to be used for quantitative assessment.

5.4 CONCLUSION

Engineering plastics, i.e., PA6 and PET, were introduced into WPCs in microfibril form through a two-step extrusion method, which allows WF to be incorporated at a relative low temperature and avoids thermal degradation. The engineering plastic microfibrils enhanced the creep resistance of both HDPE and HDPE/WF composites. Comparatively, adding WF led to better effect in terms of creep property, possibly because of its high volume percentage in the composites. Hot-stretching process resulted in finer PET microfibrils, which formed a more entangled network than the PA6 one. The microfibrils network was effective in reducing the non-recoverable viscous deformation of the composites. However, the microfibrils network may fail at high temperature, as observed in HDPE/PET system. The long-term creep deformations of the composites were predicted with the accelerated testing results and TTS assumption. Though it is not practical to examine their accuracy through experimental data, the master curves offered plausible results based on which the material can be evaluated for potential structural applications.

5.5 REFERENCES

- Bengtsson, M., N. M. Stark, and K. Oksman. 2007. Durability and mechanical properties of silane cross-linked wood thermoplastic composites. *Composites Science and Technology* **67**:2728-2738.
- Bledzki, A. K. and O. Faruk. 2004. Creep and impact properties of wood fibre-polypropylene composites: influence of temperature and moisture content. *Composites Science and Technology* **64**:693-700.
- Caufield, D., R. Jacobson, K. Sears, and J. Underwood. 2001. Fiber reinforced engineering plastics. 2nd International Conference on Advanced Engineered Wood Composites, Bethel, Maine.
- Fakirov, S., M. Evstatiev, and S. Petrovich. 1993. Microfibrillar reinforced composites from binary and ternary blends of polyesters and nylon 6. *Macromolecules* **26**:5219-5226.

- Friedrich, K., M. Evstatiev, S. Fakirov, O. Evstatiev, M. Ishii, and M. Harrass. 2005. Microfibrillar reinforced composites from PET/PP blends: processing, morphology and mechanical properties. *Composites Science and Technology* **65**:107-116.
- Klason, C., J. Kubat, and H.-E. Stromvall. 1984. The Efficiency of Cellulosic Fillers in Common Thermoplastics. Part 1. Filling without Processing Aids or Coupling Agents. *International Journal of Polymeric Materials* **10**:159 - 187.
- Lei, Y., Q. Wu, and Y. Xu. 2009a. High density polyethylene and poly(ethylene terephthalate) in situ nanostructured fibrillar blends as a matrix for wood-plastic composites. To be submitted.
- Lei, Y., Q. Wu, and Q. Zhang. 2009b. Morphology and properties of microfibrillar composites based on recycled poly (ethylene terephthalate) and high density polyethylene. *Composites Part A: Applied Science and Manufacturing* **40**:904-912.
- Liu, H., F. Yao, Y. Xu, and Q. Wu. 2009. Novel Wood Flour-filled Microfibrillar High Density Polyethylene and Nylon-6 Blend. *Bioresource Technology*:In submission.
- Marcovich, N. E. and M. A. Villar. 2003. Thermal and mechanical characterization of linear low density polyethylene/wood flour composites. *Journal of Applied Polymer Science* **90**:2775-2784.
- Nunez, A. J., N. E. Marcovich, and M. I. Aranguren. 2004. Analysis of the creep behavior of polypropylene-woodflour composites. *Polymer Engineering and Science* **44**:1594-1603.
- Sain, M. M., J. Balatinecz, and S. Law. 2000. Creep fatigue in engineered wood fiber and plastic compositions. *Journal of Applied Polymer Science* **77**:260-268.

CHAPTER 6 APPLICATION OF UHMWPE AND UV ABSORBER IN WOOD/HDPE COMPOSITE: MECHANICAL PROPERTIES AND CREEP BEHAVIOR

6.1 INTRODUCTION

Natural fiber/polymer composites (NFPCs) have been experiencing dramatic growth because of their low cost, sound mechanical properties, water resistance, and biodegradability. NFPCs can be made from recycled plastics and bio-based byproducts, reducing the use of non-biodegradable plastics and efficiently using natural resources. The natural appearance also makes this kind of material favorable for construction, decking, railing, and auto mobile components. For example, wood/thermoplastic composite lumber has been widely recognized by the construction industry and homeowners, primarily used for decking (Lundin et al. 2004). The outdoor applications of NFPCs in construction require improved mechanical properties under weathering conditions.

As introduced in Chapter 4, low impact strength is still one of the major concerns for the application of WPCs. Ultra-high molecular weight polyethylene (UHMWPE) is a polyethylene (PE) with extremely long molecular chains and high molecular weight. The long molecular chains offer this material high toughness and good wear resistance, but also make it very hard to process (Tincer and Coskun 1993). To take advantage of the good mechanical properties of UHMWPE, conventional polyethylene has been tried as additive in UHMWPE to make it more processable (Bhateja and Andrews 1983, Dumoulin et al. 1984, Kyu and Vadhar 1986, Suwanprateeb 2000, Xue et al. 2006). A major drawback of UHMWPE is its poor creep resistance, which is especially critical for its application in joint reconstruction (Deng et al. 1998). Crosslinking and additives, such as carbon fibers, were proven to be effective for the creep

enhancement of UHMWPE and HDPE/UHMWPE composite (Wright et al. 1981, Penning et al. 1994, Lewis and Carroll 2001).

Weathering is a process of degradation resulting from UV radiation of sunlight, oxygen, moisture, etc. It can change the morphology of polymeric material by means of chemical crosslinking or chain scission (Davis and Sims 1983). It was reported that UV and moisture-induced degradation significantly decreased the flexural modulus and strength of natural fiber/high-density polyethylene (HDPE) composite (Lundin et al. 2004). However, screening effect of wood particles confined the UV degradation to the surface of the composites, led to better mechanical properties of composites compared with neat polymer after UV exposure (Selden et al. 2004, LaMantia and Morreale 2008).

UV radiation has been shown to deteriorate creep resistance of polymeric materials with the effect of breaking the polymer molecular chains, which has been confirmed by the application of modern physical methods to detect the appearance of free radicals and the change of molecular weight (Regel et al. 1967). The experiments show that UV radiation increased the creep rate of different polymers and reduced their lifetime (Regel et al. 1967, Boboev et al. 1968, Boboev et al. 1969). However, UV radiation also provided a way to improve creep resistance of polymeric material when being used to create cross-linking in the material. Current research showed good effect of UV radiation to improve creep property of Ultra-High Molecular Weight Polyethylene (UHMWPE) (Penning et al. 1994, Jacobs et al. 2000).

Mineral fillers have been examined as UV stabilizer in different polymers and showed various effects. Adding talc in PP as UV stabilizer resulted in higher degradation rate compared with neat PP within an initial period (12 weeks in their research) and started to show some effect after that (Rabello and White 1996). Similar results have been found when using CaCO_3 in

HDPE composites (Valadez-Gonzalez et al. 1999). Yang et al. compared several mineral fillers for HDPE composites and found that only CaCO_3 and wollastonite had a little stabilizing effect, while kaolin, diatomite and mica accelerated UV degradation of HDPE (Yang et al. 2005).

Based on the review of previous research, the objectives of this study were 1) to evaluate the effect of UHMWPE as an impact modifier for wood flour (WF)/HDPE composite, 2) to investigate the effect of UHMWPE on the creep resistance of HDPE and the effect of WF in enhancing the creep of HDPE/UHMWPE composites, 3) to examine how UV affects the creep resistance and other mechanical properties of the composites, and 4) to explore the effect of UV absorber (UVA) on the properties of wood/HDPE composite before and after the outdoor weathering.

6.2 EXPERIMENTAL

6.2.1 Materials

The HDPE was HD6706.17 from Exxon-Mobil Chemical Co, with a melt flow index of 6.1 g/10min (190 °C, 2.16 kg) and a density of 0.952 g/cm³. UHMWPE was GUR4120 from Ticona (Houston, TX). It is a powder with a density of 0.93 g/cm³ and an average molecular weight of 5 million g/mol. DuPont DLS 210, from E.I. DuPont (New Johnsonville, TN) was used as an UVA. It is an ultrafine titanium dioxide (TiO_2) with a median particle size of 135 nm and a surface area of 45 m²/g. Wood flour (WF) was provided by American Wood Fibers Inc. (Madison, MI), with a 40-mesh particle size. A maleated polyethylene (PE-g-MA) G-2608 from Eastman Chemical Company (Kingsport, TN, USA), with a melt index of 8 g/10min (190 °C, 2.16 kg) and an acid number of 8 mg KOH/g, was used as a coupling agent for polymer matrix and WF.

The experimental design included 4 levels of UHMWPE (0%, 10%, 20%, and 30% of polymer loading), 2 levels of WF (0% and 40% of the total composite weight), and 1 level of coupling agent (5% of WF loading). In addition, 2 levels of UVA (0% and 2% of the total weight of polymer matrix) were added in the composites with UHMWPE levels of 0% and 20%. The experimental design made up 12 formulations in total.

6.2.2 Composite Preparation

HDPE, fed through the main feeder, and UHMWPE/UVA, fed through the side feeder, were first compounded through a co-rotating twin screw extruder MIC27/GL-400 (Leistritz Corporation, Allendale, NJ) with a screw length/diameter of 40:1. In the case of both powders were used, UHMWPE and UVA were well mixed by hand before feeding. The extrusion temperature profile was 140-160-180-200-210-210-210-210-200-190-180 °C from the hopper to the die and the screw rotating speed was fixed at 100 rpm. The extruded strands were cooled through water bath, and then pelletized with a BT 25 Strand Pelletizer (Scheer Bay Co., Bay City, MI).

The polymer pellets, fed through the main feeder, and WF, fed through the side feeder, were then extruded to make WPC blends with the same extruder with a temperature profile of 140-160-180-190-190-190-190-180-175-175-175 °C from the hopper to the die and a screw rotating speed of 100 rpm.

The test samples for mechanical properties were made through injection molding, using a PLUS 35 injection molding machine from Battenfeld of American Inc. (South Elgin, IL). The composites with UHMWPE were injection molded at 200 °C and those without UHMWPE were molded at 190 °C. The impact test specimens with cross-section size of around 3 mm × 12 mm were machined for creep tests.

6.2.3 Weathering

Weathering specimens were exposed outdoors in Baton Rouge, LA for 5 consecutive weeks from May to June, 2009. This was to investigate how UV radiation affects the mechanical and creep properties of the composites and the effect of UVA in protecting the material from weathering.

6.2.4 Characterization

Flexural and tensile strengths were measured according to the ASTM D790-03 and D638-03, respectively, using an INSTRON 5582 Testing Machine (Instron Co., Grove City, PA). A TINIUS 92T impact tester (Tinius Olsen, Inc., Horsham, PA, USA) was used for the Izod impact test. All samples were notched at the center point of one longitudinal side according to the ASTM D256. For each treatment level, five replicates were tested.

TA Q800 Dynamic Mechanical Analysis (DMA) instrument (New Castle, DE) was used for short-term creep tests with a 3-point bending mode. The test samples with approximate cross-section size of 3×12 mm were used for creep tests. In each test, the sample was heated to 35 °C and allowed to equilibrate for 5 minutes. A static stress level of 4 MPa was then applied for 12 hours, and the stress was released afterward to allow the sample to recover for 12 hours. The sample deformation was measured during this process.

Accelerated creep tests were performed for 30 minutes at temperature levels starting at 35 °C and increasing 10 °C in steps up to 95 °C. After equilibrating at the desired temperature for 5 minutes, 4 MPa of stress was applied and held constant for 30 minutes while the creep strain was measured.

6.2.5 Creep Modeling

The four-element Burgers model was used to fit the creep curves.

$$\varepsilon(t) = \frac{\sigma}{E_M} + \frac{\sigma}{E_K} \left[1 - \exp\left(-t \frac{E_K}{\eta_K}\right) \right] + \frac{\sigma}{\eta_M} t \quad (6.1)$$

where $\varepsilon(t)$ is the creep strain as a function of time (t) and σ is the applied stress; E_M and E_K represent elastic moduli of the springs in this model; η_M and η_K represent viscosities of the dashpots.

Statistical Analysis System (SAS) was employed to estimate the model parameters by performing nonlinear regression on the creep curves. The Gauss-Newton iterative method was implemented in this analysis to find the least-square estimates for the nonlinear model. Since the DMA instrument collected the data with an increasing step-size, every data point was weighted with the time interval of data collection.

6.3 RESULTS AND DISCUSSION

6.3.1 Mechanical Properties

6.3.1.1 UHMWPE Effect

Table 6.1 lists the mechanical properties of composites at different levels of UHMWPE with and without WF. As shown, the addition of UHMWPE effectively improved the impact strength of HDPE. For example, with the addition of 20% UHMWPE, the impact strength of HDPE was doubled. This effect may be because the lowered crystallinity of HDPE at the presence of UHMWPE and high flexibility of UHMWPE molecular chains facilitated the transfer of stress during the impact process. With the addition of rigid WF, the UHMWPE molecular chains had less free space and less flexibility. Most impact energy was transferred to and sustained by the rigid WF which is prone to break during deformation, leading to a less significant toughening effect from UHMWPE. Higher UHMWPE contents also resulted in higher toughness with the existence of WF, though the impact strength of WPCs was much lower than that of the corresponding polymer matrices.

Adding UHMWPE into HDPE showed minor improvement on the flexural and tensile strengths. However, positive effect of UHMWPE emerged at the presence of WF. Similar to the discussion above, during flexural and tensile deformations UHMWPE molecular chains facilitated the transfer of stress to the WF, which has high flexural and tensile strengths. The clear positive effect of UHMWPE on impact, flexural, and tensile properties of the HDPE/WF composite makes it a potentially valuable additive for the WPC.

Table 6.1 Mechanical properties of samples with different UHMWPE and WF loading levels

Compo- sition	HDPE/ UHM- WPE	Impact Strength (kJ/m ²)	Flexural		Tensile	
			Strength (MPa)	Modulus (GPa)	Strength (MPa)	Modulus (MPa)
HDPE/ UHM- WPE	100/0	8.4 (0.4) d	16.5 (0.3) d	0.60 (0.04) c	17.1 (0.3) e	1.01 (0.11) b
	90/10	11.2 (0.6) c	17.3 (0.3) d	0.64 (0.02) c	17.2 (0.4) e	0.98 (0.12) b
	80/20	16.7 (0.4) b	17.2 (0.1) d	0.61 (0.00) c	17.9 (0.1) e	0.89 (0.10) b
	70/30	21.8 (1.0) a	17.8 (0.3) d	0.64 (0.02) c	18.7 (0.2) e	0.84 (0.11) b
HDPE/ UHM- WPE/ WF	100/0	3.6 (0.1) h	46.2 (0.6) c	2.37 (0.05) b	29.2 (0.7) d	3.04 (0.34) a
	90/10	5.1 (0.1) g	51.4 (0.7) b	2.47 (0.05) b	37.8 (0.5) c	2.79 (0.25) a
	80/20	6.1 (0.3) f	50.8 (2.7) b	2.42 (0.17) b	42.7 (3.6) a	2.81 (0.45) a
	70/30	7.2 (0.2) e	55.7 (3.4) a	2.69 (0.26) a	39.7 (2.1) b	3.29 (0.76) a

The weight ratio of WF to HDPE/UHMWPE matrix is 40/60.

The values in parentheses are standard deviations.

Different letters indicate a significant difference at the 95% confidence level.

6.3.1.2 WF Effect

As shown in Table 6.1, the addition of WF considerably decreased the impact strength of HDPE, but it significantly strengthened the flexural properties and tensile properties at the same time. The same trend was observed for the HDPE/UHMWPE composites. The possible reason was that the rigid WF sustained stress during deformation and contributed to the composite its good flexural and tensile properties, as well as poor impact strength.

6.3.1.3 UVA Effect

Table 6.2(a) shows the mechanical properties of composites with and without the

addition of UVA before weathering. As shown, UVA showed a slight effect on these properties, with a positive effect on flexural and tensile properties and a negative one on impact strength.

This trend is similar to what was observed from the addition of WF but much less obvious.

Table 6.2(a) Comparison of mechanical properties of samples with and without UV before weathering

UV	WF	HDPE/ UHM- WPE	Impact Strength (kJ/m ²)	Flexural		Tensile	
				Strength (MPa)	Modulus (GPa)	Strength (MPa)	Modulus (MPa)
NO	NO	100/0	8.4 (0.4) c	16.5 (0.3) e	0.60 (0.04) d	17.1 (0.3) d	1.01 (0.11) d
		80/20	16.7 (0.4) a	17.2 (0.1) de	0.61 (0.00) d	17.9 (0.1) d	0.89 (0.10) d
	YES	100/0	3.6 (0.1) g	46.2 (0.6) c	2.37 (0.05) c	29.2 (0.7) c	3.04 (0.34) bc
		80/20	6.1 (0.3) e	50.8 (2.7) b	2.42 (0.17) c	42.7 (3.6) a	2.81 (0.45) c
YES	NO	100/0	7.4 (0.4) d	18.6 (0.4) d	0.70 (0.02) d	17.8 (0.2) d	1.18 (0.19) d
		80/20	14.2 (0.5) b	18.0 (0.1) de	0.64 (0.02) d	17.5 (0.1) d	0.79 (0.08) d
	YES	100/0	3.0 (0.1) h	50.5 (0.3) b	3.19 (0.03) a	31.0 (0.4) c	3.89 (0.55) a
		80/20	5.5 (0.1) f	54.7 (2.2) a	2.58 (0.16) b	40.2 (2.8) b	3.35 (0.59) b

Table 6.2(b) Comparison of mechanical properties of samples with and without UV after weathering

UV	WF	HDPE/ UHM- WPE	Impact Strength (kJ/m ²)	Flexural		Tensile	
				Strength (MPa)	Modulus (GPa)	Strength (MPa)	Modulus (MPa)
NO	NO	100/0	4.4 (0.2) e	18.7 (0.8) e	0.68 (0.06) d	18.5 (0.2) d	0.86 (0.18) b
		80/20	3.6 (0.2) f	21.5 (0.9) d	0.78 (0.06) d	19.4 (0.2) d	0.82 (0.07) b
	YES	100/0	3.4 (0.2) f	48.4 (0.5) c	2.50 (0.08) c	31.3 (0.1) c	2.57 (0.07) a
		80/20	5.7 (0.2) c	57.5 (1.8) a	2.83 (0.17) b	38.7 (4.5) b	2.74 (0.49) a
YES	NO	100/0	6.2 (0.2) b	19.8 (0.2) e	0.73 (0.02) d	18.6 (0.2) d	0.89 (0.07) b
		80/20	12.5 (0.3) a	18.9 (0.2) e	0.69 (0.02) d	18.1 (0.1) d	0.69 (0.11) b
	YES	100/0	2.8 (0.1) g	51.4 (0.8) b	3.30 (0.07) a	30.3 (0.7) c	2.90 (0.57) a
		80/20	5.3 (0.2) d	57.3 (1.6) a	2.75 (0.16) b	42.6 (2.0) a	2.90 (0.38) a

The weight ratio of WF to HDPE/UHMWPE matrix is 40/60.

The percentage of UV agent is 2% of the total weight of polymer matrix and WF.

The values in parentheses are standard deviations.

Different letters indicate a significant difference at the 95% confidence level.

6.3.1.4 Weathering Effect

Table 6.2(b) shows the mechanical properties of composites with and without the addition of UVA after weathering. Comparing Table 6.2(a) and Table 6.2(b), it can be observed that weathering greatly impaired the impact strength of pure PE by almost 50%. This decrease demonstrated the strong effect of weathering, which probably caused the breakage of HDPE chains. It was even worse for PE/UHMWPE composite, with around 80% decrease of the impact strength. UV had stronger effect on UHMWPE, of which long molecular chains are more susceptible to breakage under UV radiation. This negative influence was largely avoided for both materials by the addition of UVA, demonstrating the UV screening effect of this ultrathin titanium dioxide. The deteriorating effect of weathering on impact strength was much less at the presence of WF possibly because WF protected the polymer matrix from exposing to UV radiation, a screening effect similar to UVA.

6.3.2 Creep Behavior

6.3.2.1 UHMWPE Effect

Figure 6.1 shows the creep and recovery behavior of composite at different levels of UHMWPE with and without WF. The Burgers model parameters are presented in Table 6.3. As shown in Figure 6.1(a), the addition of UHMWPE slightly increased the creep deformation of HDPE and higher UHMWPE loading resulted in larger creep. There are two possible reasons: one is the high flexibility of UHMWPE long chains due to the lack of branches made them prone to move under stress, and the other is that the introduction of long molecular chains reduced the crystallinity of HDPE and increased the amorphous portion. The same trend was observed at the presence of WF, as shown in Figure 6.1(b).

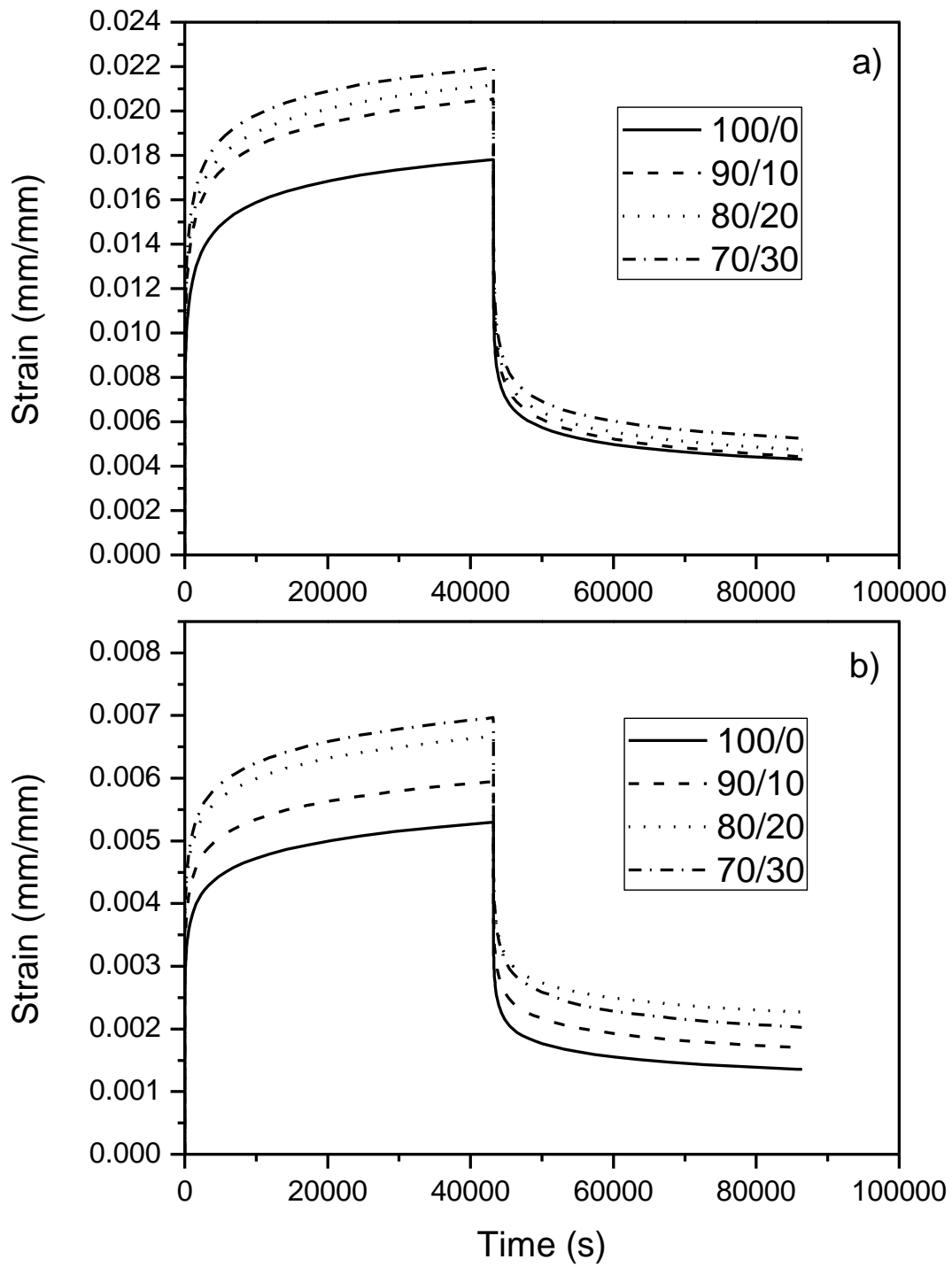


Figure 6.1 Creep and recovery curves of the composites with different HDPE/UHMWPE ratio: (a) without WF, (b) with WF.

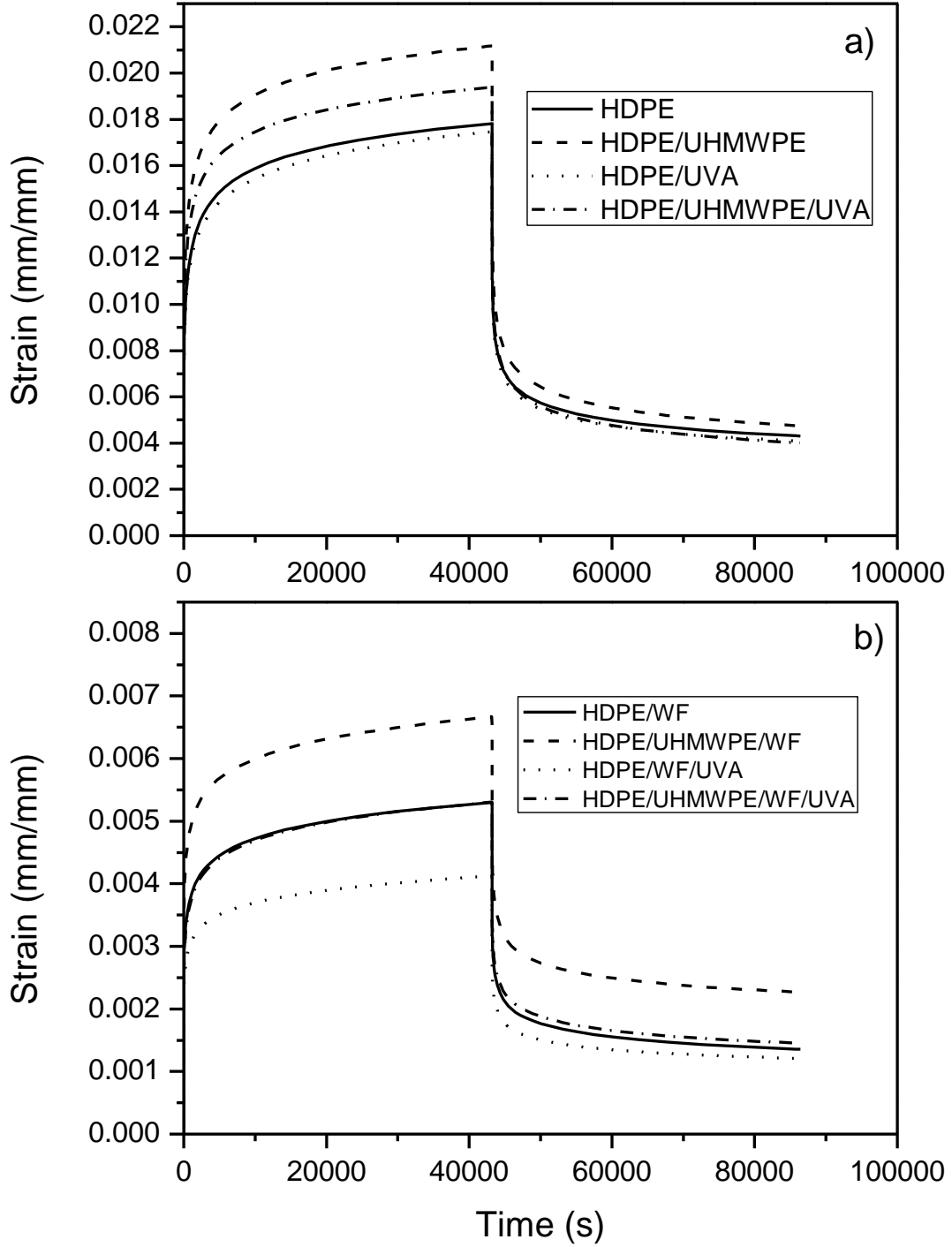


Figure 6.2 Creep and recovery curves of the composites with and without UVA: (a) without WF, (b) with WF. The HDPE/UHMWPE ratio is 80/20.

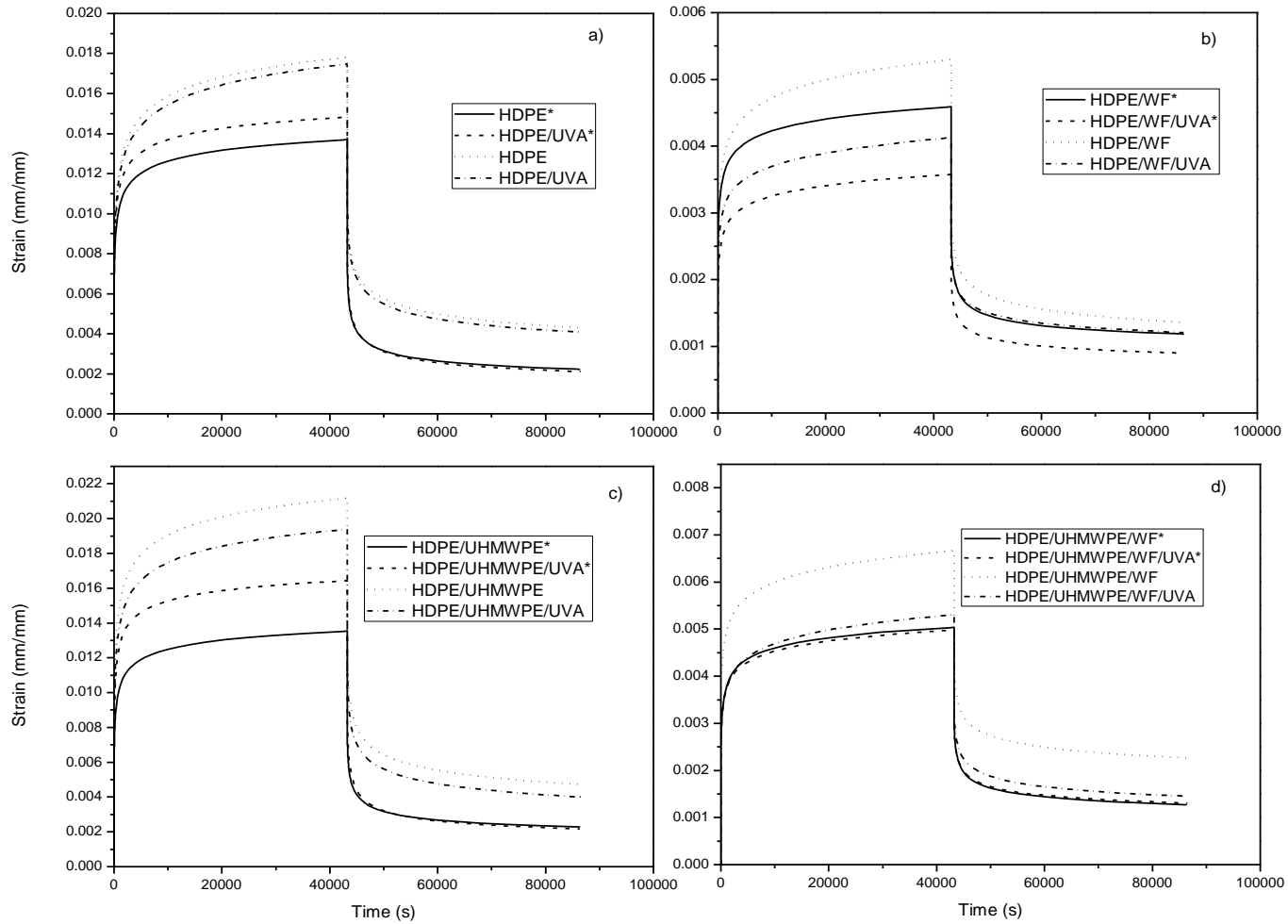


Figure 6.3 Creep and recovery curves of the composites before and after weathering (labeled with *). The HDPE/UHMWPE ratio is 80/20.

Table 6.3 Burgers parameters for samples with different UHMWPE and WF loading levels

Composition	HDPE/ UHMWPE	E_M (MPa)	E_K (MPa)	η_k (Pa s)	η_M (Pa s)
	100/0	400	707.96	1.99E+12	7.69E+13
HDPE/ UHMWPE	90/10	333.33	641.03	1.76E+12	6.93E+13
	80/20	322.58	620.16	1.62E+12	6.84E+13
	70/30	310.08	597.91	1.53E+12	6.80E+13
HDPE/ UHMWPE/ WF	100/0	1208.5	2963	9.03E+12	2.59E+14
	90/10	1036.3	2816.9	8.43E+12	2.46E+14
	80/20	921.66	2531.6	7.4E+12	2.20E+14
	70/30	896.86	2352.9	6.9E+12	2.04E+14

The weight ratio of WF to HDPE/UHMWPE matrix is 40/60.

Table 6.4(a) Burgers parameters for samples with different UHMWPE, WF and UV loading levels before weathering

UV	WF	HDPE/ UHMWPE	E_M (MPa)	E_K (MPa)	η_k (Pa s)	η_M (Pa s)
NO	NO	100/0	400	707.96	1.99E+12	7.69E+13
		80/20	322.58	620.16	1.62E+12	6.84E+13
	YES	100/0	1208.5	2963	9.03E+12	2.59E+14
		80/20	921.66	2531.6	7.4E+12	2.20E+14
YES	NO	100/0	401.61	754.72	2.27E+12	7.40E+13
		80/20	350.88	688.47	1.8E+12	7.57E+13
	YES	100/0	1481.5	4228.3	1.23E+13	3.42E+14
		80/20	1238.4	2857.1	8.93E+12	2.46E+14

Table 6.4(b) Burgers parameters for samples with different UHMWPE, WF and UV loading levels after weathering

UV	WF	HDPE/ UHMWPE	E_M (MPa)	E_K (MPa)	η_k (Pa s)	η_M (Pa s)
NO	NO	100/0	463.5	1041.7	2.42E+12	1.31E+14
		80/20	470.04	1047.1	2.36E+12	1.34E+14
	YES	100/0	1294.5	3669.7	9.17E+12	3.96E+14
		80/20	1246.1	2985.1	7.63E+12	3.31E+14
YES	NO	100/0	424.18	975.61	2.2E+12	1.25E+14
		80/20	384.62	860.22	1.76E+12	1.17E+14
	YES	100/0	1709.4	4581.9	1.24E+13	4.51E+14
		80/20	1234.6	3225.8	8.84E+12	3.29E+14

The weight ratio of WF to HDPE/UHMWPE matrix is 40/60.

6.3.2.2 WF Effect

Comparing Figure 6.1(a) and Figure 6.1(b), the creep deformation of HDPE/UHMWPE composite was greatly reduced with the addition of WF, at each loading level of UHMWPE. The enhancing effect of WF on creep resistance was much stronger than the deteriorating effect of UHMWPE. Thus, UHMWPE can be used as impact modifier for HDPE/WF composite while sustaining good creep resistance resulting from WF.

6.3.2.3 UVA Effect

As shown in Figure 6.2(a) and Figure 6.2(b), the addition of UVA reduced the creep deformation of the composites with and without WF. This effect seemed to be more obvious for the composites with WF.

6.3.2.4 Weathering Effect

As shown in Figure 6.3, the composites showed better creep resistance after weathering than before weathering, especially on long-term creep rate, represented by η_M in Table 6.4. The smaller long-term creep rate resulted in less non-recoverable viscous deformation, so that higher recoverability was observed for the composites after weathering, as shown in Figure 6.3. This enhancing effect might be attributed to the UV radiation during weathering, which broke the molecular chains and led to cross-linking. In Figure 6.3(a), HDPE showed larger creep deformation than HDPE/UVA, but the order was reversed after weathering, demonstrating the screening effect of UVA, which blocked the UV radiation and weakened its enhancing effect in creep resistance. For HDPE/WF composites with and without UVA, weathering showed a similar effect on their creep properties, suggesting that UVA had little extra protection for HDPE at the presence of WF. For HDPE/UHMWPE composites without UVA, weathering improved the creep resistance even greater, and addition of UVA effectively reduced this effect.

6.4 CONCLUSION

The addition of wood flour in HDPE composites improved main mechanical properties, such as tensile strength, tensile modulus, flexural strength, flexural modulus, and creep resistance of polymer matrix. However, the gain in these properties was at the expense of lowered impact strength. UHMWPE was successfully introduced into HDPE/WF composite as an impact modifier and improved the toughness of HDPE both with and without WF. It also improved flexural and tensile properties of the composites at the presence of WF. Although the addition of UHMWPE slightly decreased the creep resistance of HDPE/WF composites, the resulting creep property was still much better than that of pure HDPE, due to the significant enhancing effect of WF. Thus, UHMWPE and WF worked complementarily on the two properties when being used together with HDPE. Weathering dramatically impaired impact strength of HDPE and HDPE/UHMWPE, but both WF and UVA effectively inhibited this effect. A slight increase was observed in flexural property, tensile property, and creep resistance after weathering.

6.5 REFERENCES

- Bhateja, S. K. and E. H. Andrews. 1983. Thermal, mechanical, and rheological behavior of blends of ultrahigh and normal-molecular-weight linear polyethylenes. *Polymer Engineering & Science* **23**:888-894.
- Boboev, T. B., V. R. Regel, and N. N. Chernyi. 1969. Comparison of the effect of ultraviolet radiation on polymer creep rate in a vacuum and in air. *Mechanics of Composite Materials* **5**:481-483.
- Boboev, T. B., V. R. Regel, T. P. Sanfirova, and N. N. Chernyi. 1968. Effect of ultraviolet radiation on the life of stressed polymers under vacuum and in air. *Mechanics of Composite Materials* **4**:511-513.
- Davis, A. and D. Sims. 1983. *Weathering of polymers*. Elsevier Applied Science Publishers, London.
- Deng, M., R. A. Latour, A. A. Ogale, and S. W. Shalaby. 1998. Study of creep behavior of ultra-high-molecular-weight polyethylene systems. *Journal of Biomedical Materials Research* **40**:214-223.

- Dumoulin, M. M., L. A. Utracki, and J. Lara. 1984. Rheological and mechanical behavior of the UHMWPE/MDPE mixtures. *Polymer Engineering & Science* **24**:117-126.
- Jacobs, M., N. Heijnen, C. Bastiaansen, and P. Lemstra. 2000. A novel, efficient route for the crosslinking and creep improvement of high modulus and high strength polyethylene fibres. *Macromolecular Materials and Engineering* **283**:120-125.
- Kyu, T. and P. Vadhar. 1986. Cocrystallization and miscibility studies of blends of ultrahigh molecular weight polyethylene with conventional polyethylenes. *Journal of Applied Polymer Science* **32**:5575-5584.
- LaMantia, F. P. and M. Morreale. 2008. Accelerated weathering of polypropylene/wood flour composites. *Polymer Degradation and Stability* **93**:1252-1258.
- Lewis, G. and M. Carroll. 2001. Effect of crosslinking UHMWPE on its tensile and compressive creep performance. *Bio-Medical Materials and Engineering* **11**:167-183.
- Lundin, T., S. M. Cramer, R. H. Falk, and C. Felton. 2004. Accelerated Weathering of Natural Fiber-Filled Polyethylene Composites. *Journal of Materials in Civil Engineering* **16**:547-555.
- Penning, J. P., H. E. Pras, and A. J. Pennings. 1994. Influence of chemical crosslinking on the creep behavior of ultra-high molecular weight polyethylene fibers. *Colloid & Polymer Science* **272**:664-676.
- Rabello, M. S. and J. R. White. 1996. Photodegradation of talc-filled polypropylene. *Polymer Composites* **17**:691-704.
- Regel, V. R., N. N. Chernyi, V. G. Kryzhanovskii, and T. B. Boboev. 1967. Effect of ultraviolet radiation on the creep rate of polymers. *Mechanics of Composite Materials* **3**:272-275.
- Selden, R., B. Nystrom, and R. Langstrom. 2004. UV aging of poly(propylene)/wood-fiber composites. *Polymer Composites* **25**:543-553.
- Suwanprateeb, J. 2000. Binary and ternary particulated composites: UHMWPE/CACO3/HDPE. *Journal of Applied Polymer Science* **75**:1503-1513.
- Tincer, T. and M. Coskun. 1993. Melt blending of ultra high molecular weight and high density polyethylene: The effect of mixing rate on thermal, mechanical, and morphological properties. *Polymer Engineering & Science* **33**:1243-1250.
- Valadez-Gonzalez, A., J. M. Cervantes-Uc, and L. Veleza. 1999. Mineral filler influence on the photo-oxidation of high density polyethylene: I. Accelerated UV chamber exposure test. *Polymer Degradation and Stability* **63**:253-260.
- Wright, T. M., T. Fukubayashi, and A. H. Burstein. 1981. The effect of carbon fiber reinforcement on contact area, contact pressure, and time-dependent deformation in polyethylene tibial components. *Journal of Biomedical Materials Research* **15**:719-730.

Xue, Y., W. Wu, O. Jacobs, and B. Schadel. 2006. Tribological behaviour of UHMWPE/HDPE blends reinforced with multi-wall carbon nanotubes. *Polymer Testing* **25**:221-229.

Yang, R., J. Yu, Y. Liu, and K. Wang. 2005. Effects of inorganic fillers on the natural photo-oxidation of high-density polyethylene. *Polymer Degradation and Stability* **88**:333-340.

CHAPTER 7 CONCLUSIONS AND FUTURE WORK

7.1 OVERALL CONCLUSIONS

Natural fiber/polymer composites (NFPCs) are being increasingly used in construction due to its sound mechanical properties, processability, water and rot resistance, low maintenance requirement, and wood-like appearance. The increasing application of NFPCs in building products made creep resistance an important property for this material. The work described in this dissertation includes research on creep behavior of NFPCs with different polymer matrices, natural fiber types, additives and modifiers. The objectives of this research were: 1) To evaluate creep models for different applications, i.e., comparison, characterization, and prediction; 2) To develop creep models suitable for comparison, characterization and prediction of creep in NFPCs; 3) To predict long-term creep behavior of NFPCs through accelerated testing; and 4) To apply the developed techniques to investigate creep behaviors of various systems aimed to improve the overall properties of NFPCs. Based on the discussions in this dissertation, the following conclusions can be made.

The creep curves of NFPCs were fitted with both physical models and empirical models. Among these models, the 4-element Burgers model was most interpretable and fitted the overall creep curves well. The parameters obtained from the 4-element Burgers model were used to characterize the viscoelastic properties of NFPCs and to compare their creep resistances. The disadvantage of the 4-element Burgers model was that it lacks the flexibility to fully describe the transition region at the beginning of creep, tending to provide an instantaneous deformation larger than the real value. It also tended to give a larger long-term creep rate by concluding that the creep process enters the linear region during the experimental period, though the creep rate kept decreasing during that process. Thus, the 4-element Burgers model is not suitable for long-

term prediction. Generalized Burgers model, such as 6 and 8–element models, provided better fit by introducing extra Kelvin units, so that smaller instantaneous deformation and long-term creep rate were obtained. However, the Kelvin units in the generalized Burgers models only functioned within the experimental span well, predicting a linear trend starting within the experimental region, which was actually still within the nonlinear primary stage. Indexed Burgers models performed better for creep curves within primary stage in terms of both characterization and prediction.

Creep prediction was attempted using two approaches: modeling and accelerated testing. Based on the experimental data, Burgers models are not recommended for prediction because the experiments were done within the primary nonlinear stage and Burgers models predicted a linear trend before that stage was observed. Long-term experiments are needed for the Burgers model to provide a better prediction. Comparatively, the Indexed Burgers models and 2-parameter power law model performed better in terms of prediction. Accelerated creep tests were conducted at higher temperatures and smooth curves were obtained based on time-temperature superposition principle. TTS offered good prediction for creep of PVC composites but over-predicted that of HDPE composites. These assessments were based on the limited experimental data. The accuracy of long-term prediction was unable to be evaluated due to the lack of long-term experimental data.

Creep resistance of NFPCs was affected by many factors, including formulation, temperature, and weathering. Different polymers showed different creep properties due to structural and morphological differences. PVC had higher creep resistance than HDPE; HDPE showed better creep property than UHMWPE. Introducing engineering plastics to form microfibrils in HDPE matrix improved its creep performance. Recycled plastics resulted in

smaller creep deformation than the corresponding virgin resin, probably because of the additives from previous use. Natural fibers, such as bamboo flour and wood flour, greatly enhanced the creep resistance of NFPCs. This enhancing effect outweighed other effects resulting from change in polymer matrix or addition of other small-amount additives. The effect of coupling agent on creep was dependent on its modulus and coupling effect. For example, PE-g-MA improved the creep property of BF/HDPE composite but EPR-g-MA showed a reverse effect. UVA, an ultrafine titanium dioxide, slightly reduced the creep deformation of HDPE composites at a low loading level. Creep behaviors of both pure polymer and NFPCs were very sensitive to temperature. Higher temperatures led to not only larger instantaneous deformation, but also higher long-term creep rate. Weathering also affected the creep property of polymer and NFPCs. Five-week outdoor exposure led to improvement on creep resistance of HDPE composites, especially a smaller long-term creep rate. However, a long-term exposure may deteriorate this property, as reported in previous literature.

7.2 FUTURE WORK

Future work is needed to further the understanding of the creep properties of NFPCs. Based on the results shown in this dissertation, future work will need to be focused on the following aspects.

First, long-term creep tests are needed to evaluate the prediction performance of modeling techniques and accelerated testing. Our current equipment only allows one test on one sample at one time, which makes long-term creep tests impractical. New equipment would be needed to perform these long-term creep tests for a series of samples at the same time. Long-term creep data will also give better accuracy for creep modeling, especially for Burgers models.

Secondly, long-term weathering or accelerated weathering treatment is needed to simulate the circumstances in real applications. NFPCs used outdoors last for many years. Though positive effect was observed on main mechanical properties of WF/HDPE composites after 5 weeks outdoor exposure, a reverse effect may appear as weathering advances.

Finally, recovery process needs to be researched more extensively. Some brief discussion and analysis were done on recovery process of NFPCs in this dissertation, but more detailed study on this aspect will be needed to deepen the understanding of the viscoelastic behavior of polymer composites during the creep and recovery process.

APPENDIX: PERMISSION LETTER

From: **McCarthy, Stephen** <Stephen_McCarthy@uml.edu>
Date: Mon, Jul 20, 2009 at 6:52 AM
Subject: RE: permission for reprint of my paper as part of dissertation
To: Yanjun Xu <yxu6@tigers.lsu.edu>

Yes, that is fine

----- Forwarded message -----

From: **Yanjun Xu** <yxu6@tigers.lsu.edu>
Date: 2009/7/9
Subject: permission for reprint of my paper as part of dissertation
To: [Stephen McCarthy@uml.edu](mailto:Stephen_McCarthy@uml.edu)

Dear Dr. McCarthy,

This is Yanjun Xu, PhD candidate at Louisiana State University. I published the following article on your journal and I am writing to ask for permission to reprint it as part of my dissertation.

Xu, Y., Q. Wu, Y. Lei, F. Yao, and Q. Zhang. 2008. [Natural Fiber Reinforced Poly\(vinyl chloride\) Composites: Effect of Fiber Type and Impact Modifier](#). Journal of Polymers and the Environment 16(4):250-257.

Thanks and best regards,

Yanjun

Yanjun Xu
PhD Graduate Research Assistant
School of Renewable Natural Resources
Louisiana State University, Baton Rouge, LA 70803
Tel: 225-578-4358; Cell: 225-362-0275
E-mail: yxu6@tigers.lsu.edu

VITA

Yanjun Xu was born in August 1979 in Changshu, Jiangsu, China. He has an older sister. He attended Sichuan University and received his Bachelor's degree in polymer science and engineering in 2002 and Master's degree in polymer processing engineering in 2005. After that, he joined Shanghai Kingfa Sci. & Tech. Co. Ltd. and worked there until December 2005. Yanjun Xu will graduate with a Doctor of Philosophy degree in forestry and a Master in applied statistics from Louisiana State University in December 2009. He and his wife are expecting their first baby in January 2010.